NASA CR-152109

AN INVESTIGATION OF WING BUFFETING RESPONSE AT SUBSONIC AND TRANSONIC SPEEDS: PHASE I F-111A FLIGHT DATA ANALYSIS

VOLUME I - SUMMARY OF TECHNICAL APPROACH, RESULTS AND CONCLUSIONS

by

David B. Benepe, Atlee M. Cunningham, Jr.
and W. David Dunmyer

Prepared under Contract No. NAS 2-7091 by
GENERAL DYNAMICS CORPORATION
Fort Worth Division
Fort Worth, Texas

for

AMES RESEARCH CENTER
NATIONAL AERONAUTICS AND SPACE ADMINISTRATION

NASA CR-152109

AN INVESTIGATION OF WING BUFFETING RESPONSE AT SUBSONIC AND TRANSONIC SPEEDS: PHASE I F-111A FLIGHT DATA ANALYSIS

VOLUME I - SUMMARY OF TECHNICAL APPROACH, RESULTS AND CONCLUSIONS

by

David B. Benepe, Atlee M. Cunningham, Jr.
and W. David Dunmyer

Prepared under Contract No. NAS 2-7091 by
GENERAL DYNAMICS CORPORATION
Fort Worth Division
Fort Worth, Texas

for

AMES RESEARCH CENTER
NATIONAL AERONAUTICS AND SPACE ADMINISTRATION

TABLE OF CONTENTS

TABLE OF CONTENTS (Cont'd)

LIST OF TABLES

LIST OF FIGURES

AN INVESTIGATION OF WING BUFFETING RESPONSE AT SUBSONIC AND TRANSONIC SPEEDS: PHASE I F-111A FLIGHT TEST DATA ANALYSIS

VOLUME I - SUMMARY OF TECHNICAL APPROACH, RESULTS AND CONCLUSIONS

by
David B. Benepe, Arlee M. Cunningham, Jr.,
and W. David Dunmyer

SUMMARY

The structural response to aerodynamic buffet during moderate to high-g maneuvers at subsonic and transonic speeds was investigated. The measurements which consisted of shear, bending moment and torque at four wing span stations, vertical accelerations at the wing tips, center of gravity and pilot's seat and lateral accelerations at the center of gravity and pilot's seat had been previously obtained during the Loads Demonstration flight program on a variable sweep fighter-bomber aircraft.

Existing flight data for one wing sweep were extracted from magnetic tape records and subjected to statistical analyses to determine the power spectra and root-mean-square values of response for each of the measurements at several angles of attack for each of seven maneuvers. The frequency content of the various responses is correlated with results of ground vibration tests to identify the response modes. The rms values of response are plotted against angle of attack to show the variations of intensity of response during the maneuvers.

The investigation showed that the structural response to buffet is very complex. Almost all of the natural vibration modes of the aircraft, both symmetric and antisymmetric, are excited during buffet encountered in a moderate to high-g maneuver. Some of the sensors show pronounced changes in the relative modal contributions to the total response as penetration beyond buffet onset increases. The fluctuating shear and bending moment loads on the wing are small in terms of design loads except near the wing tip. The wing structural response in torsion is larger than anticipated on the basis of previously published buffet studies and amounts to between 1/3 and 1/2 of the rms values of wing bending response at high angles of attack. For the particular aircraft geometry and structure examined, there is some evidence of bending-torsion coupling starting at angles of attack between 9 and 12 degrees at Mach numbers of 0.80 and 0.87.

The investigation is reported in three volumes. NASA CR-152109 presents a summary of the technical approach, the results and conclusions drawn from the results. NASA CR-152110 presents plotted variations of Power Spectral Density (PSD) data with frequency for each structural response item for each data sample analyzed during the course of the investigation. NASA CR-152111 presents Power Spectral Density (PSD) data in tabular form for the convenience of those who might wish to perform additional analysis.

SYMBOLS

Note: Quantities are presented in the International System of Units (U.S. customary units in parenthesis). The work was performed using U.S. customary units.

b	wing span - m, (ft)
$B.M._{DES}$	design value of wing bending moment, N-m. (in - lb)
c.g.,C.G.	"center of gravity"
f	frequency, hertz
f_o	spectral base frequency or analysis bandwidth, hertz
F_Z	wing vertical shear as measured by strain gages - N, (lb)
g	gravitational acceleration
M	Mach number
M_X	Wing Bending Moment as measured by strain gages N-m, (in - lb)
M_Y	Wing torsional moment - N-m, (in - lb)
n_{max}	maximum maneuver load factor - g's
S	theoretical wing area (leading and trailing edges of swept panel extended to airplane centerline m^2, (ft^2)
T	length of input frame in spectral analysis - seconds
T_1	start time of interval for spectral analysis - seconds
T_2	stop time of interval for spectral analysis - seconds
ΔT	time interval used for spectral analysis = T_2-T_1,sec
V_{DES}	design value of wing vertical shear, N, (lb)
$\ddot{y}$	lateral acceleration g's
$\ddot{z}$	vertical acceleration g's

SYMBOLS (Continued)

α	indicated angle of attack referenced to wing manufacturing chord plane
α_{max}	maximum indicated angle of attack - deg.
α_{nom}	nominal angle of attack representing time interval ΔT
α_{1}	indicated angle of attack at time T_1, deg
$\Delta\alpha$	increment in indicated angle of attack during time interval ΔT, deg
β	indicated sideslip angle, deg
σ_{a}	rms value of acceleration fluctuations - g, rms
$\sigma_{V_{max}}$	maximum rms value of wing vertical shear fluctuations - N, rms, (lb, rms)
$\sigma_{BM_{max}}$	maximum rms value of wing bending moment fluctuations - N-m, rms, (in - lb, rms)
Ψ_T	average rms value determined from power spectral analysis

ABBREVIATIONS

Alt	altitude
Asym	antisymmetric
B.M.	bending moment
Cross-PSD, XPSD	Cross power spectral density
dB	decibel
Dyn Press	dynamic pressure
FM	frequency modulation
H_z	hertz
hor, hori	horizontal
in-lb, IN-LB	inch-pound
inb'd	inboard
L	left
lb, LB	pound
L/H	left hand
LWT	left wing tip
m	meter
N	newton
N-m, N-M	newton-meter
outbd	outboard
P.S.	pilot seat
PSD	power spectral density
R	right
R/H	right hand

ABBREVIATIONS, (Continued)

rms	root-mean-square
RWT	right wing tip
Sym	symmetric
TOR	torsion
W.S.	Wing Station for strain gage measurements

SECTION 1

INTRODUCTION

The phenomenon of aerodynamic buffet has been a challenge to aircraft design teams for many years. With the advent of truly high performance fighter aircraft which are capable of operating at high angles of attack, the intensity of buffet and the magnitudes of the aircraft structural responses to buffet have become important design considerations.

The state-of-the-art of buffet research is such that development of a valid method of predicting aircraft structural response to buffet appears feasible in the near future. A significant problem that exists is the dearth of published flight data to provide an adequate test of the validity of a prediction method.

The investigation described in this report is an attempt to supply data of sufficient scope in terms of the number and types of flight measurements and in terms of the depth of analysis of the measurements to use for correlation with predicted response characteristics. A secondary, though no less important, objective of the investigation is to add to the aeronautical community's understanding of buffet phenomena which has advanced rapidly in recent years.

Considerable effort has been expended in research programs conducted by the National Aeronautics and Space Administration's Ames, Langley, and Flight Research Centers (Refs. 1-7), by the armed services (Refs. 8-14), and by airframe manufacturers (Refs. 15-17). Each of these previous efforts has contributed something of significance to our understanding of buffet and of aircraft responses to buffet.

Results of various flight test programs have shown that a most reliable indicator of maneuvering buffet onset is the abrupt change in rms response of a wing-tip accelerometer. It can also be inferred that wing-tip accelerometer response is a good indicator of the variation of buffet intensity with angle of attack. However, measurements need to be obtained of accelerations at several points on an aircraft and of the spanwise distributions of dynamic structural loads on the wing to obtain a true test of a prediction method. Additionally, the power spectra data are needed for each measurement over a range of frequencies which covers the important natural vibration modes of the aircraft structure.

Recent developments in flight test instrumentation and data recording and data processing systems permit the use of powerful techniques of random data analysis to study the buffet problem. Power spectral density (PSD) plots can be readily constructed to obtain the needed variations of response with frequency and

calculate root-mean-square values (rms) of the accelerations and loads to obtain statistical measures of the variations of responses with angle of attack.

The duration of the flight maneuvers is short, therefore the data samples are usually not long enough to strictly satisfy the mathematical criteria for obtaining a high level of confidence in the spectral or rms estimates. Nevertheless, spectral estimates and rms values are much more meaningful quantities than the peak-to-peak or half-amplitude measurements prevalent in early studies of the buffet problem.

It is appropriate at this point to describe the philosophy of this report. The main body of this report serves to describe, in detail, the techniques used in obtaining the flight data, the instrumentation, the data reduction and data analysis procedures and discuss and interpret selected results which illustrate the major findings of the investigation. Included in the appendix are time histories of pertinent data items in plotted form.

The flight program from which data have been extracted for use in this study was primarily for F-111A flight loads demonstration. The test aircraft was therefore instrumented with numerous strain-gage sensors and accelerometers. Flight maneuvers included wind-up turns, pull-ups and roller coasters at various altitudes, Mach numbers, and target load factors. While it was not a particular goal of the flight program to investigate buffeting, many of the flight test conditions were such that significant levels of buffeting occurred. An opportunity thus existed to subject the extensive flight data to analyses specifically aimed at providing detailed buffeting response characteristics.

The basic approach used in the study is described in the following paragraphs.

The various records pertinent to the Flight Loads Demonstration program were surveyed to identify candidate flight points for the investigation. About 90 combinations of wing sweep, Mach number, altitude and target load factor were selected for initial investigation. Analog strip-chart playouts of thirty items of instrumentation were then made for each candidate flight point. The strip charts were used primarily to identify the particular flight maneuvers in which the wing responses were of sufficient magnitude to be meaningful in the study and to eliminate points

in which excessive wing spoiler activity might "contaminate" the response data.

Since the investigation was aimed at providing flight data for comparison with predictions an additional criterion in the selection of flight points for detailed analysis was the existence of corresponding wind tunnel data in terms of wing sweep and Mach number. The investigation finally was concentrated on seven flight maneuvers all of which were performed at one nominal wing sweep. Existing digital data for the selected flight points were then reviewed and plots were made of the variations of Mach number, angle of attack and load factor as functions of time during the particular maneuvers. Specific time intervals corresponding to nominal average angles of attack were selected for each maneuver and stochastic (statistical) analyses were performed on the outputs from seven accelerometers and twelve strain-gage sensors for each selected time interval.

The major effort in the stochastic analysis was devoted to obtaining power spectral density (PSD) plots as a function of frequency and root-mean-square (rms) values of the magnitudes of wing shear, bending moment, and torque at four wing span stations and accelerations at the wing tips, center of gravity and pilot's seat. These PSD and rms data are essential for correlation with prediction methods. In addition the PSD plots were used to

identify the frequencies and magnitudes of the major responses for each time interval. The particular vibration modes associated with the major responses were then identified insofar as possible from the results of extensive ground vibration tests performed at an earlier time on F-111A aircraft (References 18 and 19).

The variations of rms values of the various outputs (for specific ranges of frequencies) of instrumentation were plotted against angle of attack and comparisons made to observe trends with changes of altitude or Mach number.

SECTION 2

AIRCRAFT DESCRIPTION

The test aircraft was F-111A Number 13. A drawing showing the general features of the aircraft is presented as Figure 1. Detailed geometry associated with the aircraft and its components appears in Table 1. The aircraft has a variable sweep wing and a convention was adopted early in the development program that all aerodynamic coefficients would be referenced to geometric characteristics at a specific wing sweep, namely, Λ_{LE} = 16 degrees. The variations of some key geometric characteristics of the wing with wing leading-edge sweep angle are presented in Figure 2.

Although the aircraft is fitted with a high lift system consisting of multisegment leading-edge slats and multisegment double-slotted trailing-edge flaps, these devices were in their retracted positions for all maneuvers analyzed in this study.

Two-segment upper surface spoilers on each wing are used at low wing sweeps in addition to differentially controlled all-movable horizontal tails to achieve roll control.

The aircraft has a three-axis stability augmentation system which was operational on all maneuvers analyzed in this investigation.

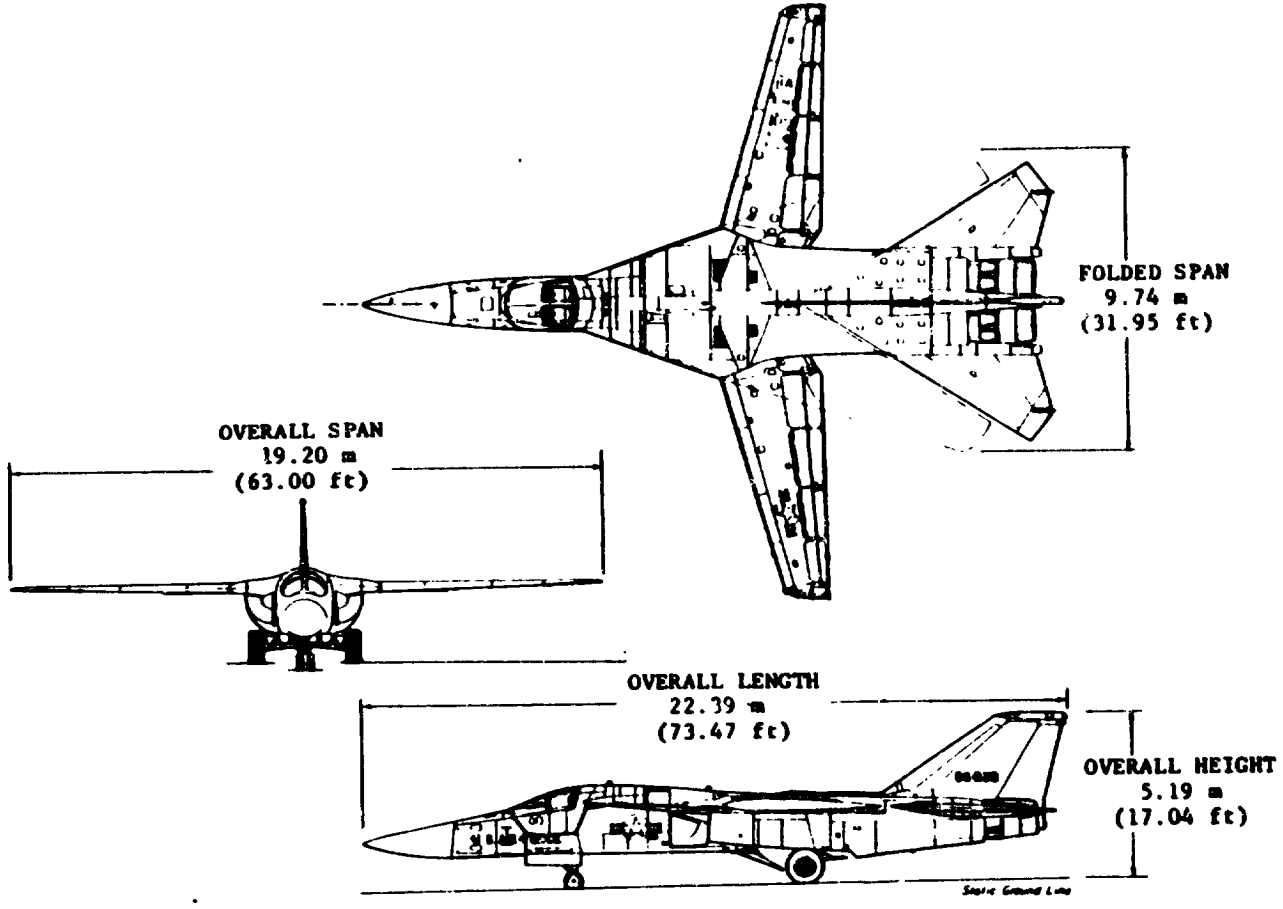

Figure 1. F-111A THREE-VIEW

Table 1

PHYSICAL CHARACTERISTICS OF THE
F-111A AIRPLANE (NUMBER 13)

Wing –	
Airfoil section, at pivot	NACA 64A210.7 (modified)*
Airfoil section, tip	NACA 64A209.8 (modified)*
Sweep, deg (leading edge)	16 to 71.5
Incidence, deg	1
Dihedral, deg	1
Span, area, mean aerodynamic chord	(See fig. 2)
Leading-edge slats	
Area (planform projected), $ft^2(m^2)$	60.7(5.64)
Span, percent of exposed wing-panel span	96.5
Deflection, maximum, deg	45
Trailing-edge flaps	
Type	Double Slotted Fowler
Area (aft of hinge line), $ft^2(m^2)$	117.8(10.94)
Span, percent of exposed wing panel span	
Deflection, maximum, deg	37.5
Spoilers:	
Area (planform projected), $ft^2(m^2)$	28 [illegible](2.66)
Span, ft(m)	11.8(3.6)
Deflection, maximum, deg	45
Wing pivot	
Distance from airplane nose, ft(m)	40.16(12.25)
Distance from airplane centerline, ft(m)	5.86(1.79)
Horizontal tail (all movable) –	
Airfoil section	BICONVEX
Incidence, deg	1
Dihedral, deg	-1
Sweep at leading edge, deg	57.5
Span, ft(m)	29.3(8.93)
Area (exposed), $ft^2(m^2)$	174.3(15.74)
Area (movable), $ft^2(m^2)$	154.2(13.92)
Aspect ratio	1.42
Mean aerodynamic chord (exposed), in. (cm)	137.5(349.3)
Deflection, maximum, deg:	
As elevators	
Trailing-edge up	(approx.) 25
Trailing-edge down	(approx.) 10
As ailerons (total)	(approx.) ±15
Surface stops	
Trailing-edge up	(approx.) 31
Trailing-edge down	(approx.) 16
Vertical tail –	
Airfoil section	BICONVEX
Sweep at leading edge, deg	55
Span, ft(m)	8.9(2.71)
Area, $ft^2(m^2)$	111.7(10.09)
Aspect ratio	1.42
Mean aerodynamic chord, in.(cm)	159.3(404.6)
Rudder	
Span, ft(m)	7.8(2.38)
Area, $ft^2(m^2)$	29.3(2.65)
Deflection, maximum, deg	±30
Speed brake –	
Area, $ft^2(m^2)$	26.5(2.39)
Deflection, maximum, deg	77
Ventrals –	
Area (total), $ft^2(m^2)$	25(2.26)
Power plants –	
P & W TF30-P-3 engines	2

* $\Lambda_{LE} = 16°$

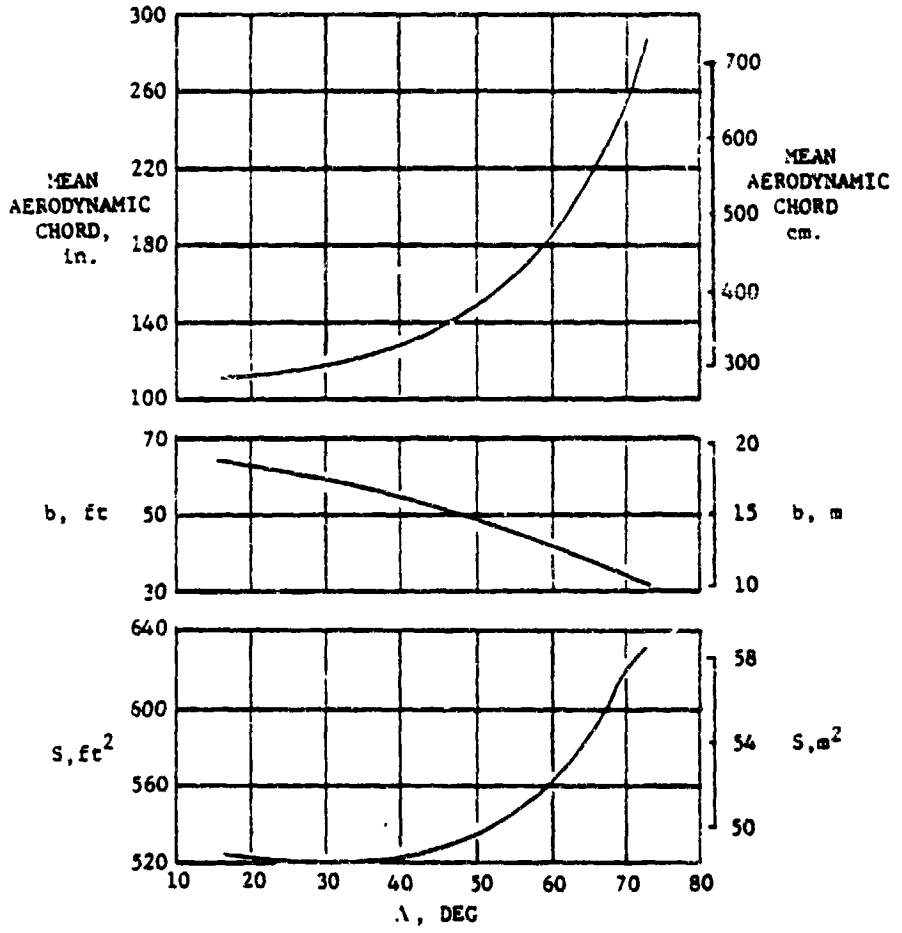

Figure 2 F-111A WING GEOMETRY AS A FUNCTION OF WING-SWEEP ANGLE

SECTION 3

AIRCRAFT INSTRUMENTATION

The instrumentation system installed in the aircraft consisted of two 30 track and one 14 track FM analog magnetic tape recorders and various transducers throughout the airplane. IRIG B time reference signals were recorded on each tape recorder to provide time correlation. The general locations of the accelerometers pertinent to the buffet study are shown in Figure 3. The actual locations in terms of aircraft geometry references are listed in Table 2.

The characteristics of the accelerometers most of which were commercially available units, are indicated in Table 3. The accuracies quoted refer to the nominal flat frequency response up to the limit frequency quoted. No calibration data exist above the quoted limit of flat frequency response, however, the natural resonant frequencies are well beyond 100 hertz for all of the accelerometers. There is no reason to suspect a significant deviation from the basic calibration factors quoted for frequencies up to 100 hertz.

The locations of the strain gage sensors pertinent to the

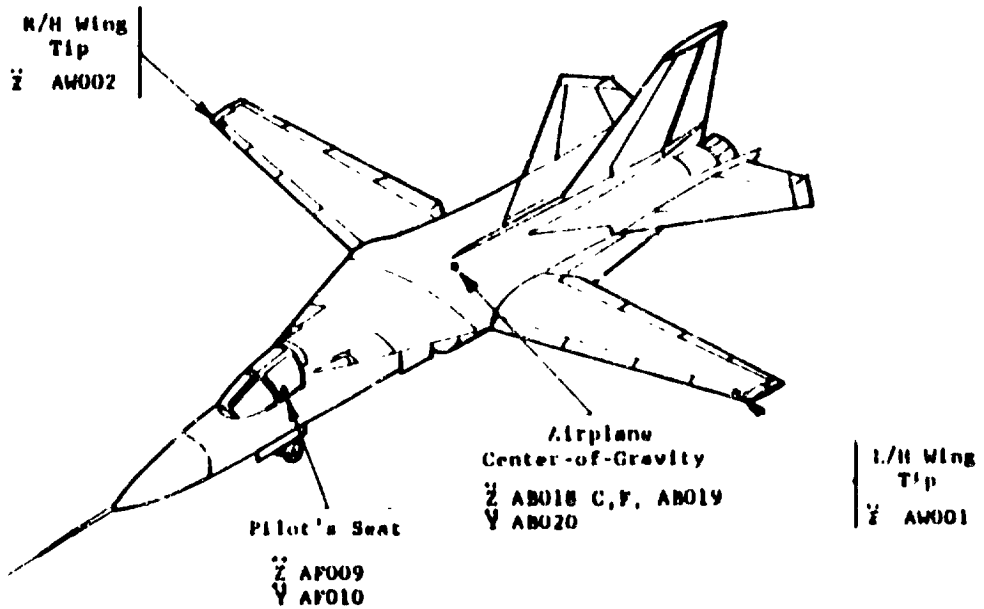

Figure 3. ACCELERATION MEASUREMENTS

Table 2

ACCELEROMETER LOCATIONS

ITEM CODE	MEASUREMENT	LOCATION					
		FUSELAGE STATION		WATERLINE		BUTT LINE	
		METERS	INCHES	METERS	INCHES	METERS	INCHES
AB018	c g vertical	12.996	(511 64)	4.740	(186.62)	0	0
AB019	c.g. vertical	12.996	(511 64)	4.740	(186 62)	0	0
AB020	c.g. lateral	12.996	(511.64)	4.740	(186 62)	-.023	(- .8')
AF009	Pilot seat vertical	6 462±.127	(254 40±5.0)	4.245±.127	(167.12±5 0)	-.133	(-5.25)
AF010	Pilot seat lateral	6 462±.127	(254 40±5.0)	4.245±.127	(167.12±5.0)	- 133	(-5.25)
AW001	Left wing tip - vertical	Front spar station 9 500 meters (374 inches)					
AW002	Right wing tip - vertical	Wing span station 9.157 meters (360.5 inches) @ Λ_{LE} = 16°					

Table 3

ACCELEROMETER CHARACTERISTICS

ITEM CODE	MEASUREMENT	NOMINAL FULL SCALE RANGE*	SPECIFIED ACCURACY % FULL SCALE**	SPECIFIED FLAT FREQUENCY RESPONSE TO HZ.	RESONANTS NAT. FREQ HZ	FLIGHTS
AB018	C.G. Vertical	-3.5 to +6 5	±5	25	Not Available	48, 60
AB018	C.G. Vertical	±15	±3	42	530	70, 77, 78, 79
AB019	C.G. Vertical	±10	±5	325	--	ALL
AB020	C.G. Lateral	±7.5	±5	275	--	ALL
AF009	Pilot Seat Vertical	±10	±3	32	400	ALL
AF010	Pilot Seat Lateral	±7.5	±5	275	--	ALL
AW001	Left Wing Tip Vertical	±25	±5	500	--	ALL
AW002	Right Wing Tip Vertical	±25	±5	500	--	ALL

*The actual range calibrated varied from these nominal values.
**Over range of flat frequency response and at all temperatures between -70° and +250°F

buffet study are shown in Figure 4. Shear, bending moment and torque were measured at each of the four indicated wing stations on the right wing. The sensitivities of these measurements were governed by the fact that the wing loads were to be measured during maneuvers at load factors up to the maximum capability of the aircraft. As a consequence the signal-to-noise ratios for the present buffet studies were lower than is desirable. The calibration slopes for each channel of information are shown in Table 4.

In several cases the frequency response upper limit for the measurements was set by the subchannel characteristics of the flight recording system. Table 5 lists the appropriate nominal limit of frequency response for each item of instrumentation based on the recorder subchannel arrangements for each flight selected for detailed analysis.

Correlating items such as angle of attack, airspeed, Mach number, altitude, gross weight, and control surface position indication of the spoilers and horizontal tail surface deflections were also recorded on the FM tapes.

A special test nose boom was fitted to the aircraft to obtain angle of attack, sideslip angle, altitude and Mach number data.

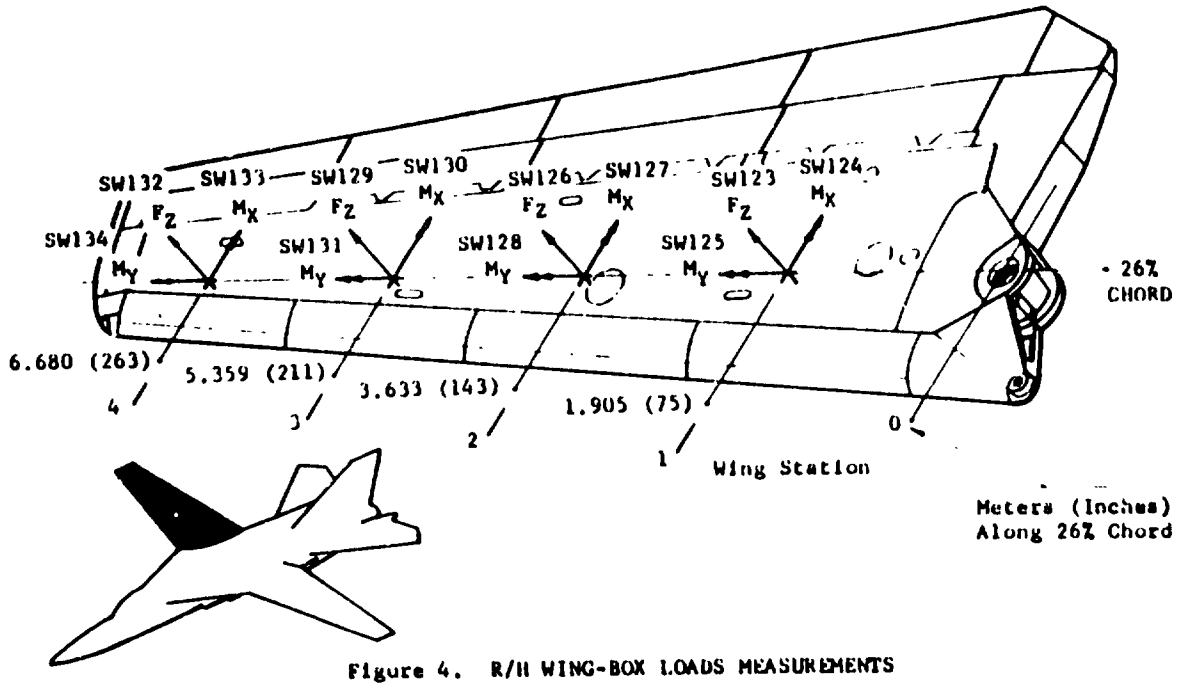

Figure 4. R/H WING-BOX LOADS MEASUREMENTS

TABLE 4

CALIBRATION SLOPES – UNITS/PERCENT OF BANDWIDTH

ITEM	MEASUREMENT	S.I. UNITS	U.S. CUST. UNITS	FLT 48 S.I.	FLT 48 CUST.	FLT 60 S.I.	FLT 60 CUST.	FLT 76 S.I.	FLT 76 CUST.	FLTS 77, 78 S.I.	FLTS 77, 78 CUST.	FLT 79 S.I.	FLT 79 CUST.
AW001	LWT-Vert.	g's	g's		50304		.50304		.33578		.33578		33578
AW002	RWT-Vert.	g's	g's		.50232		50232		33322		.33322		33322
AB018C	CG-Vert.	g's	g's		.130		.130		.10690		.10313		18339
AB018F	CG-Vert.	g's	g's		.010		.010		---		---		---
AB019	CG-Vert.	g's	g's		.20142		.20142		.20172		.20172		20172
AB020	CG-Vert.	g's	g's		.05129		.05129		.05052		.05052		.05052
AF009	P.S.-Vert.	g's	g's		.15306		.15306		.29280		.29280		.29280
AF010	P.S.-Lat	g's	g's		.10232		.10232		.10128		.10128		.10128
AB015	Ang. Roll	rad/sec^2	rad/sec^2		.53569		.53569		.3012		.3012		.3012
AB016	Ang. Pitch	rad/sec^2	rad/sec^2		.32175		.32175		.0998		.0998		.0998
SW123	Shear-W.S.1	N	lbs	8011	1801	8011	1801	11770	2464	11770	2464	11926	2681
SW124	B.M.-W.S.1	m-N	in-lbs	22517	202896	22517	202896	37110	334383	37110	334383	37393	336937
SW125	TOR.-W.S.1	m-N	in-lbs	4136	37264	4136	37264	3913	35263	3913	35263	3969	35767
SW126	Shear-W.S.2	N	lbs	5124	1152	5124	1152	9475	2130	9475	2130	9608	2160
SW127	B.M.-W.S.2	m-N	in-lbs	9981	89935	9981	89935	9828	88557	9828	88557	9897	89181
SW128	TOR.-W.S.2	m-N	in-lbs	1251	11268	2501	22535	2798	25215	2798	25215	2834	25539
SW129	Shear-W.S.3	N	lbs	2358	530	2358	530	3479	782	3479	782	3523	792
SW130	B.M.-W.S.3	m-N	in-lbs	2800	25228	2800	25228	4160	37481	4160	37481	4197	37821
SW131	TOR.-W.S.3	m-N	in-lbs	1008	9084	1008	9804	964	8690	964	8690	982	8847
SW132	Shear-W.S.4	N	lbs	801	180	801	180	1561	351	1561	351	1588	357
SW133	B.M.-W.S.4	m-N	in-lbs	393	3541	393	3541	758	6835	758	6835	765	6896
SW134	TOR.-W.S.4	m-N	in-lbs	188	1694	188	1694	344	3100	344	3100	349	3147
DH001C	α	deg	deg		.875		.875		.875		.875		875
DH001F	α	deg	deg		.080		.080		.080		.080		.080
DH002F	β	deg	deg		080		.080		.080		.080		.080
DW001	L Inbd Spoil	deg	deg		.60		.60		.60		.60		60
DW002	R Inbd Spoil	deg	deg		.60		.60		.60		.60		.60
DW003	L Outb Spoil	deg	deg		.60		.60		.60		.60		.60
DW001	R Outb Spoil	deg	deg		.60		.60		.60		60		.60
DT003C	L Hor T.	deg	deg		.88		.88		.88		.88		88
DT004C	R Hor T.	deg	deg		.88		.88		.88		.88		.88
PD016F	Mach	---	---		.0034		.0034		.0034		.0034		.0034
PD004F	Alt	m	Ft	15.24	50	15.24	50	---	---		---		---
PH022F	Alt	m	Ft	---	---	---	---	12.192	40	12.192	40	12.192	40

Table 5

FLIGHT RECORDER FREQUENCY RESPONSE CHARACTERISTICS

ITEM CODE	FLIGHTS 48, 60		FLIGHTS 70, 77, 78, 79	
	IRIG CHANNEL	FILTER FREQ. - HZ	IRIG CHANNEL	FILTER FREQ. - HZ
AW001	8	45	11	110
AW002	12	160	12	160
AB018	14	330	11	110
AB019	9	60	8	45
AB020	14	330	9	60
AF009	11	110	12	160
AF010	12	160	10	80
SW123	10	80	7	35
SW124	11	110	8	45
SW125	12	160	9	60
SW126	13	220	10	80
SW127	8	45	11	110
SW128	9	60	12	160
SW129	10	80	13	220
SW130	11	110	6	25
SW131	12	160	7	35
SW132	13	220	8	45
SW133	8	45	9	60
SW134	9	60	10	80

SECTION 4

BASIC DATA PROCESSING METHODS

During the Loads Demonstration Flight Program, the FM analog magnetic tapes containing raw flight test data were processed by automated techniques. The real time data were first displayed on strip chart recorders for instrumentation verification. Next, the data were digitized at sample rates of 1 to 20 samples per second under computer control. The specific sample ratio depended on user group requirements. The digitized data were then scaled, calibrated and output in computer listings and computer tapes for additional processing on an IBM System/360. Second generation computer runs were made to obtain corrected flight condition data such as gross weight, Mach number, altitude, dynamic pressure and fuel distribution at 1-second intervals.

Microfilm records of the computer listings from the original flight program data reduction were used in the present program to make plots of angle of attack, normal load factor, Mach number and dynamic pressure as functions of flight time and to identify the gross weights and altitudes for the selected flight maneuvers. The Mach number, altitude and dynamic pressure data include corrections for position error. The angles of attack are indicated angles and do not include the effect of upwash at the nose boom.

The following formula can be used to obtain an estimate of the true geometric angle of attack values if desired:

$$\alpha_T = 0.318 + 0.931\,\alpha \text{(degrees)}$$

This correction was not applied to the data presented in this report because the magnitude is not large in the range of angles of attack covered by the flight data and is within the uncertainty of the flight measurements taken under buffeting conditions with an aeroelastic aircraft.

Time histories were made of about 30 items of instrumentation which were considered pertinent to the buffet study. Examples of each of the strip chart records are presented in Figure 5. Additional time histories for the selected flight maneuvers are contained in the appendix. The particular groupings of items on the strip charts permit assessment of the time phasing of the build-up of the wing responses to buffet as angle of attack increases during the maneuver. The chart speed was nominally 20 mm/sec and the frequency response limit of the pen recorders is about 50 hertz. For correlation purposes, a time reference trace with pen deflections each second appears in the lower border of the strip chart. The flight times associated with the particular maneuvers are annotated below the time trace.

The Mach number, altitude and angle of attack traces represent uncorrected indicated values. Occasionally these items show finite jumps from one bound of the record to the other.

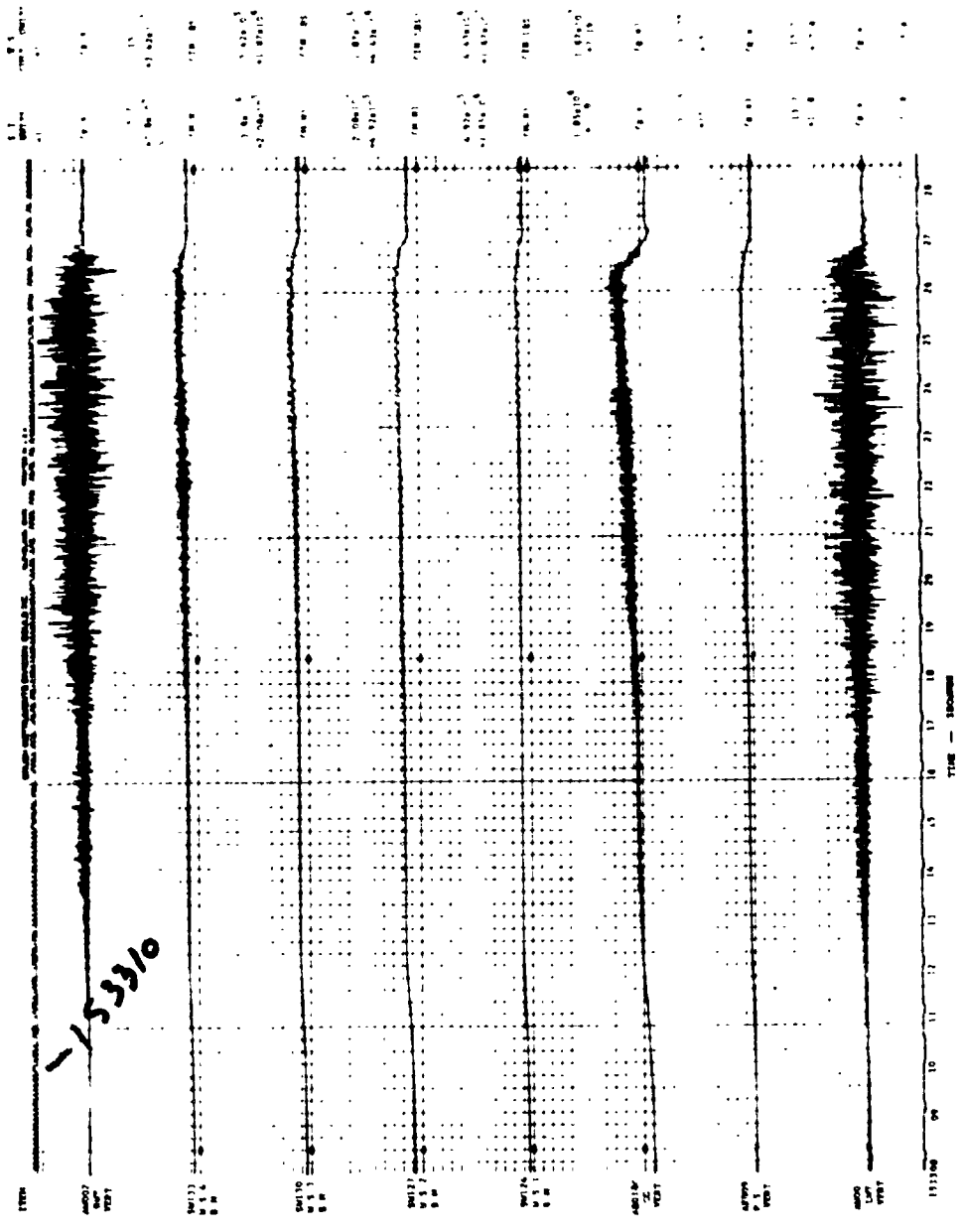

(a)

Figure 5. TIME HISTORIES OF INSTRUMENTATION OUTPUT FOR WINDUP TURN FLIGHT 77, RUN S&C-R

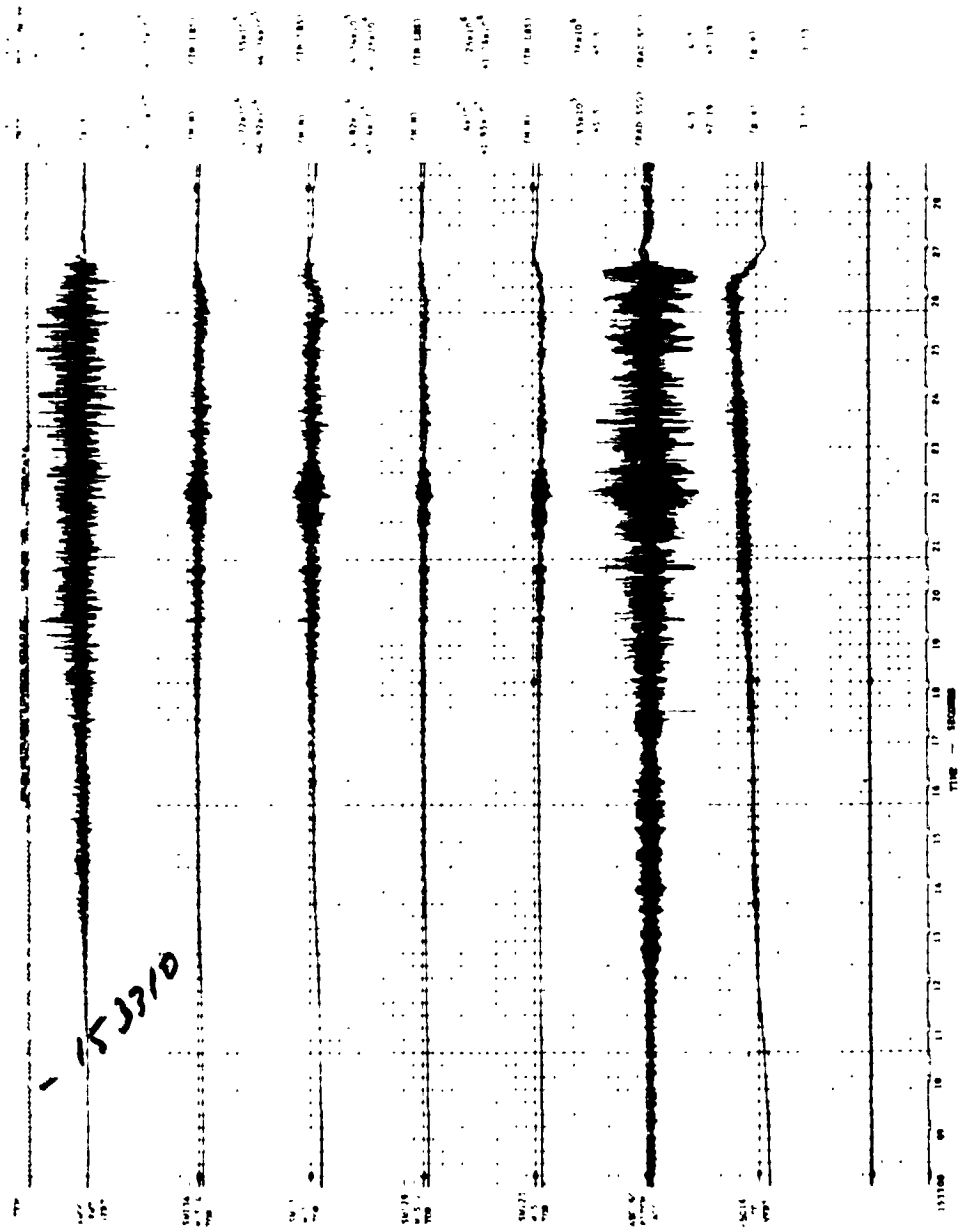

(b)

Figure 5. Continued

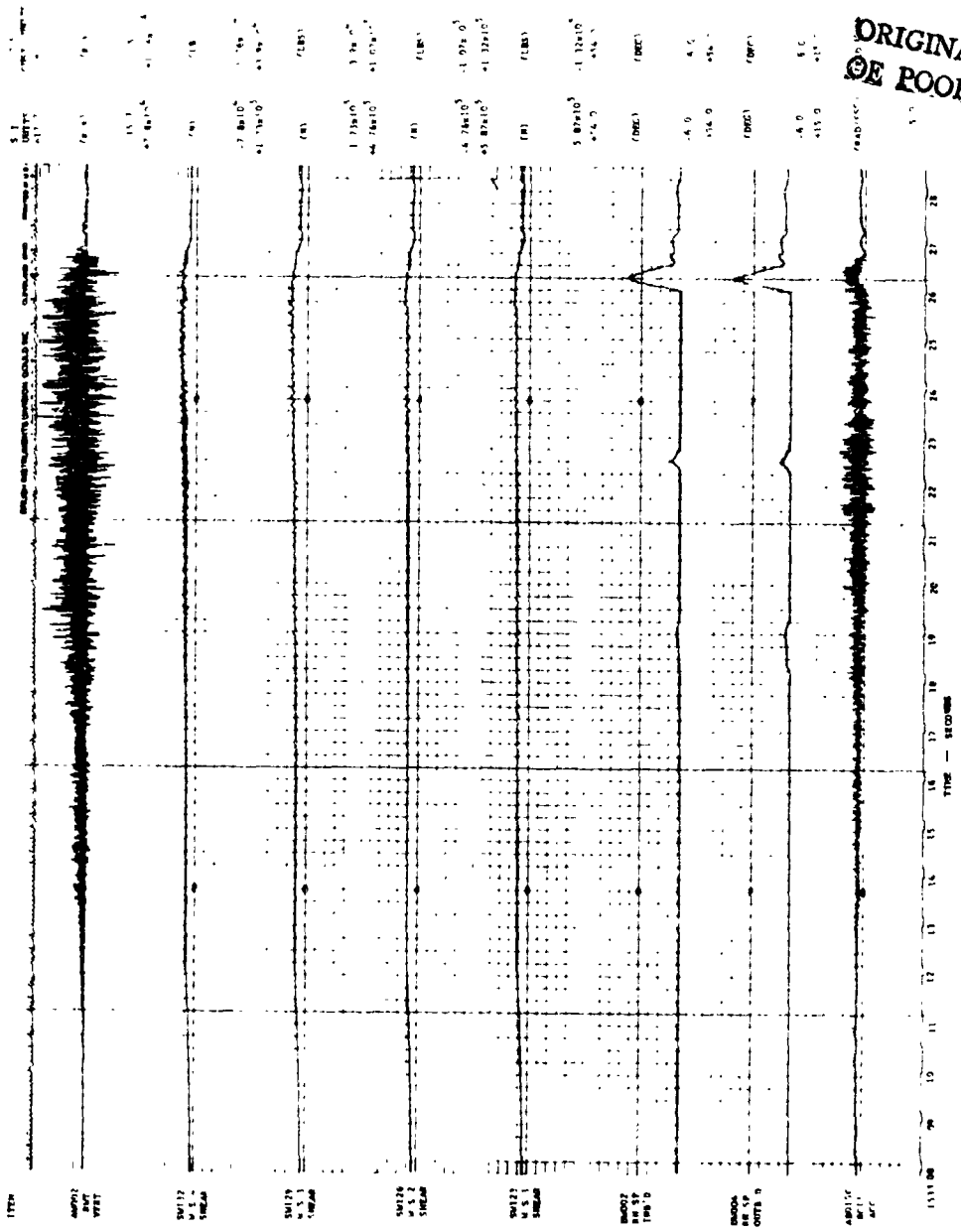

(c)

Figure 5. Continued

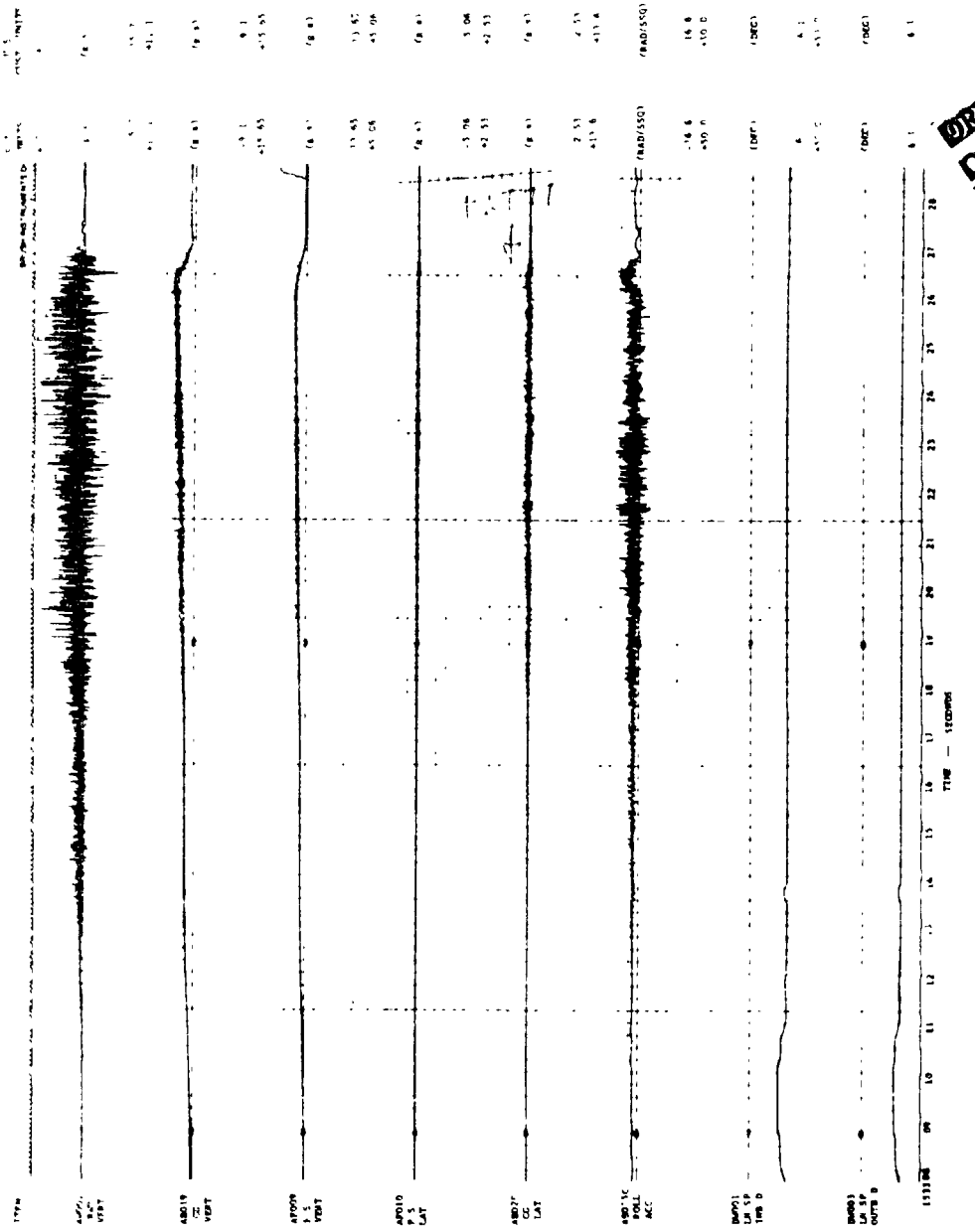

(d)

Figure 5. Continued

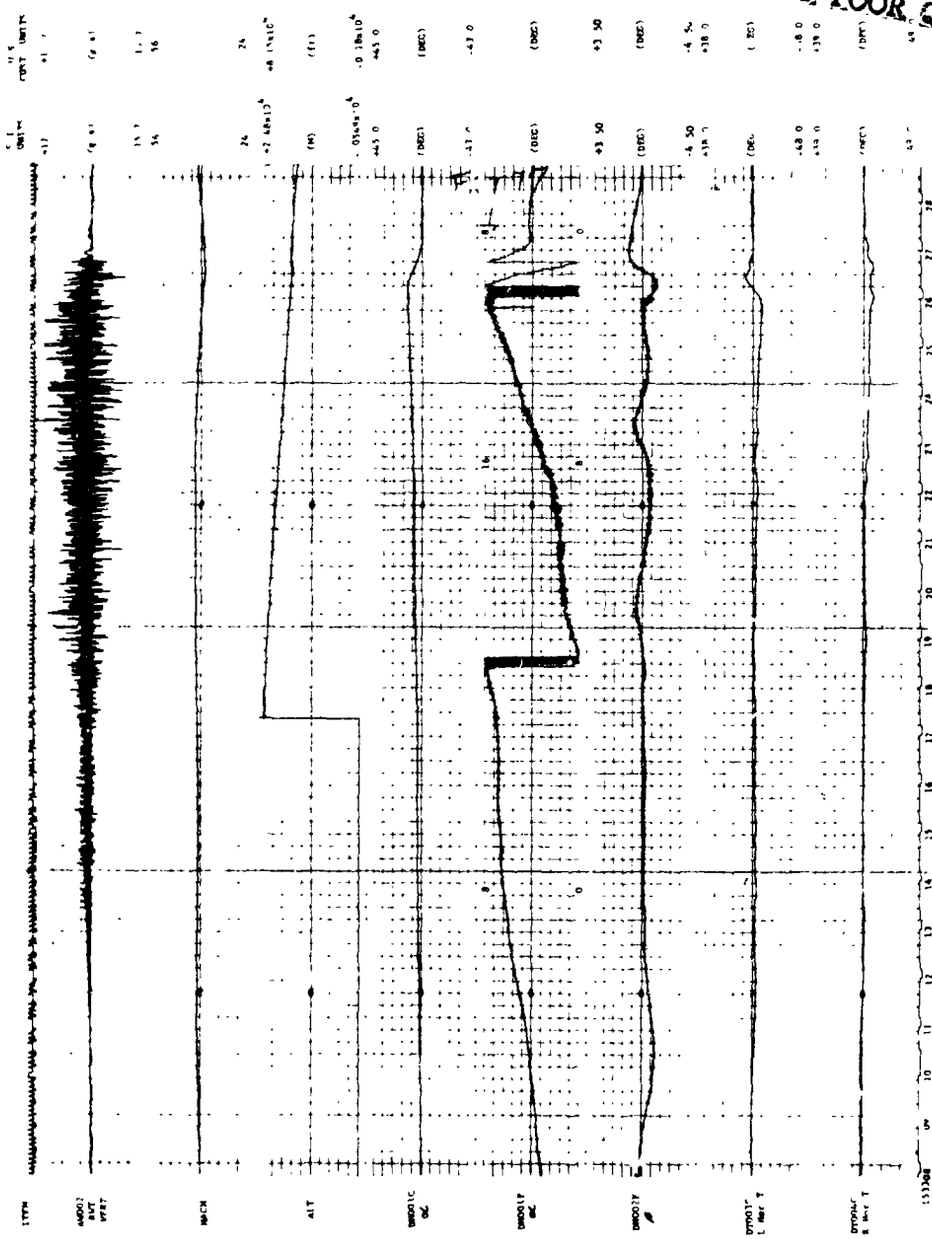

(e)

Figure 5. Concluded

This situation occurs because the calibration is a multi-stepped function and the measurements cross the boundaries of one or more ranges of values.

SECTION 5

FLIGHT CONDITIONS SELECTED FOR DETAILED ANALYSIS

The time histories for the 90 candidate flight maneuvers were studied thoroughly to determine which maneuvers might provide a set of flight buffet data that would serve as a good test of a prediction method. Five basic criteria were used in the selection process:

First, the wing responses should be large enough to make a detailed analysis meaningful.

Second, the nominal flight conditions should closely approximate Mach number and angle of attack conditions which had already been obtained in a wind tunnel test program.

Third, effects of Mach number (flow field) and altitude (aeroelasticity) should be included, if possible.

Fourth, the selected maneuvers should be free from effects of spoiler deflection, if possible.

Fifth, one of the selected points should closely approximate a flight point that had already been obtained in a NASA/FRC flight test program which used F-111A Number 6 (Reference 5).

The seven maneuvers selected for detailed analysis are listed in Table 6. They consist of two wind-up turns, four pull ups and one roller coaster, all performed at a nominal wing sweep of 26 degrees. The Mach numbers are approximately 0.70, 0.80, and 0.87 for the three high altitude maneuvers (above 6000 meters). At the two higher Mach numbers the selected maneuvers are for three altitudes, nominally 1500, 3700 and above 6000 meters. The gross weights range from 266,000 N to 330,500 N.

Variations of angle of attack, load factor, Mach number and dynamic pressure with flight time are presented in Figure 6 for each of the selected maneuvers. Inspection of Figures 6(a) through 6(g) shows that the wind-up turns are gradual maneuvers whereas the pull ups and roller coaster are rather abrupt maneuvers. As a consequence, it was feasible to select more points within each of the wind-up turns for stochastic analysis than for the other maneuvers.

Table 7 lists the segments of each maneuver selected for detailed analysis. In most cases the time duration of the records is one second, but some longer records were used particularly for the wind-up turn of Flight 77, S&C-R. The table also lists the indicated angle of attack at the start of each record (α_1), at the end of each record (α_2) and in a few cases the maximum indicated angle of attack (α_{max}) occurring during the record.

Table 6

SELECTED FLIGHT MANEUVERS

FLT	RUN	MANEUVER	WING SWEEP DEG	NOMINAL FLIGHT CONDITIONS		
				MACH	ALTITUDE	GROSS WEIGHT
48	6	Windup Turn	26.6	.70	7,559 m (24,800 ft)	294,472 N (66,200 lb)
77	S&C-R	Windup Turn	25.6	.80	6,035 m (19,800 ft)	266,004 N (59,800 lb)
78	5	Pullup	26.2	.80	3,780 m (12,400 ft)	327,389 N (73,600 lb)
79	9R	Pullup	26.7	.80	1,494 m (4,900 ft)	323,386 N (72,700 lb)
60	10	Roller Coaster	26.6	.87	8,382 m (27,500 ft)	307,817 N (69,200 lb)
78	4	Pullup	26.3	.87	3,688 m (12,100 ft)	330,503 N (74,300 lb)
70	2	Pullup	26.8	.86	1,494 m (4,900 ft)	328,800 N (73,800 lb)

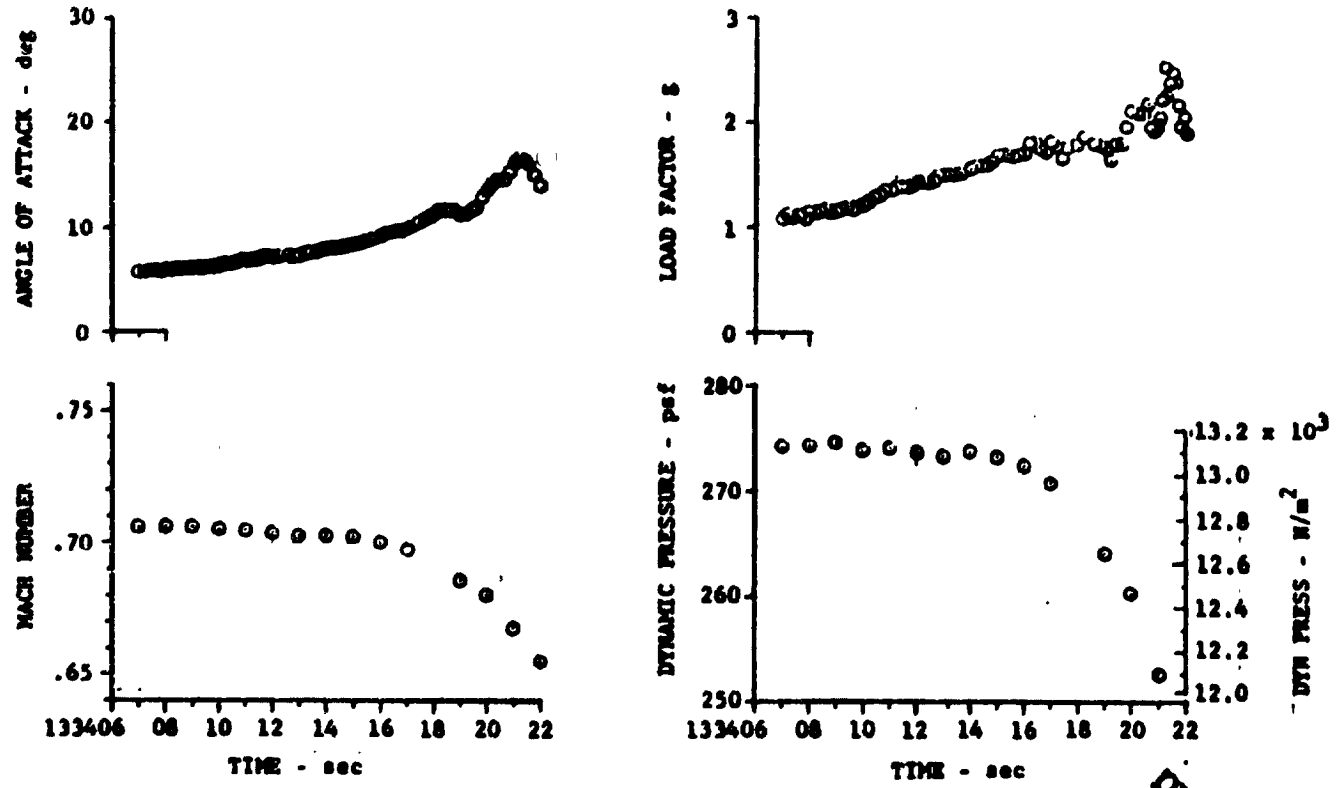

(a) FLIGHT 48, RUN 6, WINDUP TURN

Figure 6. FLIGHT CONDITIONS FOR SELECTED MANEUVERS

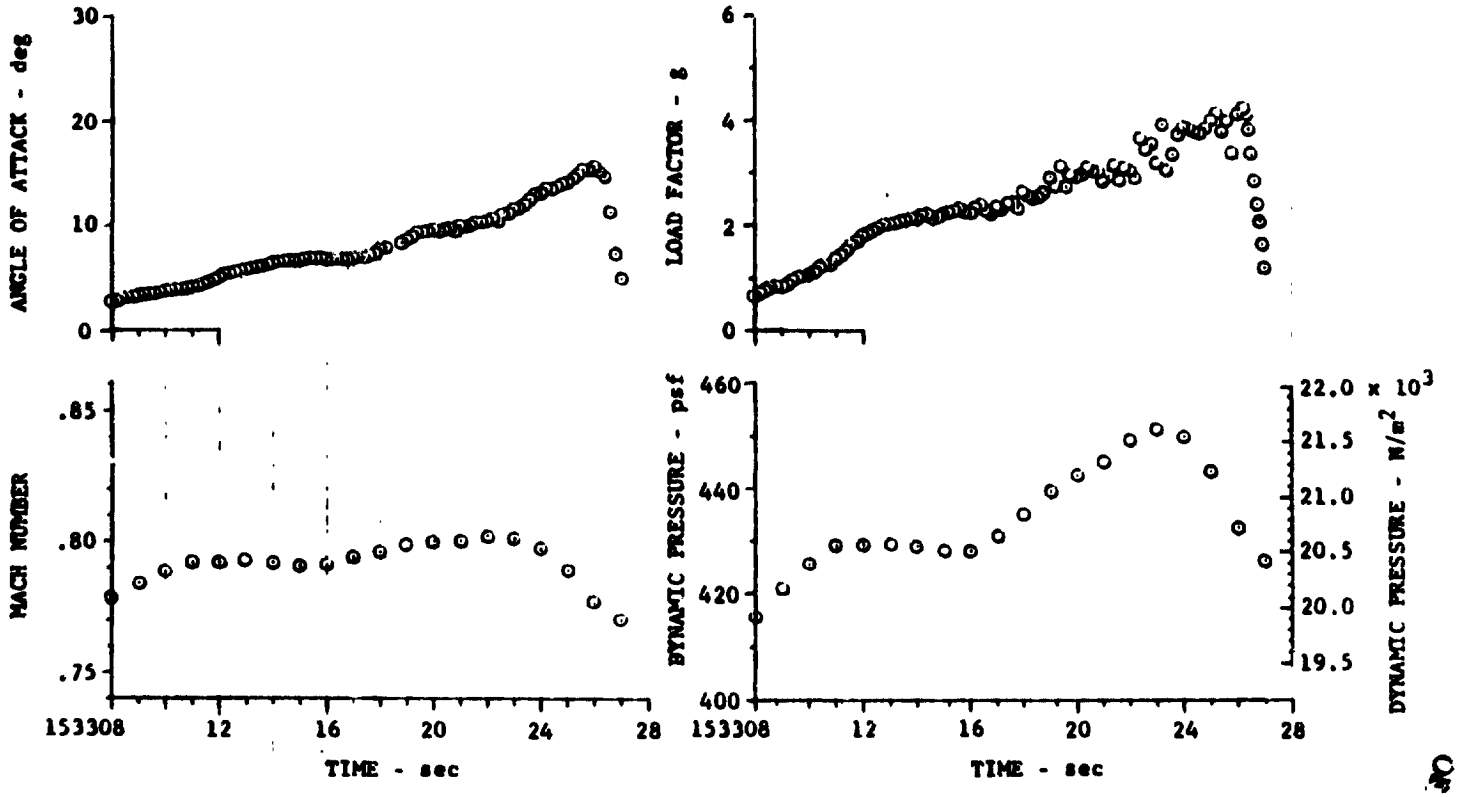

(b) FLIGHT 77, RUN S&C-R, WINDUP TURN

Figure 6. Continued

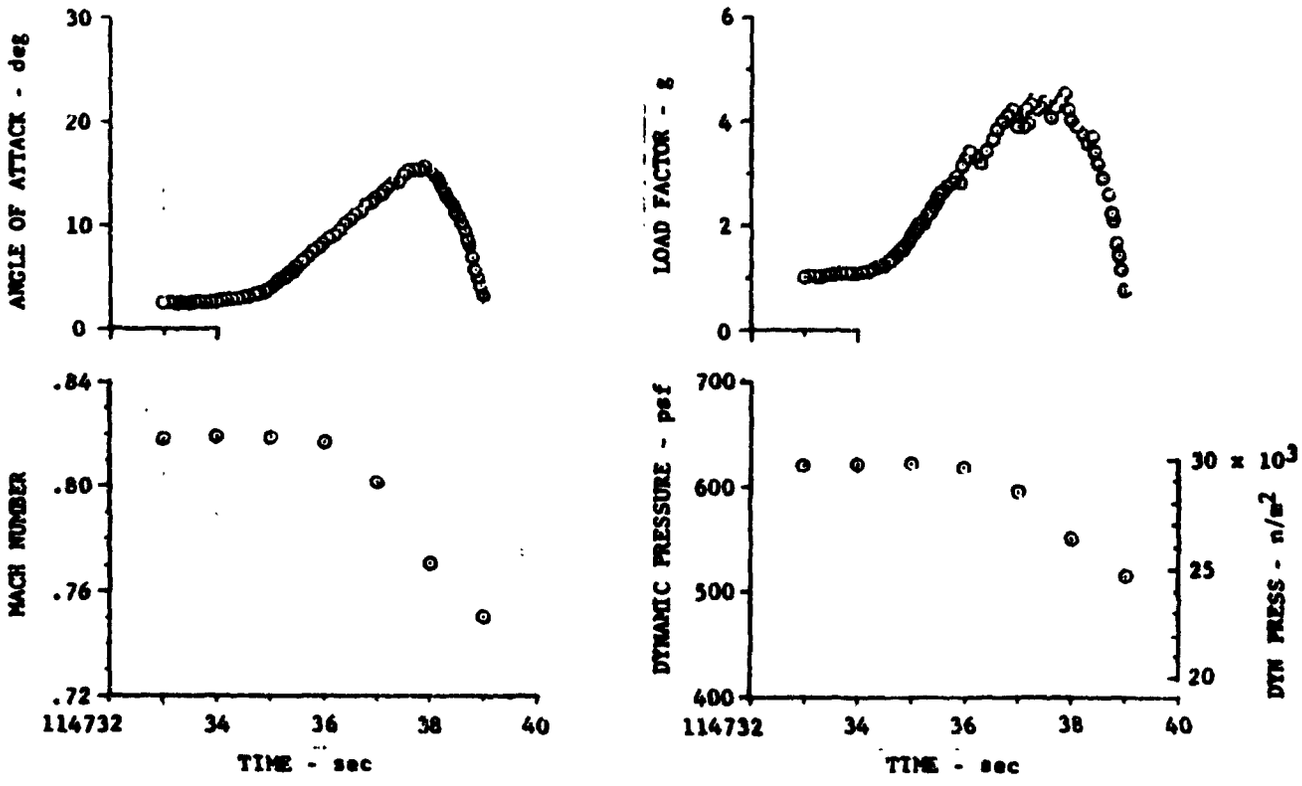

(c) FLIGHT 78, RUN 5, PULLUP

Figure 6. Continued

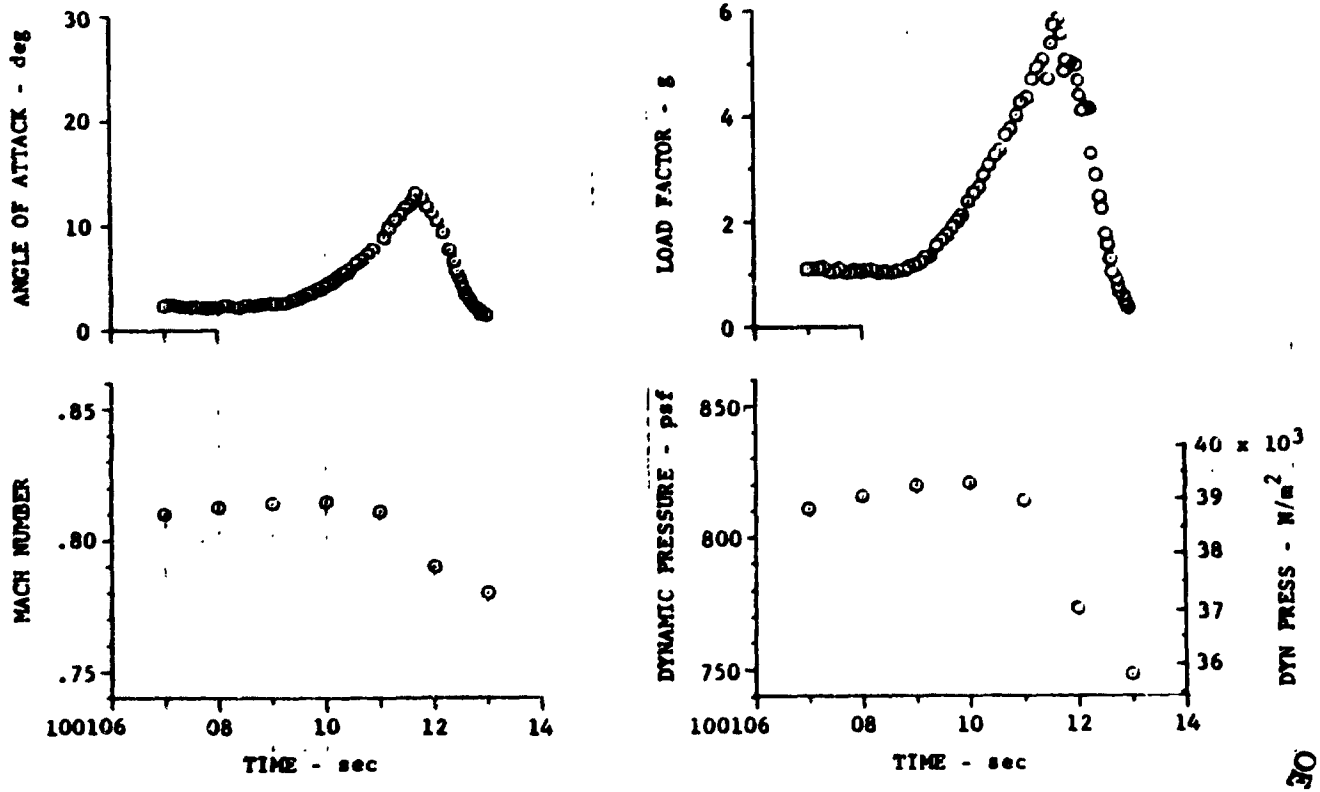

(d) FLIGHT 79, RUN 9R, PULLUP

Figure 6. Continued

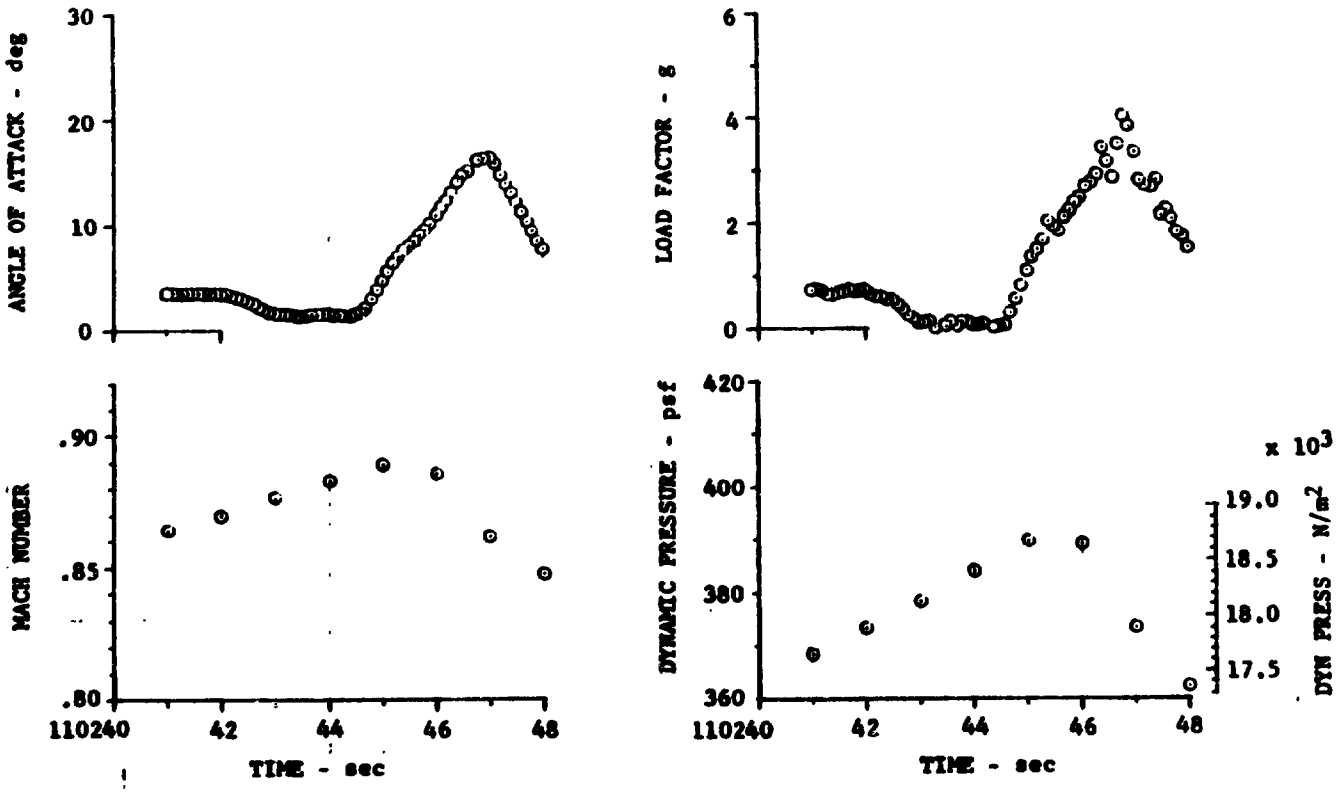

(e) FLIGHT 60, RUN 10, ROLLER COASTER

Figure 6. Continued

(f) FLIGHT 78, RUN 4, PULLUP

Figure 6. Continued

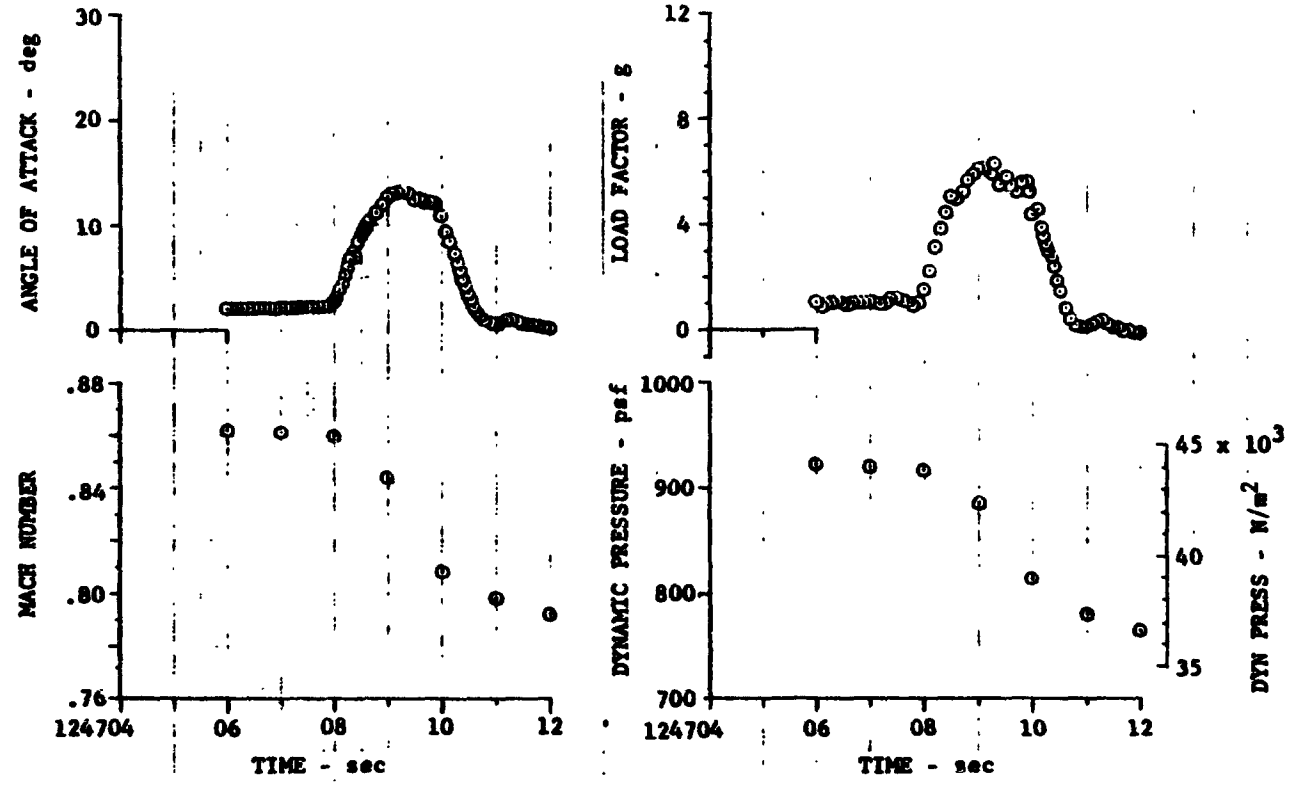

(g) FLIGHT 70, RUN 2, PULLUP

Figure 6. Concluded

TABLE 7

FLIGHT POINTS SELECTED FOR STOCHASTIC ANALYSIS

FLT	RUN	POINT	START TIME T_1	STOP TIME T_2	ΔT (SEC)	α_1 (DEG)	α_2 (DEG)	α_{MAX} (DEG)	α_{NOM} (DEG)	$\Delta\alpha$ (DEG)
48	6	1	133412.5	133413.5	1	7.25	7.62		7.4	0.37
		2	133414.0	133415.0	1	7.82	8.40		8.1	0.58
		3	133415.0	133416.0	1	8.72	9.55		9.1	0.83
		4	133416.7	133417.7	1	9.70	10.75		10.2	1.05
		5	133417.3	133418.3	1	10.30	11.75		11.1	1.45
		6	133419.0	133420.0	1	11.15	13.55		12.3	2.40
		7	133420.3	133421.3	1	14.25	16.60		15.3	2.35
		8	133420.0	133422.0	2	13.55	13.70	16.60	15.1	3.05

TABLE 7 CONTINUED

FLT	RUN	POINT	START TIME T_1	STOP TIME T_2	ΔT (SEC)	α_1 (DEG)	α_2 (DEG)	α_{MAX} (DEG)	α_{NOM} (DEG)	$\Delta\alpha$ (DEG)
77	S&C-R	1	153310.0	153311.0	1	3.72	4.22		4.0	0.50
		2	153311.5	153312.5	1	4.70	5.62		5.1	0.92
		3	153316.0	153317.0	1	6.90	7.08		7.0	0.18
		4	153319.0	153320.0	1	8.75	9.65		9.2	0.90
		5	153322.85	153323.85	1	11.45	13.00		12.2	1.55
		6	153325.3	153326.3	1	14.60	15.35	15.55	15.2	0.95
		7	153311.0	153313.0	2	4.22	5.98		5.1	1.76
		8	153315.5	153317.5	2	7.60	7.22		7.1	0.32
		9	153318.5	153320.5	2	8.45	9.65		9.2	1.24
		10	153322.35	153324.35	2	10.85	13.40		12.2	2.55
		11	153324.35	153326.35	2	13.40	15.35	15.55	14.8	2.15
		12	153323.0	153326.0	3	11.65	15.55		13.6	3.88

TABLE 7 CONTINUED

FLT	RUN	POINT	START TIME T_1	STOP TIME T_2	ΔT (SEC)	α_1 (DEG)	α_2 (DEG)	α_{MAX} (DEG)	α_{NOM} (DEG)	$\Delta\alpha$ (DEG)
78	5	1	114732.0	114733.0	1	2.60	2.60		2.60	$\pm$.05
		2	114734.8	114735.8	1	3.60	7.40		5.1	3.80
		3	114735.7	114736.7	1	7.00	11.20		9.2	4.20
		4	114736.4	114737.4	1	10.10	14.40		12.2	4.30
		5	114737.2	114738.2	1	13.35	14.00	15.40	14.6	2.05
79	9R	1	100109.4	100110.4	1	2.95	5.50		4.1	2.55
		2	100110.3	100111.3	1	5.12	10.50		7.1	5.38
		3	100110.6	100111.6	1	6.30	12.10		9.2	5.80
		4	100111.15	100112.15	1	9.30	9.95	12.60	10.8	3.30

TABLE 7 CONCLUDED

FLT	RUN	POINT	START TIME T_1	STOP TIME T_2	ΔT (SEC)	α_1 (DEG)	α_2 (DEG)	α_{MAX} (DEG)	α_{NOM} (DEG)	$\Delta\alpha$ (DEG)
60	10	1	110241.0	110242.0	1	3.50	3.45		3.5	$\pm$.05
		2	110244.65	110245.65	1	2.10	8.70		5.15	6.60
		3	110245.2	110246.2	1	6.35	12.30		9.3	5.95
		4	110245.7	110246.7	1	9.07	15.60		12.3	6.53
		5	110246.15	110247.15	1	12.60	15.20	16.30	14.8	4.30
78	4	1	114454.0	114455.0	1	3.35	3.30		3.3	$\pm$.05
		2	114455.6	114456.85	1	4.35	8.35		6.35	4.00
		3	114456.55	114457.55	1	6.95	11.90		9.40	4.95
		4	114457.05	114458.05	1	9.10	14.55		12.0	5.45
		5	114457.65	114458.65	1	12.45	16.65		14.6	4.20
		6	114457.4	114459.4	2	11.05	11.20	16.65	13.6	3.55
70	2	1	124705.7	124707.7	2	2.10	2.10		2.10	$\pm$.05
		2	124708.5	124709.5	1	9.05	12.60	13.25	12.3	4.20
		3	124708.9	124709.9	1	11.95	12.05	13.25	12.5	1.30

Also presented is the increment in angle of attack during the record ($\Delta\alpha$) which is relatively large for the pullup and roller coaster maneuvers. A nominal angle of attack (α_{nom}) has been assigned to each segment which is used later to plot trends in the variations of instrument responses with angle of attack.

An adjunct to the point selection process was the determination of the buffet onset characteristics for each of the maneuvers from the time histories. The criterion used for buffet onset was the first detectable change in level of response from any of the wing instrumentation which was followed by an ever increasing level of response. The results of the buffet onset determinations are presented in Figure 7. It was possible to obtain buffet onset points for six of the seven maneuvers. The aircraft was slightly into buffet even at 1-g trim conditions for Flight 78, Run 4. Figure 7(a) shows that the variation of angle of attack for buffet onset with Mach number is smooth despite the significant differences in dynamic pressure and pitch rates for the various maneuvers. Figure 7(b) shows that the normal force coefficients for buffet onset show a slight trend of increasing with a decrease in altitude (increase in dynamic pressure). This result is likely due to the fact that less horizontal tail deflection is required to produce the maneuvers and the loss in lift due to tail deflection is then smaller at the lower altitudes.

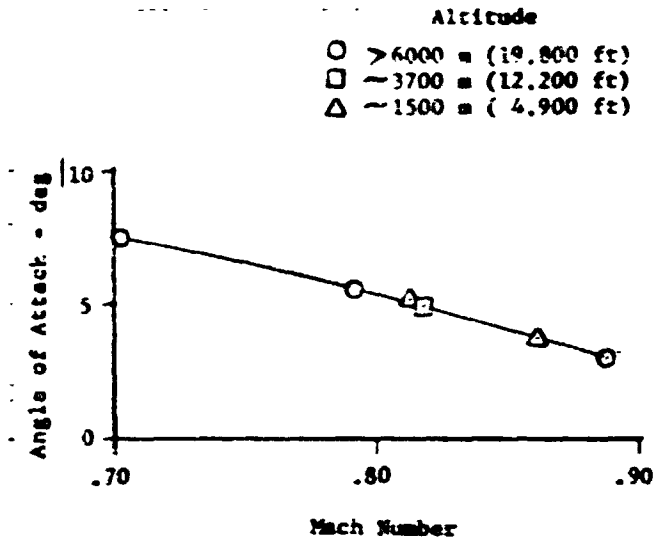

(a) ANGLE OF ATTACK

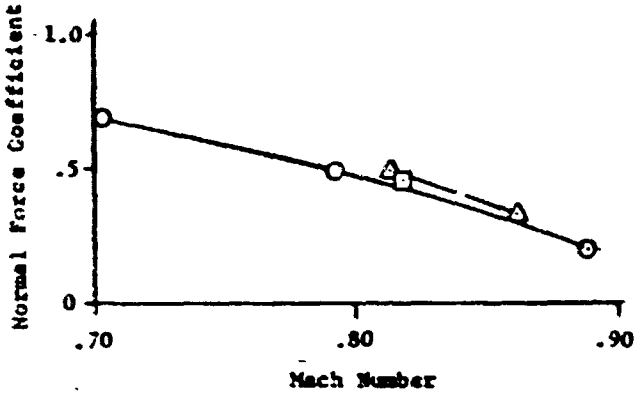

(b) NORMAL FORCE COEFFICIENT

Figure 7. ANGLE OF ATTACK AND NORMAL FORCE COEFFICIENT FOR BUFFET ONSET

SECTION 6

STOCHASTIC ANALYSIS TECHNIQUES

The analysis techniques used in this study are compatible with American National Standard (ANS S2.10-1971) recommended methods for analysis and presentation of shock and vibration data. A quick-look examination was performed on each time-history measurement to determine the data classification, degree of stationarity, record length, and recoverability.

Measurements

Data reduction was performed on the following data:

1. Shear, bending moment, and torsion at four wing stations (12 measurements).
2. Two wing-tip accelerometers (vertical)
3. Two C.G. vertical and one C.G. lateral accelerometers.
4. Pilot seat vertical and lateral accelerometers.

The analysis performed on these items consisted of PSD (including an average rms value), cross-PSD, and Probability Density and was distributed as follows:

PSD (all items)	779 plots
Cross-PSD (AW001 and AW002)	7 photographs
Probability Density	126 photographs

In addition to the plots and photographs, a digital magnetic tape recording was made of spectral coefficients of all PSD's and Cross-PSD's. The magnetic tape format (shown in Fig. 8) for a single PSD consists of two adjacent records; the first record for identification and the second for raw data.

Special-Purpose Processing

A block diagram of the special-purpose stochastic equipment is shown in Fig. 9. The FM signal is discriminated to recover the analog signal. Band-pass filters at 3 Hz and 100 Hz (48 dB per octave) were used to reject unwanted frequencies and to minimize aliasing effects on the sampled data. The data is calibrated at this point and converted to non-dimensional quantities. The 1/D 100 Analyzer was used to compute the PSD's, cross-PSD's, and Probability Densities. The stochastic algorithms utilized by the T/D 100 to perform these functions are discussed below.

After each PSD or cross-PSD was plotted, the spectral coefficients were punched, in ASCII format, on perforated paper tape. This paper tape was then fed into an SEL-810A mini-computer for transcription to magnetic tape. This was done to increase storage density, for ease of handling, and for speed of subsequent playback.

- RECORD 1, 3, 5, ..., N

WORD NUMBER	FORMAT	CONTENTS
0-2	A2	KEY, AAAAAA
3-7	A1	ITEM ID
8	A1	TEST TYPE, P FOR PSD AND X FOR CROSS PSD
9-10	A1	RUN ID
11-19	A1	FRAME NUMBER AS 011225.55
20	A1	LENGTH
21-27	A1	CONSTANT AS 2.05+01
28-143	?	JUNK

- RECORD 2, 4, 6, ...,(N-1)

WORD NUMBER	FORMAT	CONTENTS
0-2	A2	KEY, BBBBBB
3-103	I6	DATA VALUE
104-143	?	JUNK

- RECORD LAST

END OF FILE (N+2)

Figure 8. STOCHASTIC DATA TAPE FORMAT

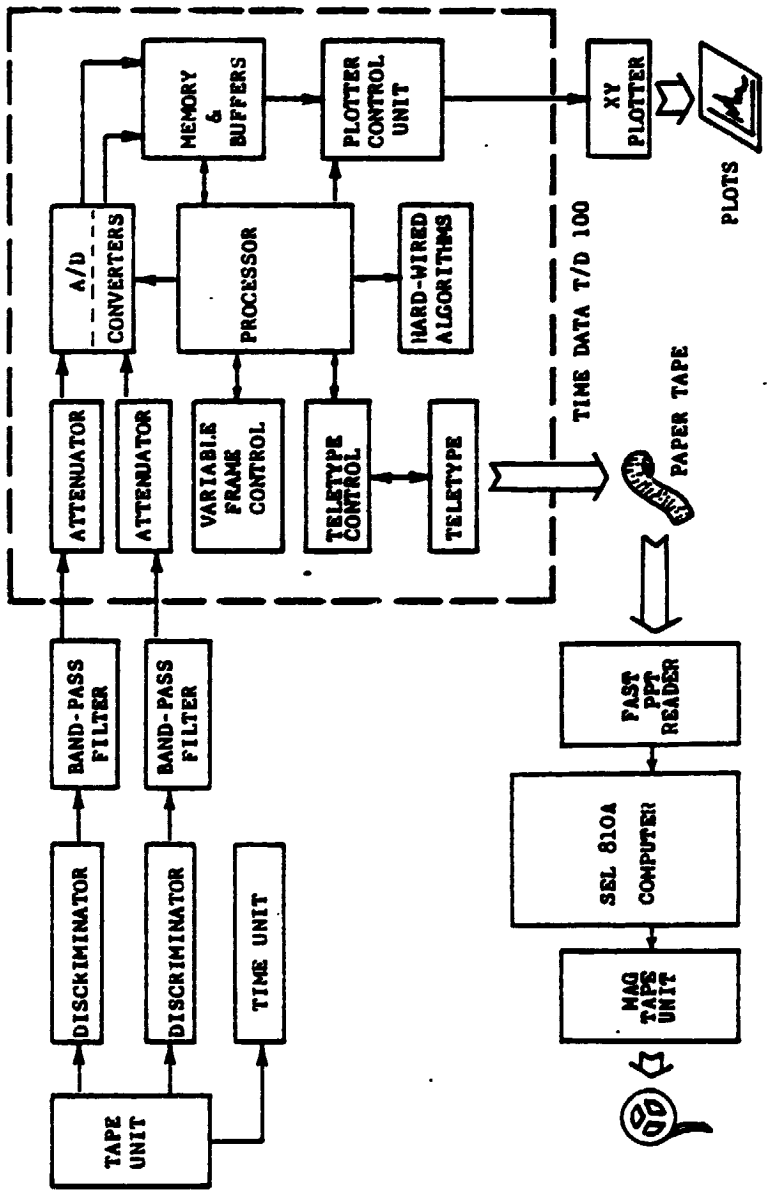

Figure 9. STOCHASTIC SPECIAL-PURPOSE EQUIPMENT

Auto-Spectral Density (PSD)

The T/D 100 computes the PSD coefficients by first approximating the complex Fourier transform of the input signal. The Fourier transform of the time-domain input function x(t) is given by:

$$G(jf) = \int_{-}^{+} x(t)(\cos 2\pi ft - j \sin 2\pi ft)\, dt \qquad (1)$$

where $j = \sqrt{-1}$. Since the time-domain input is sampled and quantitized in the analyzer, and only a finite number of samples are available, the finite transform is used, and separated into its real P(f) and imaginary Q(f) components can be written as follows:

$$P_T(f) = \int_{-T/2}^{T/2} x(t) \cos 2\pi ft \; dt \qquad (2)$$

$$Q_T(f) = \int_{-T/2}^{T/2} x(t) \sin 2\pi ft \; dt \qquad (3)$$

where T is the length of the input frame, which is assumed to be centered about time t=0.

Replacing the continuous input, x(t), with a set of 2N+1 discrete samples at intervals of $t_o = \frac{1}{2N}$, and replacing the sinusoidal functions by corresponding values, the continuous integrals may be expressed as the sum of products:

$$P(kf_o) = \sum_{n=-N}^{+N} x(nt_o) \cos \left[2 \quad kf_o(nt_o) \right] \tag{4}$$

$$Q(kf_o) = -\sum_{n=-N}^{+N} x(nt_o) \sin \left[2 \quad kf_o(nt_o) \right] \tag{5}$$

where k is a series of 2N integers and f_o is the base frequency which is equal to $\frac{1}{2T}$.

The PSD coefficients $\left[S(kf_o)\right]$ are then computed from (4) and (5) by the equation:

$$S(kf_o) = \left|P(kf_o)\right|^2 + \left|Q(kf_o)\right|^2 \tag{6}$$

Cross-Spectral Density (XPSD)

The T/D 100 computes the XPSD (S_{AB}) by simultaneously computing the complex Fourier transform of channel A ($P_A + jQ_A$) and channel B ($P_B + jQ_B$) and multiplying the channel A transform by the complex conjugate of the channel B transform as follows:

$$\begin{aligned} S_{AB} &= (P_A + jQ_A)(P_B - jQ_B) \\ &= P_AP_B + Q_AQ_B + j(P_BQ_A - P_AQ_B) \end{aligned} \tag{7}$$

The spectrum is then separated into its real ($S_{P\cdot AB}$) and imaginary ($S_{Q\cdot AB}$) components as follows:

$$\begin{aligned} S_{P\cdot AB} &= P_AP_B + Q_AQ_B \\ S_{Q\cdot AB} &= P_BQ_A + P_AQ_B \end{aligned} \tag{8}$$

The T/D 100 then puts the real component into the channel A output buffer and the imaginary component into the channel B output buffer.

Probability Density

On the T/D 100 the Probability Density of a time-domain input is ascertained by performing an Amplitude Histogram on the input function. This algorithm counts the number of times that each of 255 discrete amplitudes occurs at the input. Zero-amplitude occurrences appear mid-scale of the output display with negative-amplitude occurrences increasing to the left of mid-scale and positive-amplitude occurrences increasing to the right.

Average rms (Ψ_T)

The average rms of the input signal is calculated from the PSD coefficients $\left[S(kf_o)\right]$ by the following equation:

$$\Psi_T = \sqrt{f_o \sum_{k=0}^{2N} S(kf_o)}$$

where $f_o = \frac{1}{2NT}$ is the base frequency or analysis bandwidth.

SECTION 7

DISCUSSION OF RESULTS

This discussion will review the major findings of the investigation and illustrate each of these findings with appropriate examples of the stochastic analysis results.

The major findings of this study are as follows:

1. The structural response of the aircraft to buffet during moderate-g and high-g maneuvers is very complex. Almost all natural vibration modes of the aircraft (symmetric and antisymmetric) can be excited to a significant intensity level at some time during the maneuvers.
2. As a consequence of 1, above, several different types and locations of instrumentation are needed to obtain an adequate description of the structural responses.
3. Some of the sensors show pronounced changes in the relative modal contributions to the total response as penetration (angle of attack) beyond buffet onset increases.
4. The fluctuating shear and bending moment loads for the test conditions examined are small in terms of design loads except near the wing tip.

5. The wing structural response in torsion is much larger than anticipated on the basis of previous buffet studies, amounting to between 1/3 and 1/2 of the rms values of wing bending response at high angles of attack.
6. There is some evidence of bending-torsion coupling starting at angles of attack between 9 and 12 degrees at Mach numbers of 0.80 and 0.87.
7. The stochastic analysis techniques employed in this investigation provide useful and consistent sets of data despite the short sample times and the abruptness of some of the maneuvers. Proper interpretation of the analysis results must include consideration of the ranges of angle of attack, Mach number and dynamic pressure that occur during the time duration of each record.

Characteristics of the Structural Responses

During the course of the study approximately 800 power spectral density plots were obtained. These data have two primary uses. First they permit identification of the significant modal contributions through comparison with the ground vibration test data

obtained in the F-111 development program. Second they provide the data base for future assessment of prediction methods.

Natural Vibration Modes

A summary of measured natural vibration modes of the F-111A at 26 degrees leading-edge sweep is presented in Table 8. Most of the values were taken from tests previously conducted on Airplane No. 12 which is structurally the same as Airplane No. 13 (Reference 18). A few of the measurements were taken on Airplane No. 1 and were not repeated on Airplane No. 12 because the parts and associated structure had not changed (Reference 19). Data are presented for two fuel loading conditions: fuselage empty, wing empty and fuselage full, wing empty. Note that the difference in fuselage fuel load affects some of the natural frequencies.

Table 9 presents calculated values of symmetric vibration mode frequencies obtained using a math model of the aircraft structure for two gross weight conditions which represent specific loadings occuring on maneuvers investigated in this study. These calculated mode frequencies serve the purpose of clarifying some measured responses which were not clearly identified in the ground vibration tests because of the close proximity of other modes.

TABLE 8 - MEASURED F-111A NATURAL VIBRATION MODES

Predominant Mode (Airplane No. 12 Tests)	Frequency - Hz			
	Fuse. Empty, Wing Empty		Fuse. Full, Wing Empty	
	Symmetric	Antisymmetric	Symmetric	Antisymmetric
Wing First Bending	5.2	7.6	5.1	7.1
Fuselage First Vertical Bending	8.6	---	8.0	---
Fuselage First Lateral Bending	---	---	---	8.7
Wing Fore and Aft Bending	7.9	9.3	8.8	8.7
Wing Second Bending	16.9	29.2	17.8	29.0
Wing-Horizontal Tail	---	16.2, 17.5	---	17.5
First Wing Torsion	25.2	25.4	25.7	26.1
Horizontal Tail First Bending	13.6	13.3	13.8	13.1
Horizontal Tail Fore and Aft	15.2	15.3	16.3	16.2
Horizontal Tail Pitch	34.4	37.3, 31.0	30.9	29.5, 36.1
Vertical Tail Bending	---	9.9	---	9.6
Vertical Tail Torsion	---	28.0	---	11.7
Rudder Rotation	---	32.7	---	28.3
Rudder Torsion	---	45.0	---	44.8
Rotating Glove	27.4			
Leading Edge Bending	44.3			
Yaw	50.9			
Pitch	63.8			
Aft End Bending				
Spoiler Modes (From Airplane No. 1 Tests)				
Spoiler No. 1			46,56,62	53,60
Spoiler No. 2			55,65,72	68

TABLE 9 - CALCULATED SYMMETRIC VIBRATION MODES

Mode No.	Mode Description	Frequency - Hz	
		Gross Weight - lbs	
		59,800	72,600
1	First Wing Bending	4.794	4.772
2	First Fuselage Vertical Bending	7.013	6.708
3	Horizontal Tail Bending + Sec. Wing Bend. + Sec. Fus. Bend.	13.930	13.249
4	Horizontal Tail Bending + Second Wing Bending	14.828	14.723
5	Second Wing Bending	17.010	16.401
6	Third Fuselage Bending + Wing Torsion	22.853	21.618
7	First Wing Torsion	24.064	23.970
8	Horizontal Tail Second Bending	27.521	26.073
9	Third Wing Bending	30.666	30.273
10	Horizontal Tail Torsion	33.893	33.865
11	Fuselage Fourth Bending + Second Wing Torsion	37.573	36.391
12	Second Wing Torsion	39.229	37.986

Power Spectra

Representative examples of power spectra will be presented and discussed to illustrate several of the major findings of the investigation. All of the plotted PSD's are presented in Appendix B and tabulated PSD data are presented in Appendix C for future comparisons with predictions.

The power spectra are presented on a consistent semi-log format in which normalized values of power spectral density are plotted against frequency over the range from 0 to 100 Hz (see Figure 10(a)). The normalizing factor (scale factor) in each case is the sum of the spectral estimates at each frequency from 1 to 100 Hz. The scale factor is presented above each plot in both S.I. units and U.S. customary units (if appropriate). The values plotted at 0 and 1 Hz are ficticious and are used only to set the scales for the automatic plotting routine that was used to generate these presentations. Any data point which falls on the lower bound of the plot at frequencies other than 1 Hz actually represents a value below the threshold of the dynamic range of the analysis system for the particular analysis. Finally, although all the power spectra estimates are plotted from 2 to 100 Hz, the valid upper limit of frequency for each instrumentation item and flight condition is approximately that indicated previously in Table 5 because of the flight recorder frequency

response characteristics. Values for frequencies much above the limits indicated in Table 5 probably are caused by cross-talk between recorder channels and should be ignored.

Near Buffet Onset

The particular set of PSD data presented in Figure 10 is for point 8 of Flight 77, Run S&C-R. The nominal angle of attack is 7.1 degrees and the length of the sample record is two seconds. The aircraft is slightly beyond buffet onset at this condition. The wing shear strain-gage data are presented first for each of the four wing stations, followed by the wing bending gage and torsion gage data. The various accelerometer data complete the presentation for this point. Each plot is annotated with the vibration mode at which each of the major responses occur.

Examination of the shear data shows that at Wing Station 1 the major responses are in the first and second wing bending modes, the first fuselage bending mode, the first wing torsion mode and a combined wing-tail mode. Further outboard on the wing some additional modes can be identified including the second antisymmetric wing bending mode and several horizontal tail pitch and torsion modes. In addition, the levels of the power spectra at the higher frequencies increase to the point that the first wing bending and first fuselage vertical bending mode are no longer the dominant modes at Wing Station 4.

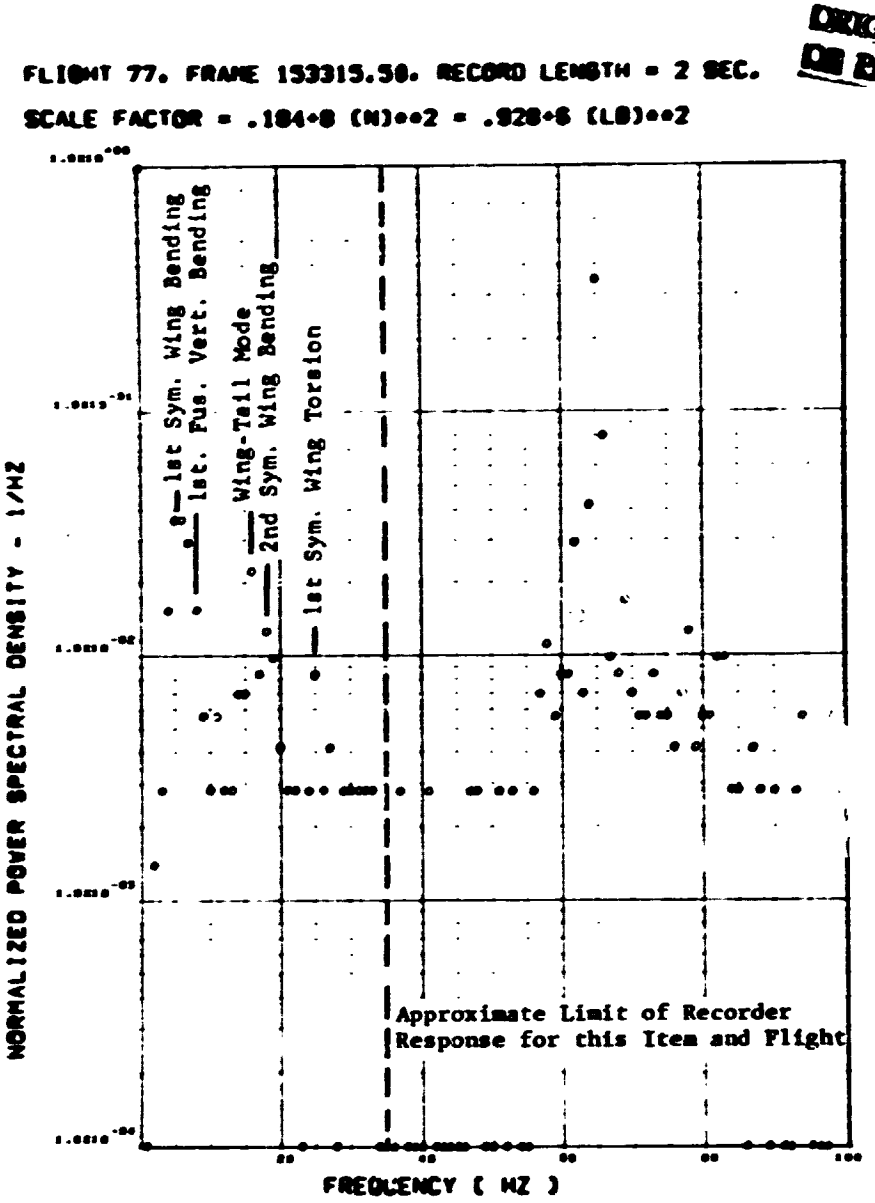

Figure 10. POWER SPECTRA, FLIGHT 77, RUN S&C-R, POINT 8
M~0.80, h~6035 m (19,800 ft), α_{NOM} = 7.1 deg

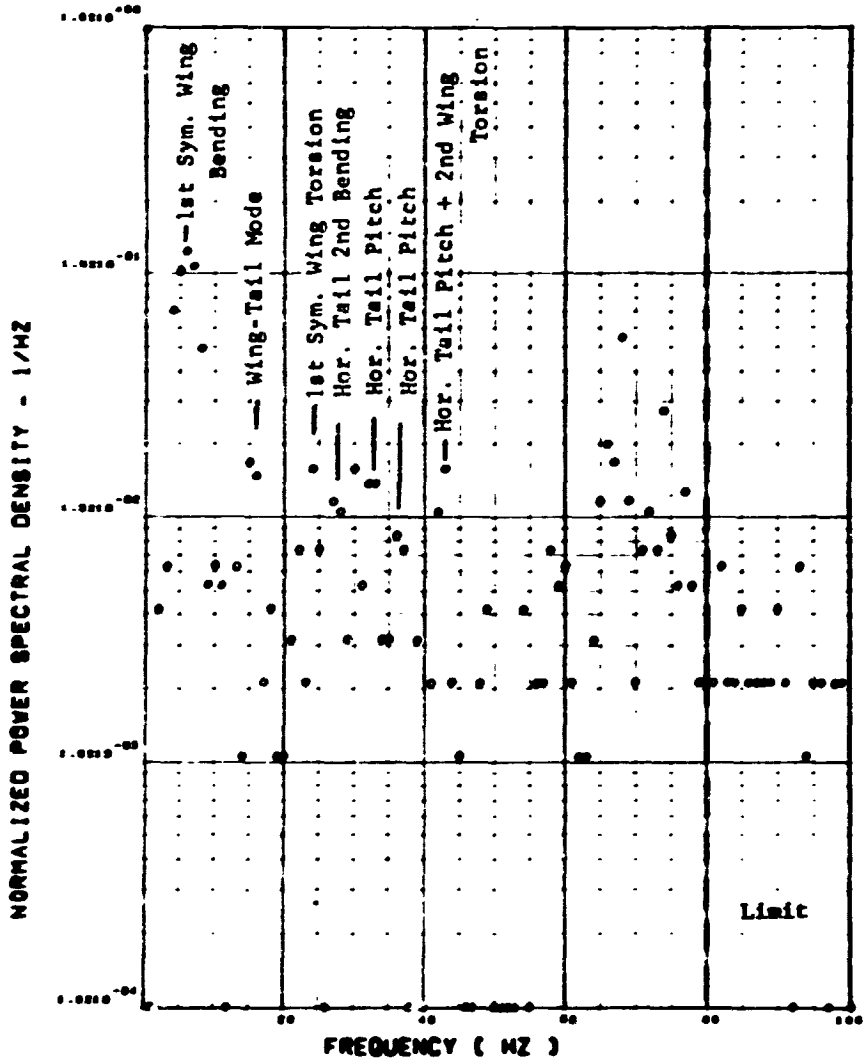

(b) SW12B SHEAR AT WING STATION 2

Figure 10. Continued

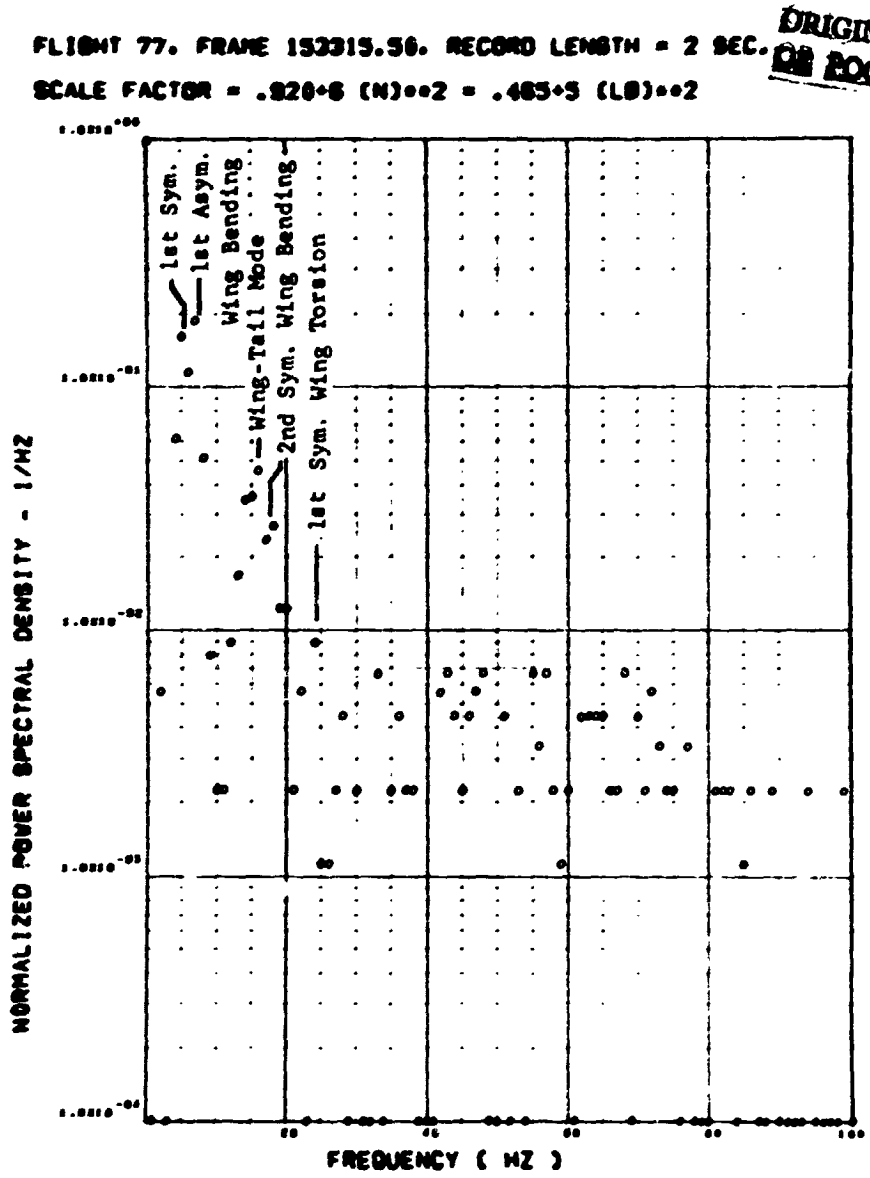

(c) SV120 SHEAR AT WING STATION 3

Figure 10. Continued

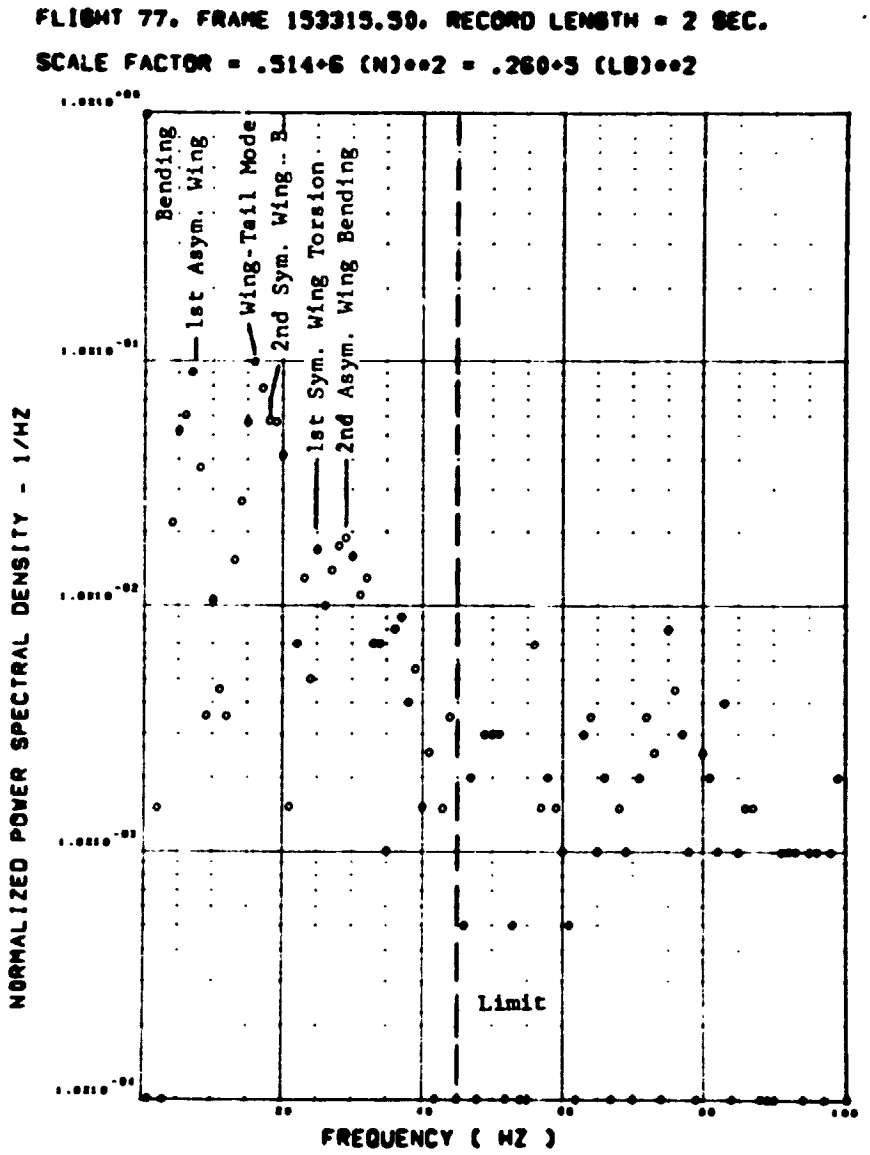

(d) SV132 SHEAR AT WING STATION 4

Figure 10. Continued

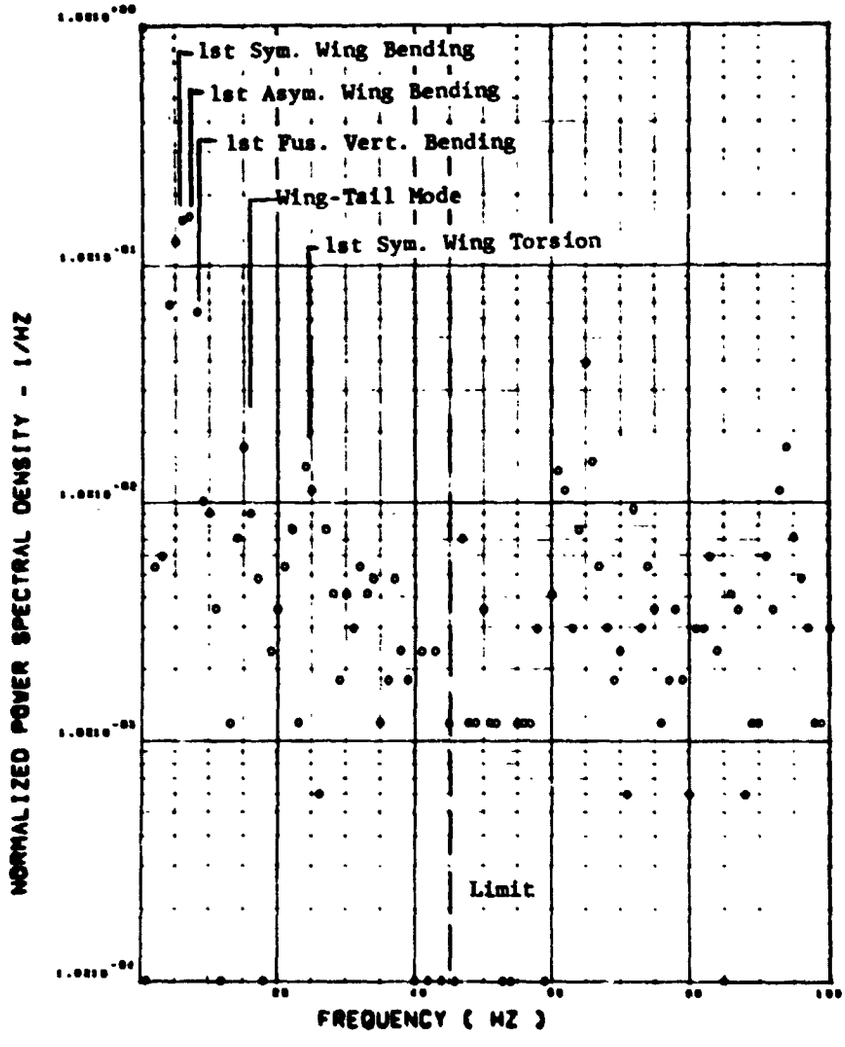

(e) SV124 BENDING MOMENT AT WING STATION 1

Figure 10. Continued

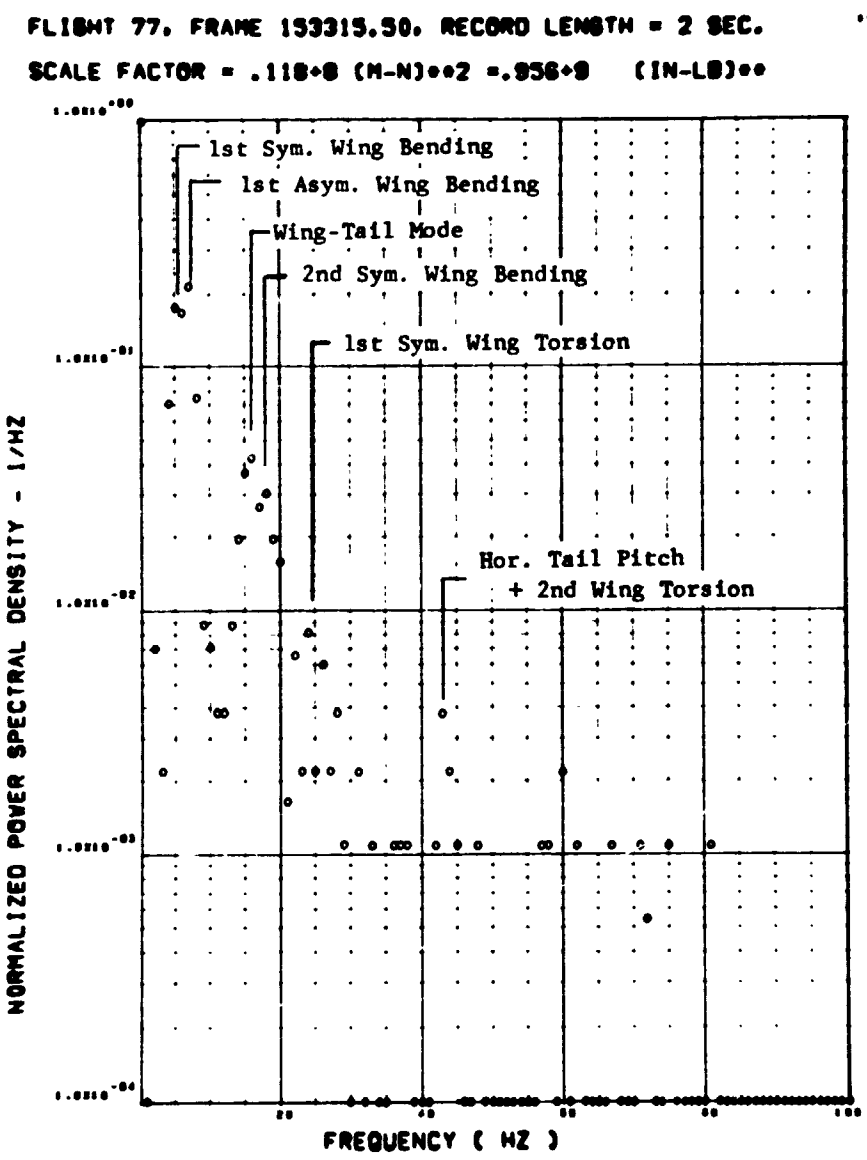

(f) SW127 BENDING MOMENT AT WING STATION 2

Figure 10. Continued

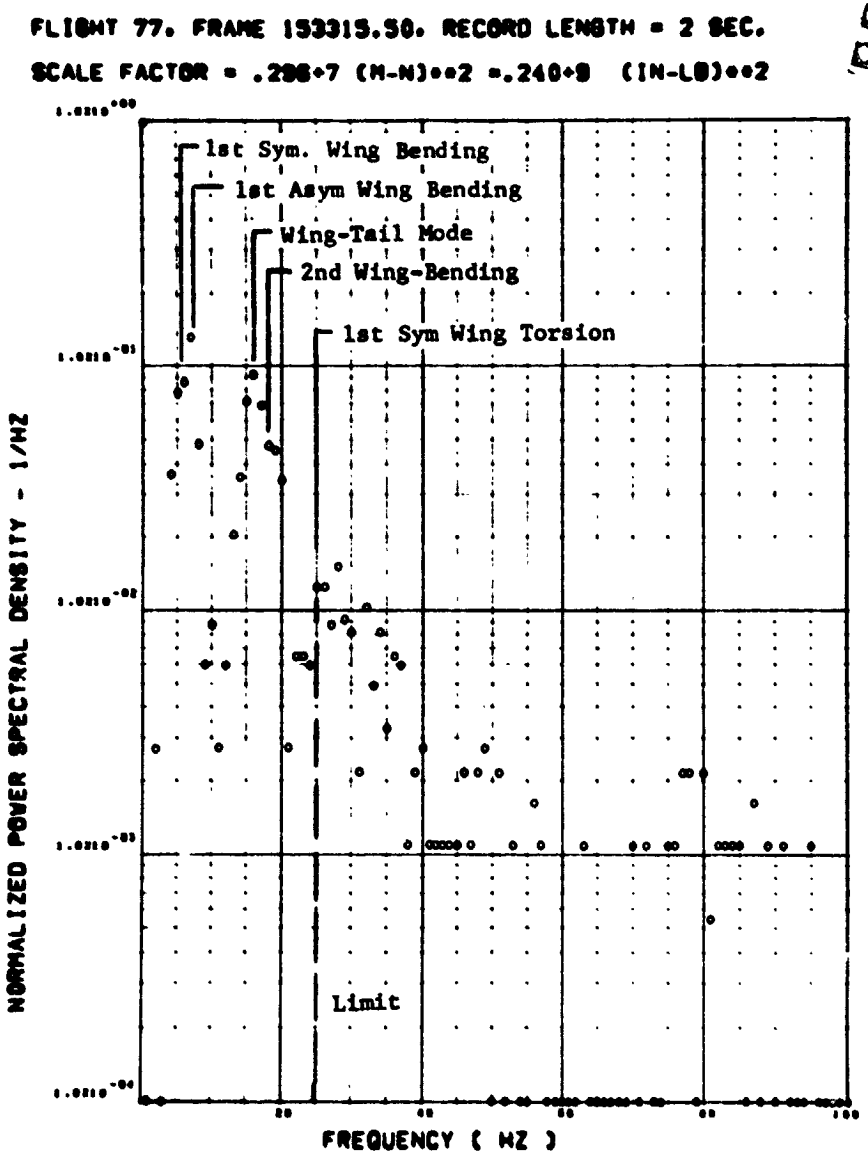

(g) BV130 BENDING MOMENT AT WING STATION 3

Figure 10. Continued

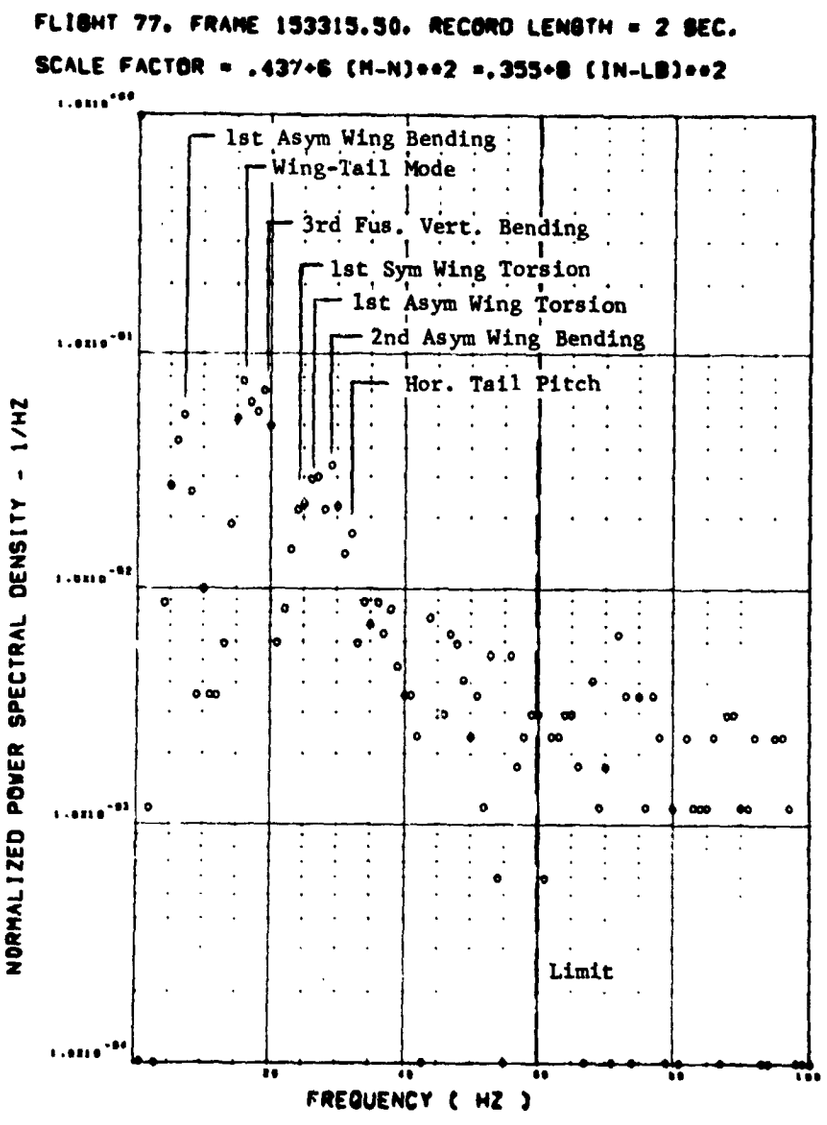

(h) SW133 BENDING MOMENT AT WING STATION 4

Figure 10. Continued

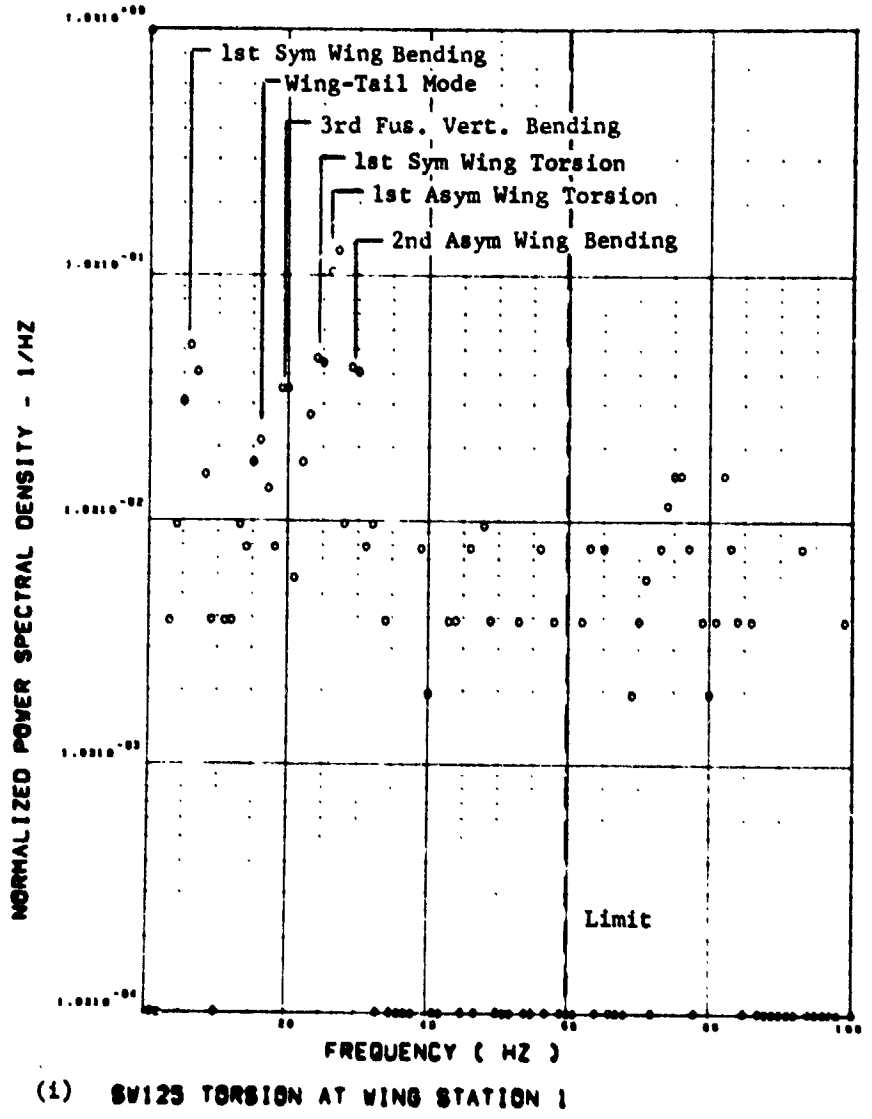

Figure 10. Continued

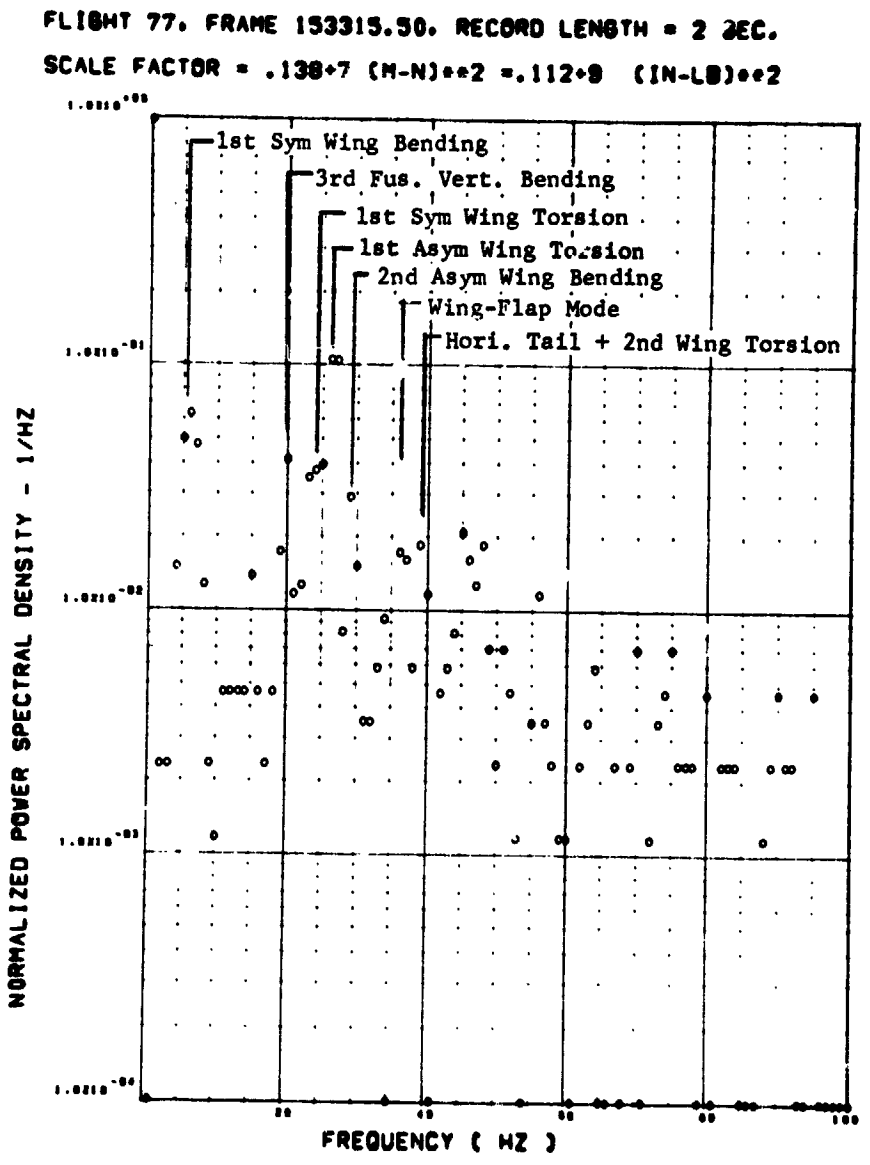

(j) SW12B TORSION AT WING STATION 2

Figure 10. Continued

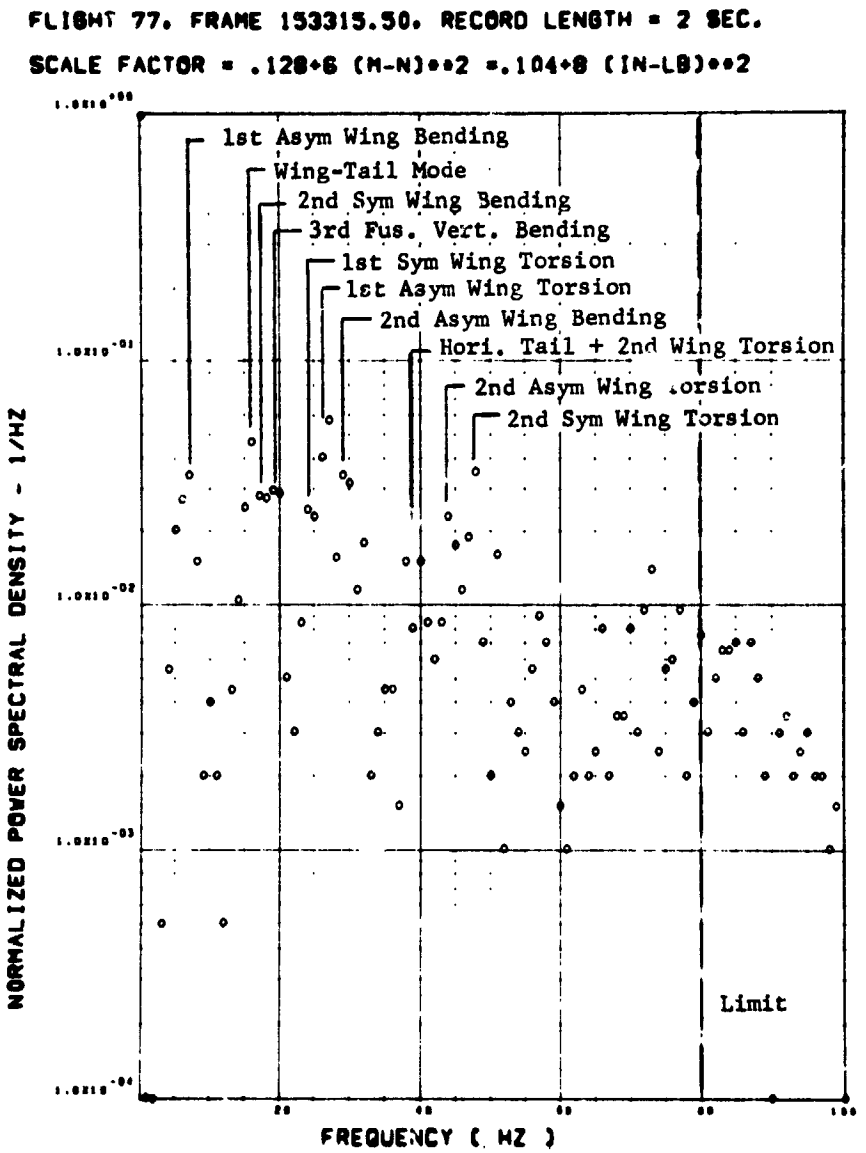

Figure 10. Continued

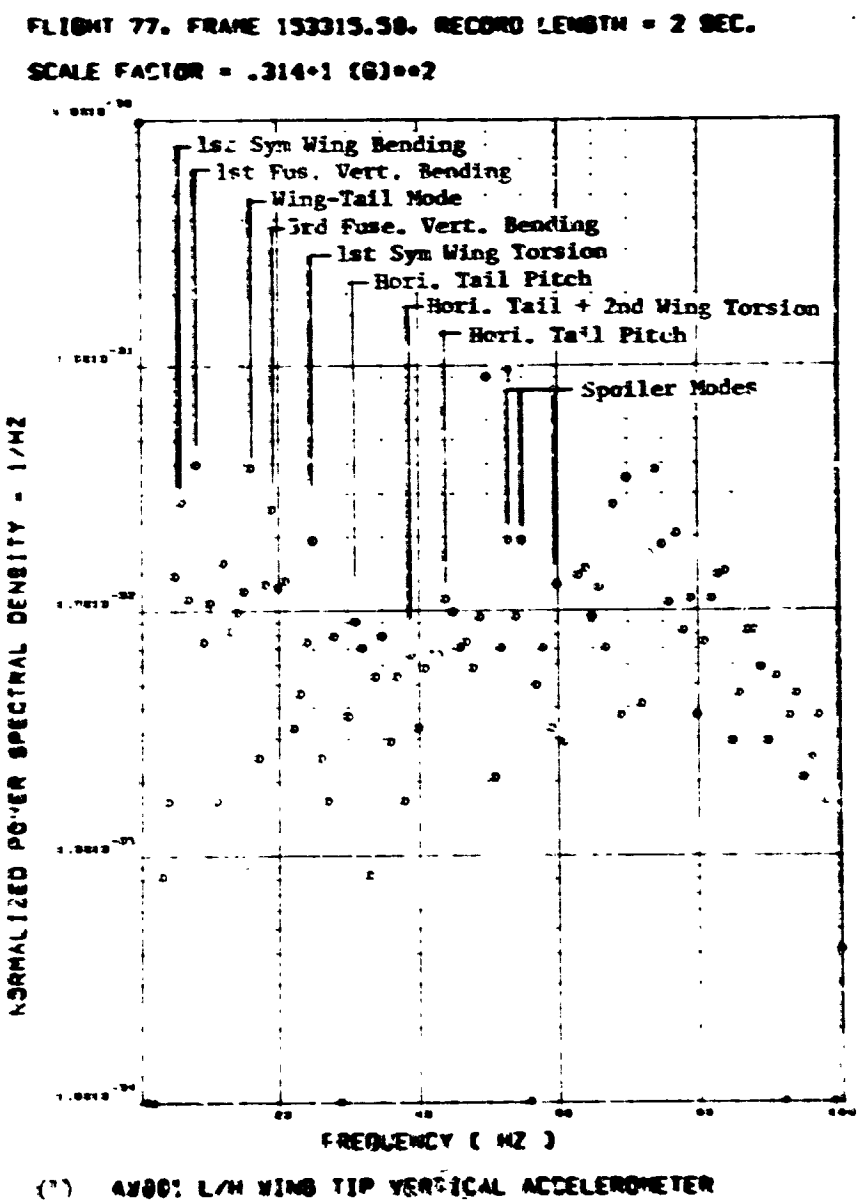

Figure 10. Continued

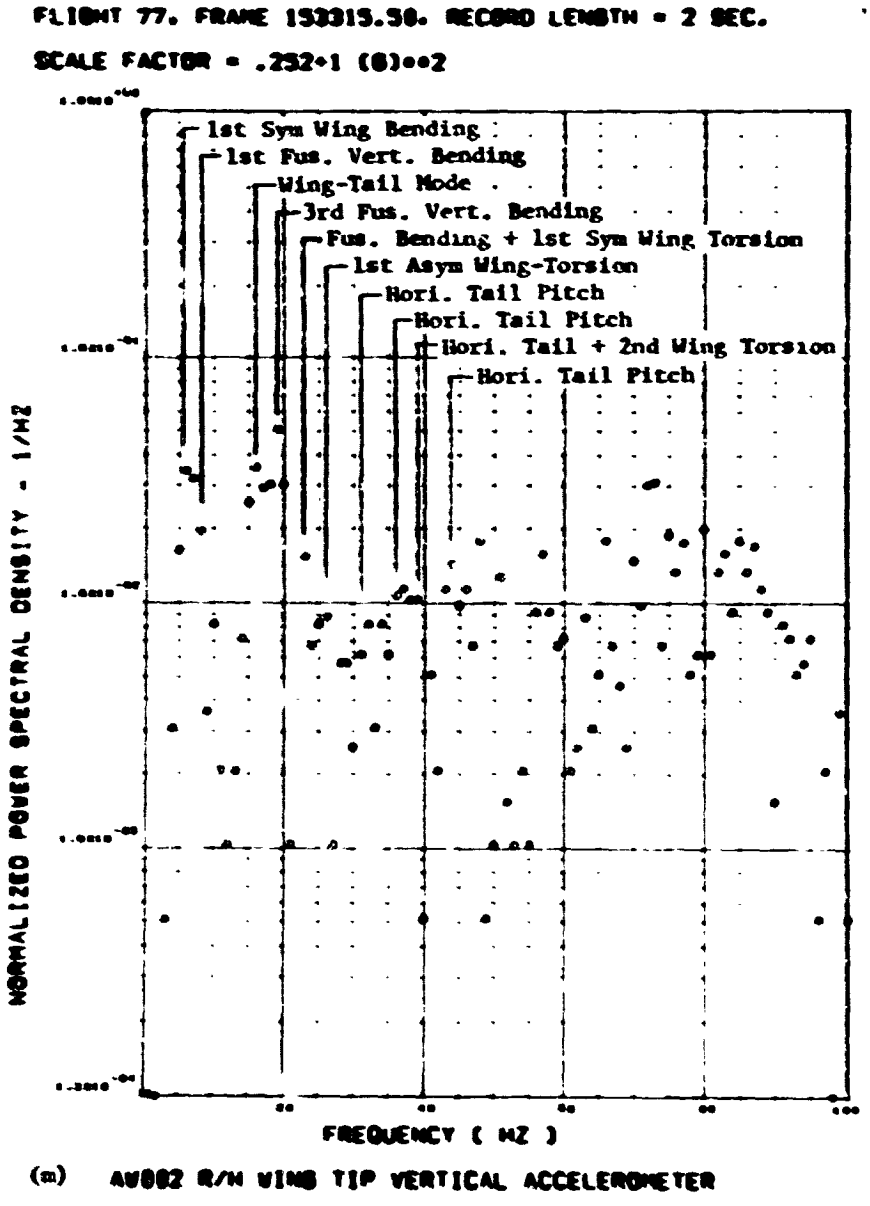

(m) AV002 R/H WING TIP VERTICAL ACCELEROMETER

Figure 10. Continued

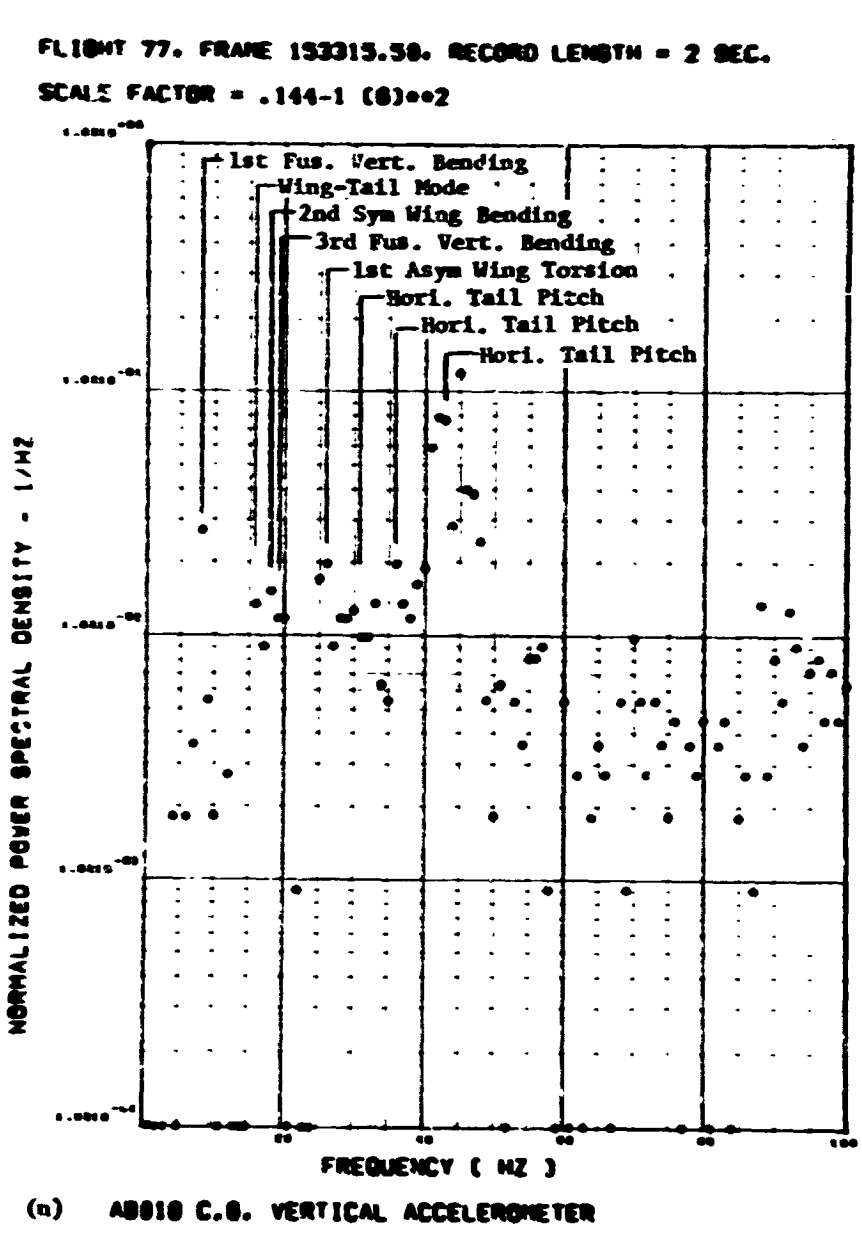

(n) AB010 C.G. VERTICAL ACCELEROMETER

Figure 1C. Continued

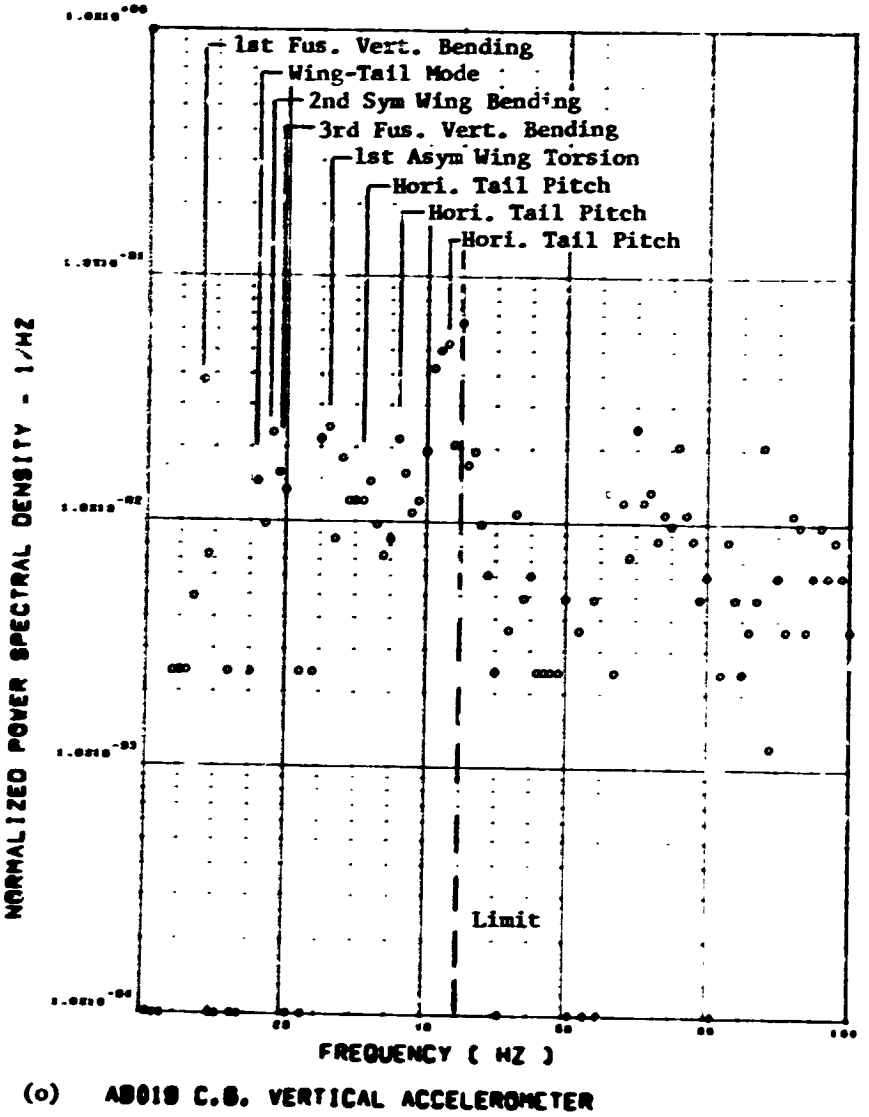

(o) AD018 C.G. VERTICAL ACCELEROMETER

Figure 10. Continued

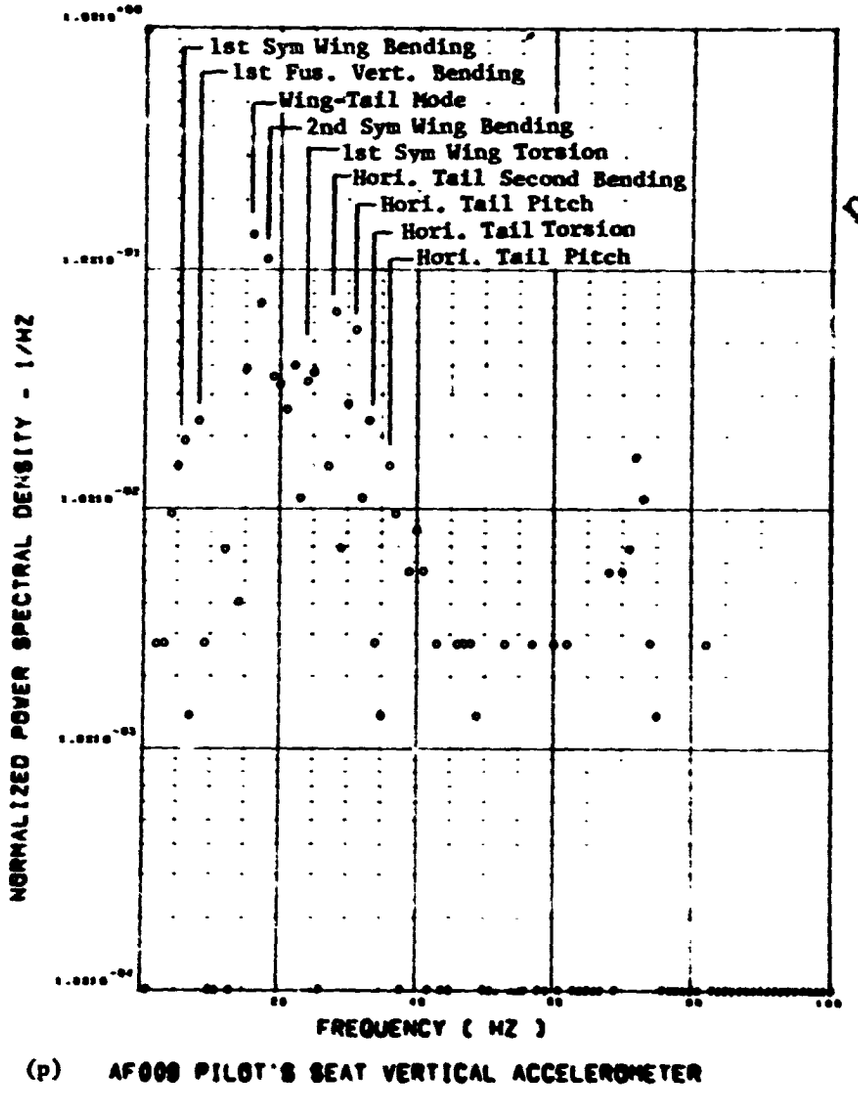

(p) AF008 PILOT'S SEAT VERTICAL ACCELEROMETER

Figure 10. Continued

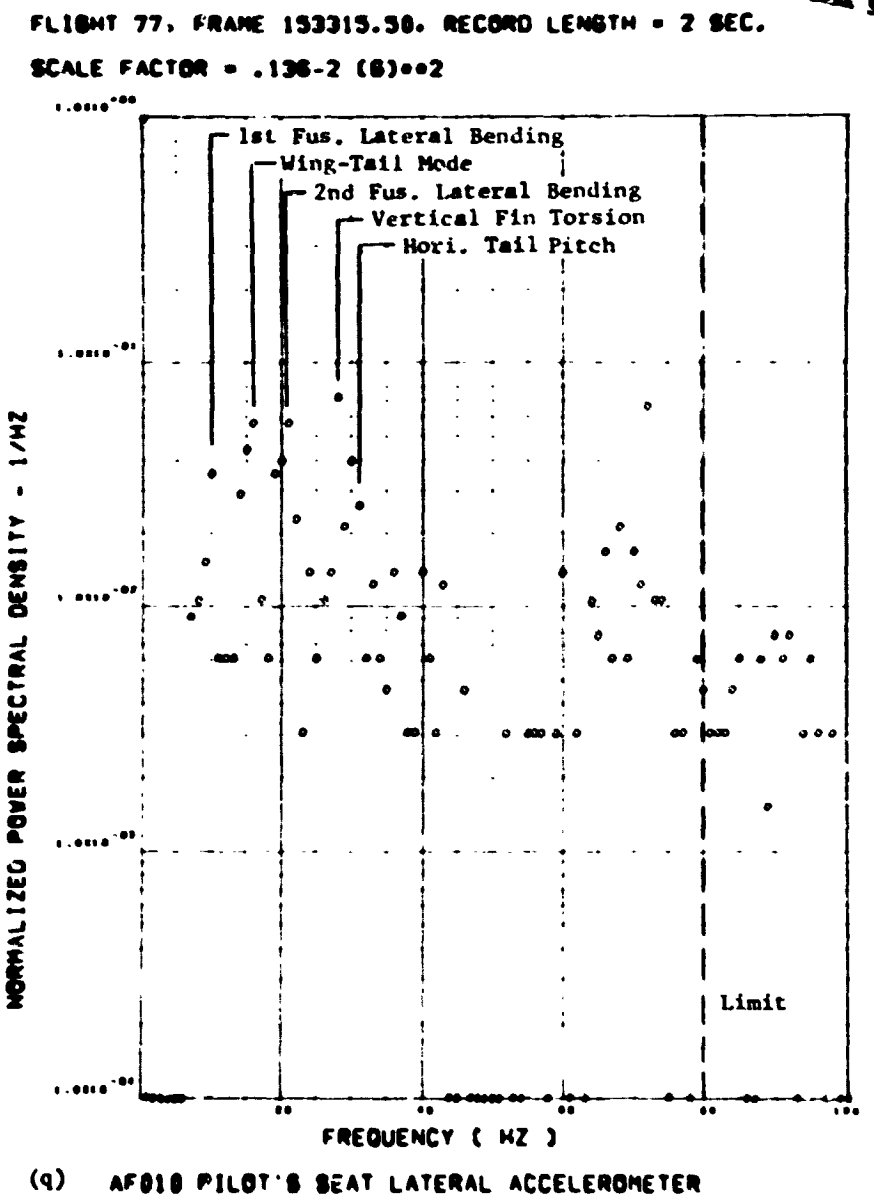

(q) AF010 PILOT'S SEAT LATERAL ACCELEROMETER

Figure 10. Continued

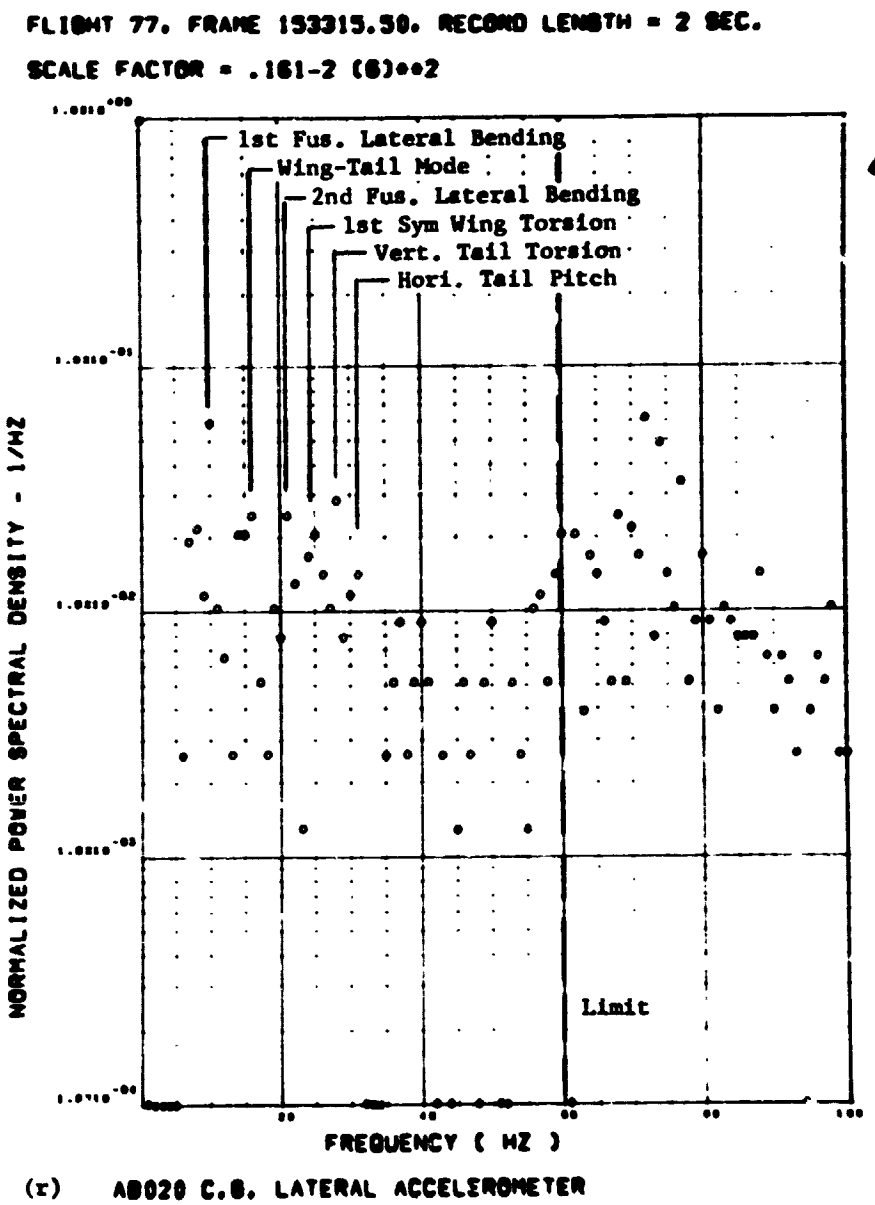

Figure 10. Concluded

The responses shown by the wing bending gages at each wing station track the responses shown by the shear gages at the corresponding stations, except that at the inboard two stations the first wing bending mode dominates the responses.

The wing torsion responses are strong at the first wing torsion frequency with a major contribution occurring also at the first wing bending frequency. There is some response shown at a frequency of about 20 Hz which can be attributed to a fuselage bending mode.

The wing tip accelerometers show responses in most of the modes already identified from the strain gage sensors plus several responses at higher frequencies between 40 and 80 Hz. Note that while the PSD plots for the left-hand and right-hand wing tip accelerometers are similar they are not identical in detail.

The fuselage mounted accelerometers show very little response in the first wing bending modes. The two C.G. vertical accelerometers show very similar responses and the dominant response is in a band of frequencies from 40 to 45 Hz which includes some higher order horizontal tail pitch modes. The other significant responses are attributable to first fuselage vertical bending, wing-tail, horizontal tail second bending, first antisymmetric wing torsion and lower order horizontal tail pitch

modes. The dominant responses shown by the pilot station vertical accelerometer include the wing-tail, horizontal tail second bending, first wing torsion, and lower order horizontal tail pitch modes. Only small responses occur at first wing bending and first fuselage vertical bending modes. The lateral accelerometers at the C.G. and pilot's seat respond at frequencies for first and second fuselage lateral bending, antisymmetric wing-tail, first wing torsion, second wing antisymmetric bending, and horizontal tail pitch modes. Responses are also noted at high frequencies between 60 and 80 Hz but these are not readily identifiable modes.

Near Maximum Buffet

From the data just presented it can be seen that the aircraft responses just beyond buffet onset are quite complex and many vibration modes are excited. It is observed that a higher angle of attack condition where the rms values of response are much larger, the relative model contributions change significantly.

Figure 11 presents the power spectra for point 10 of Flight 77, Run S&C-R which corresponds to a nominal angle of attack of 12.2 degrees. Examination of the shear data at Wing Station 1 reveals a very large response in first wing bending, some contributions in the wing second bending mode and new major contributions in the first wing torsion and second antisymmetric wing bending mode. At Wing Station 2 the contributions due to

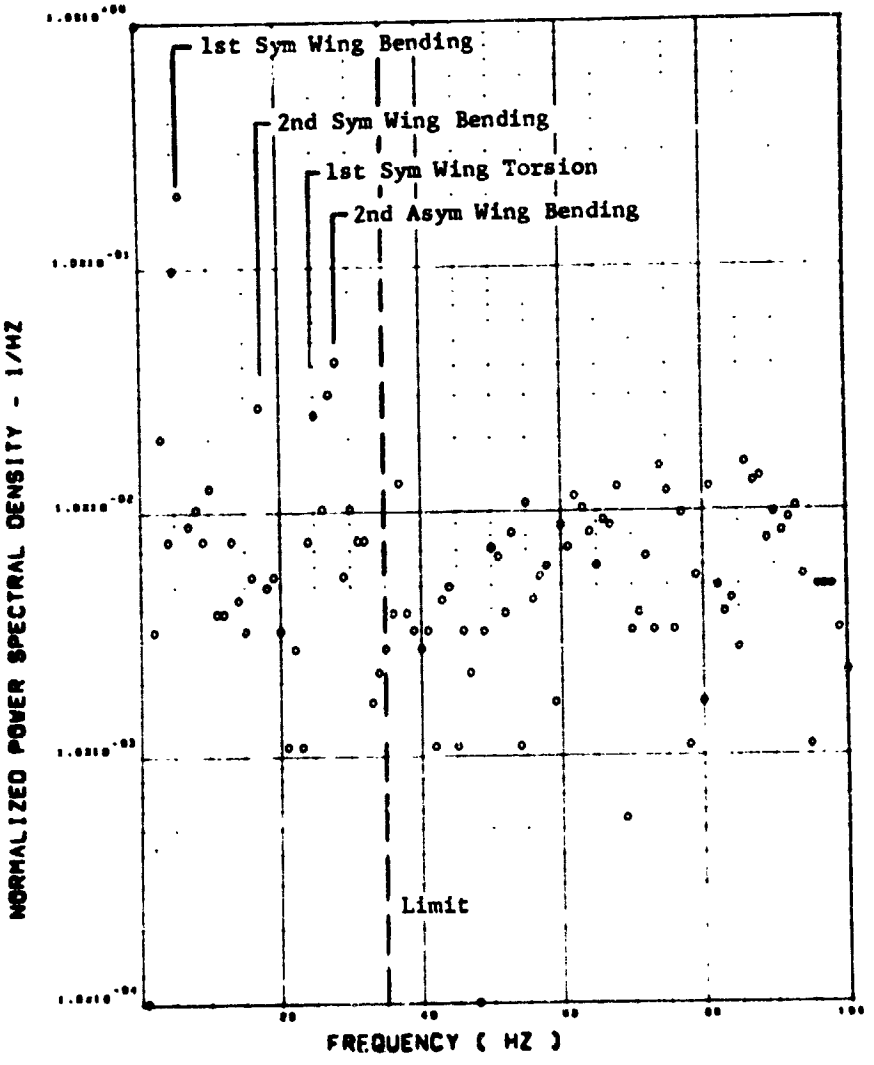

Figure 11. POWER SPECTRA, FLIGHT 77, RUN S&C-R, POINT 10
M ~ 0.80, h ~ 6035 m (19,800 ft), α_{NOM} = 12.2 deg

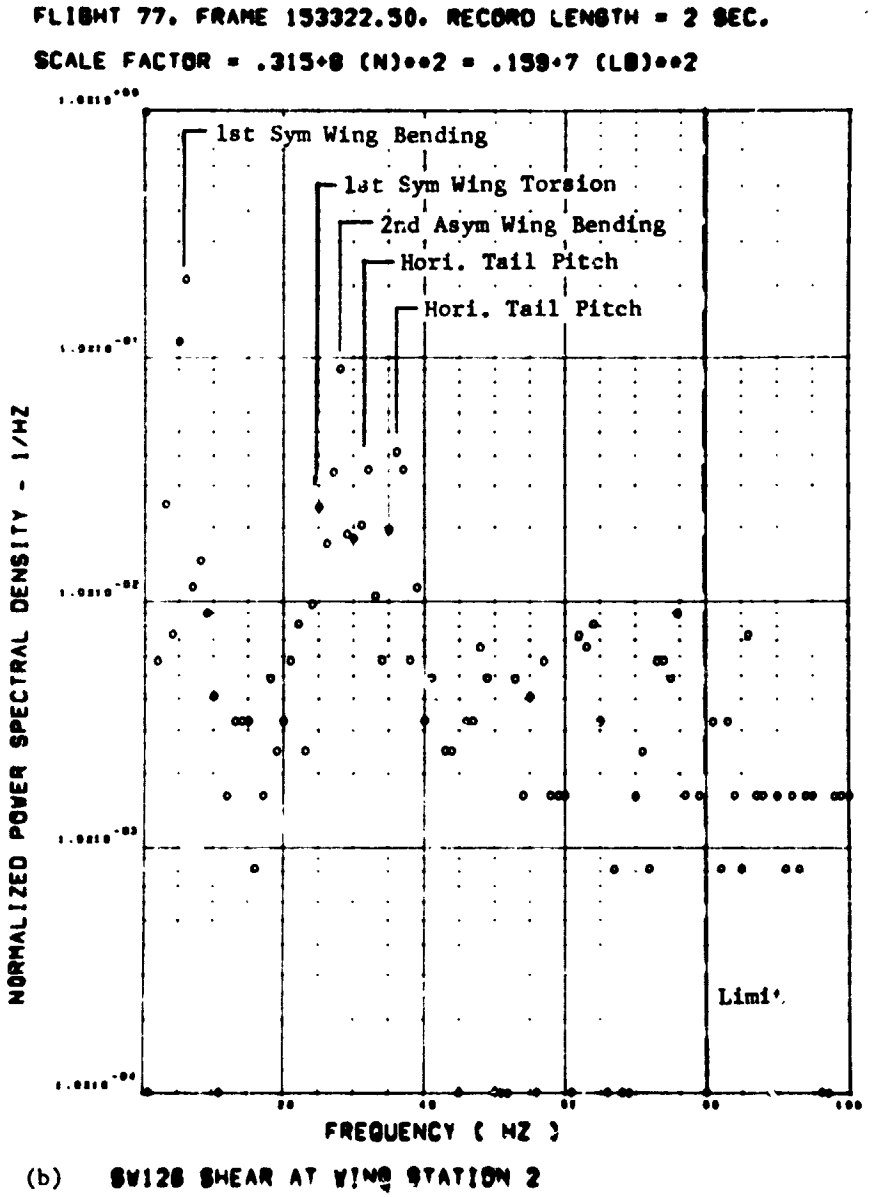

(b) SW12B SHEAR AT WING STATION 2

Figure 11. Continued

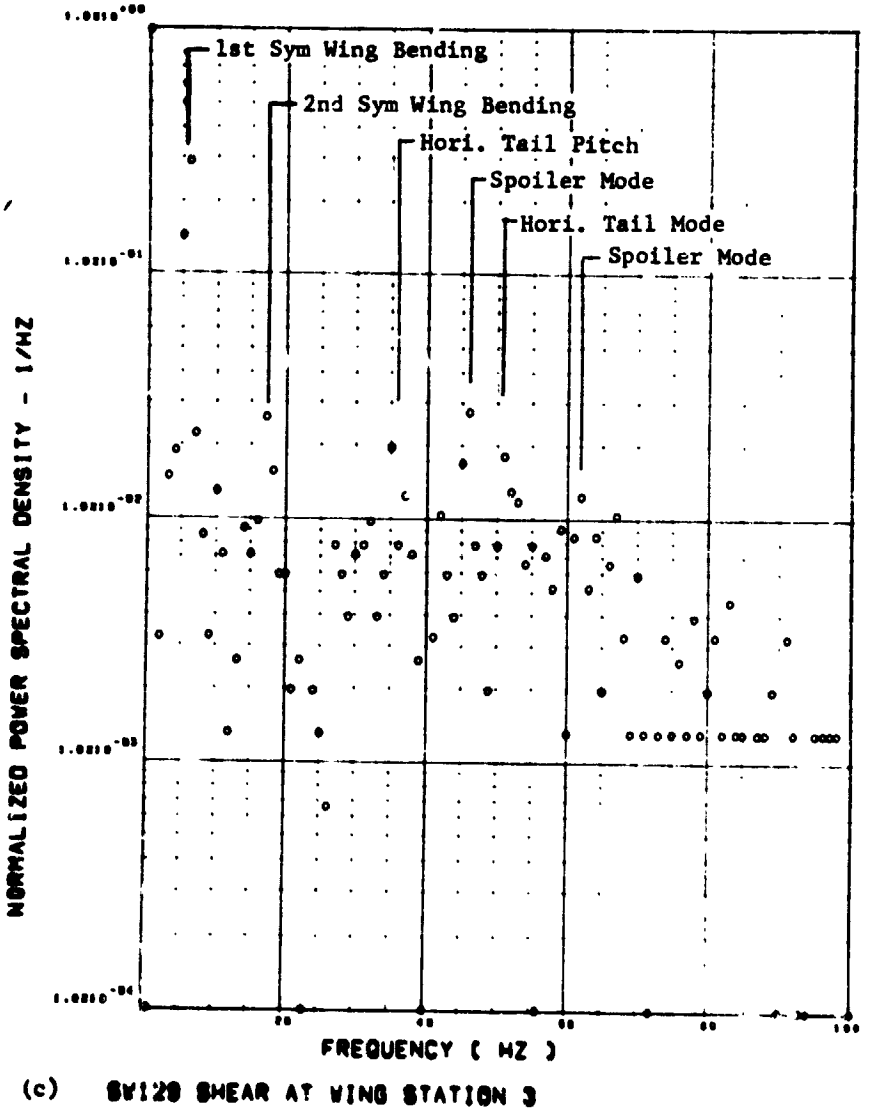

Figure 11. Continued

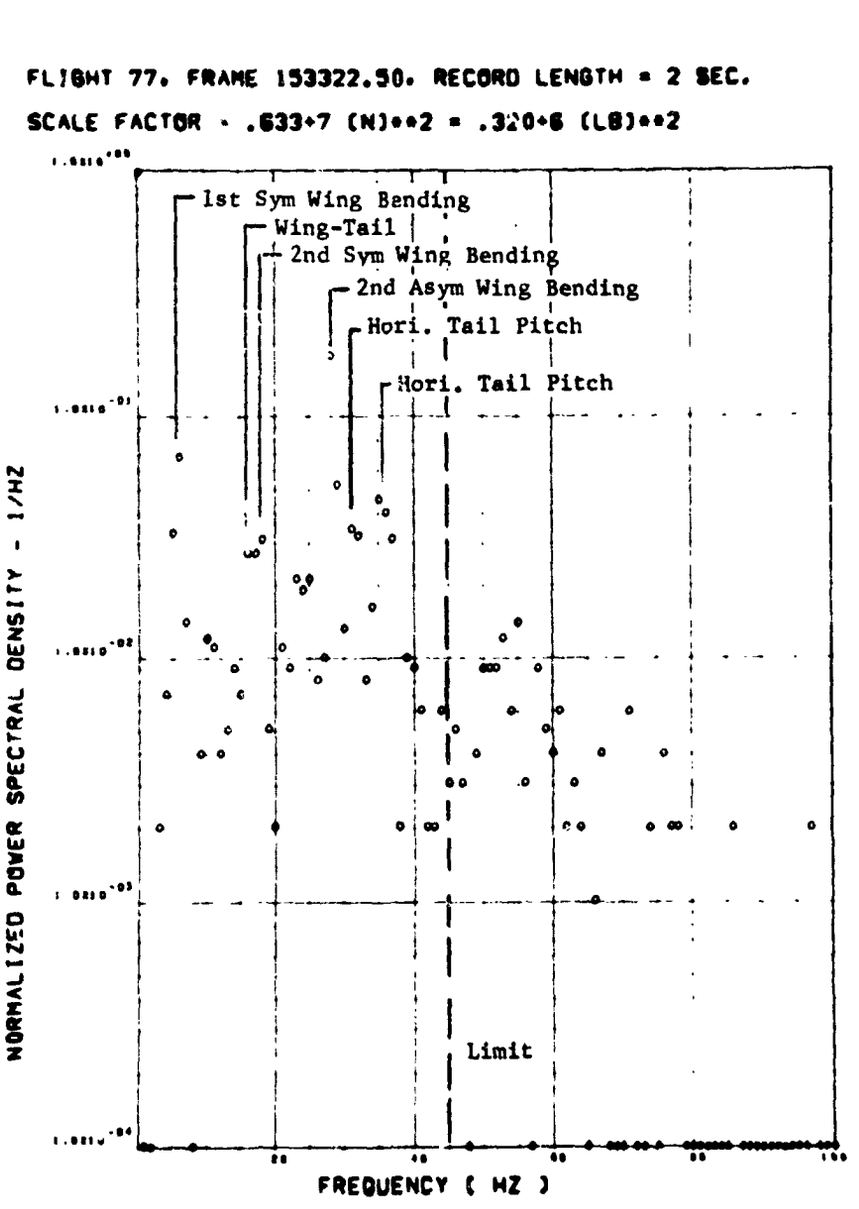

(d) SW132 SHEAR AT WING STATION 4

Figure 11. Continued

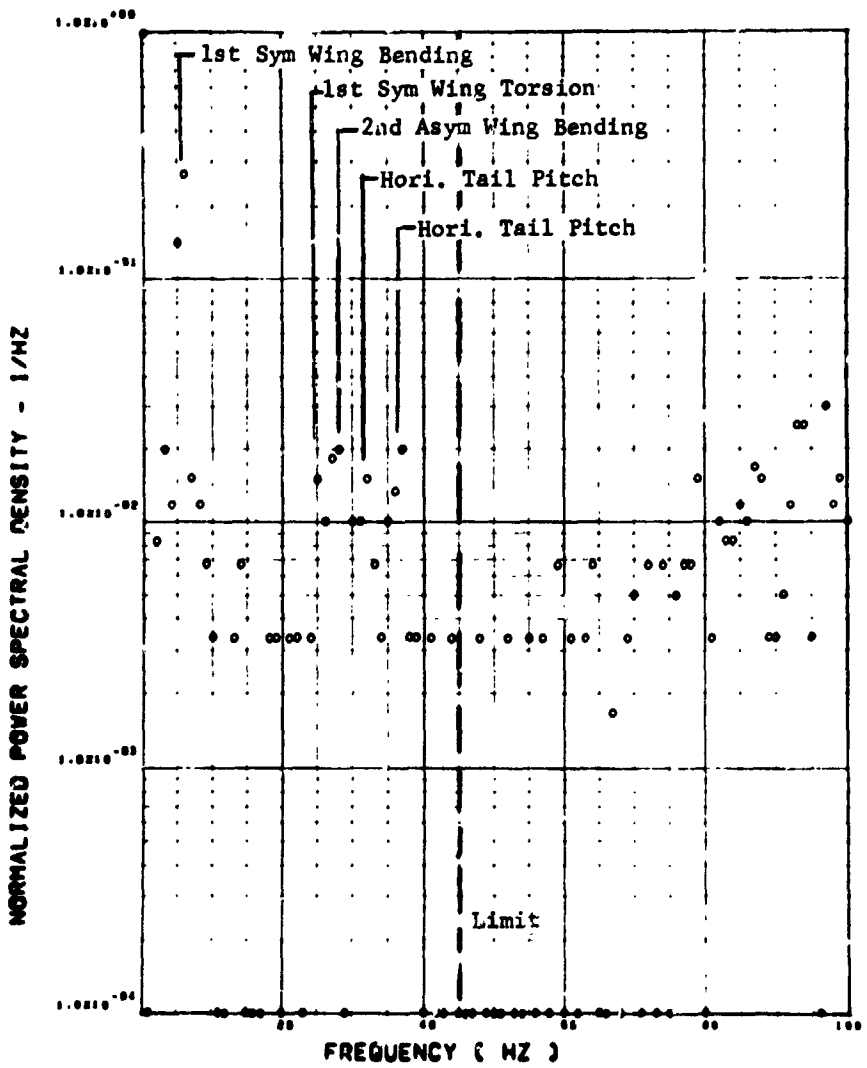

(e) SW124 BENDING MOMENT AT WING STATION 1

Figure 11. Continued

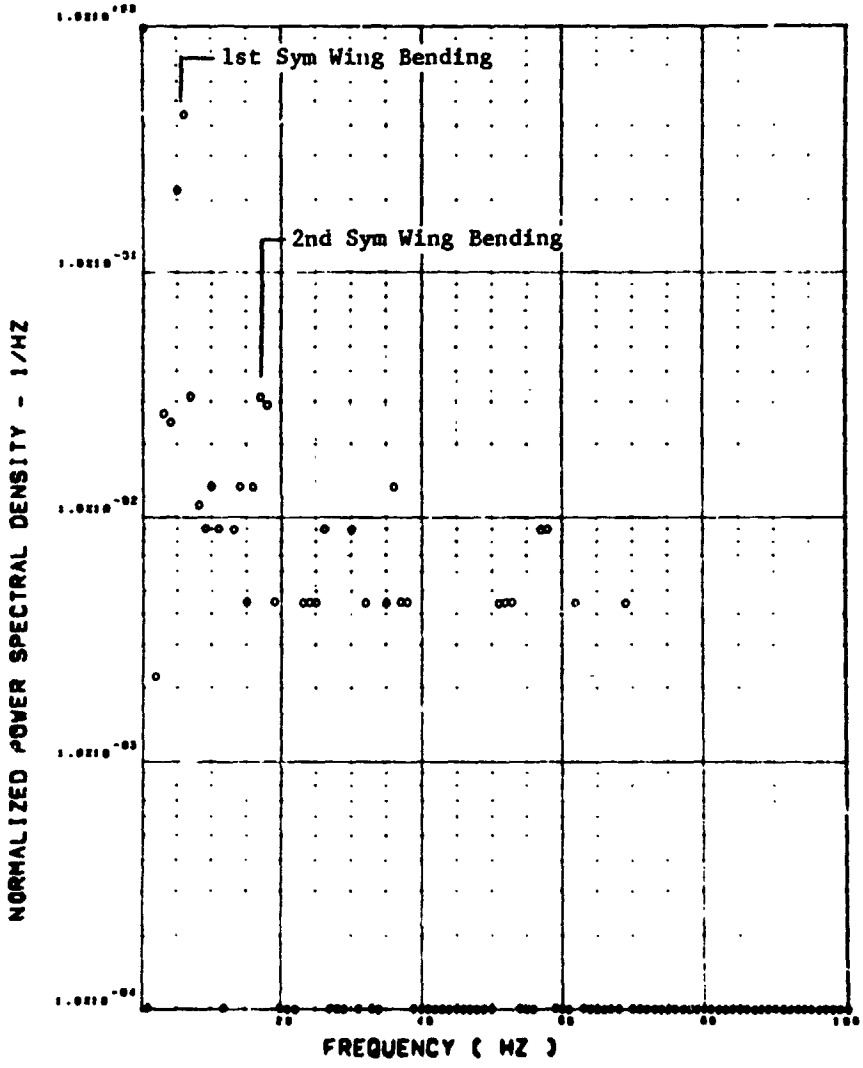

(f) SW127 BENDING MOMENT AT WING STATION 2

Figure 11. Continued

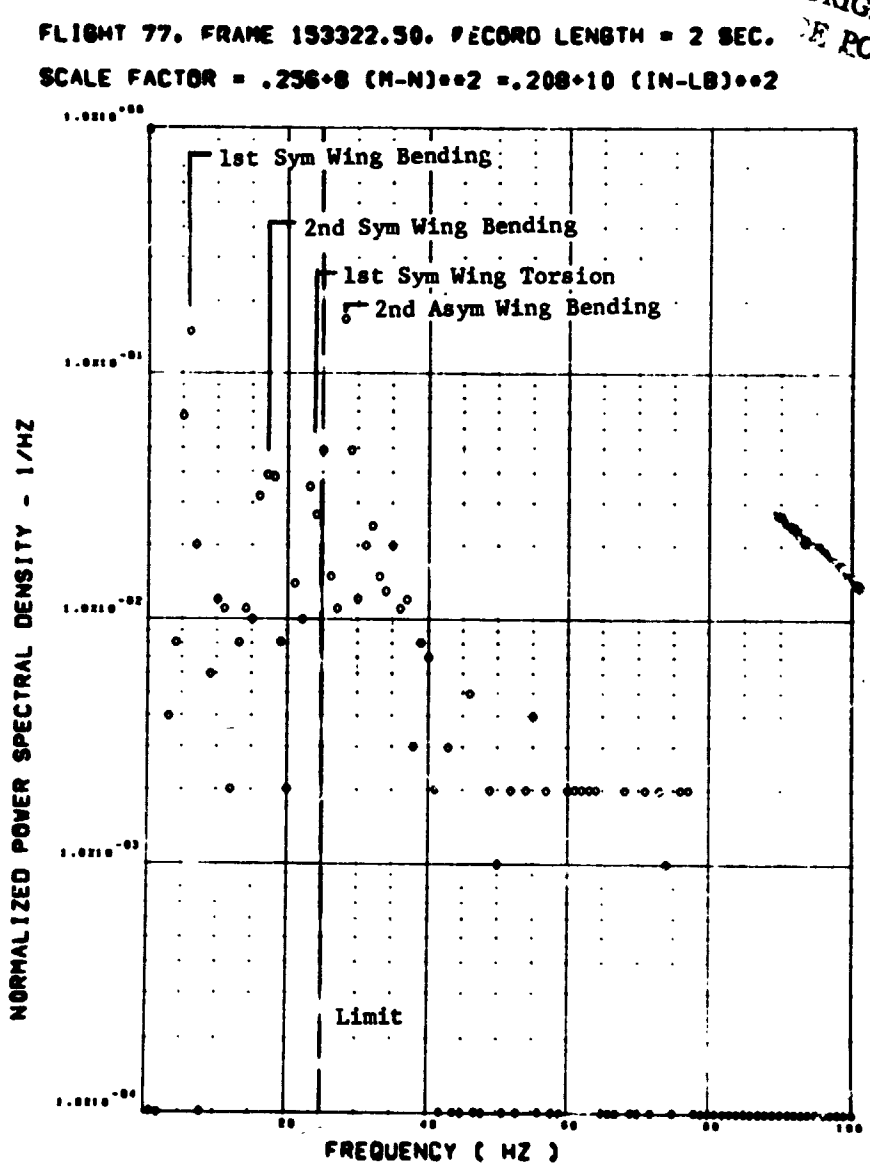

(g) SV130 BENDING MOMENT AT WING STATION 3

Figure 11. Continued

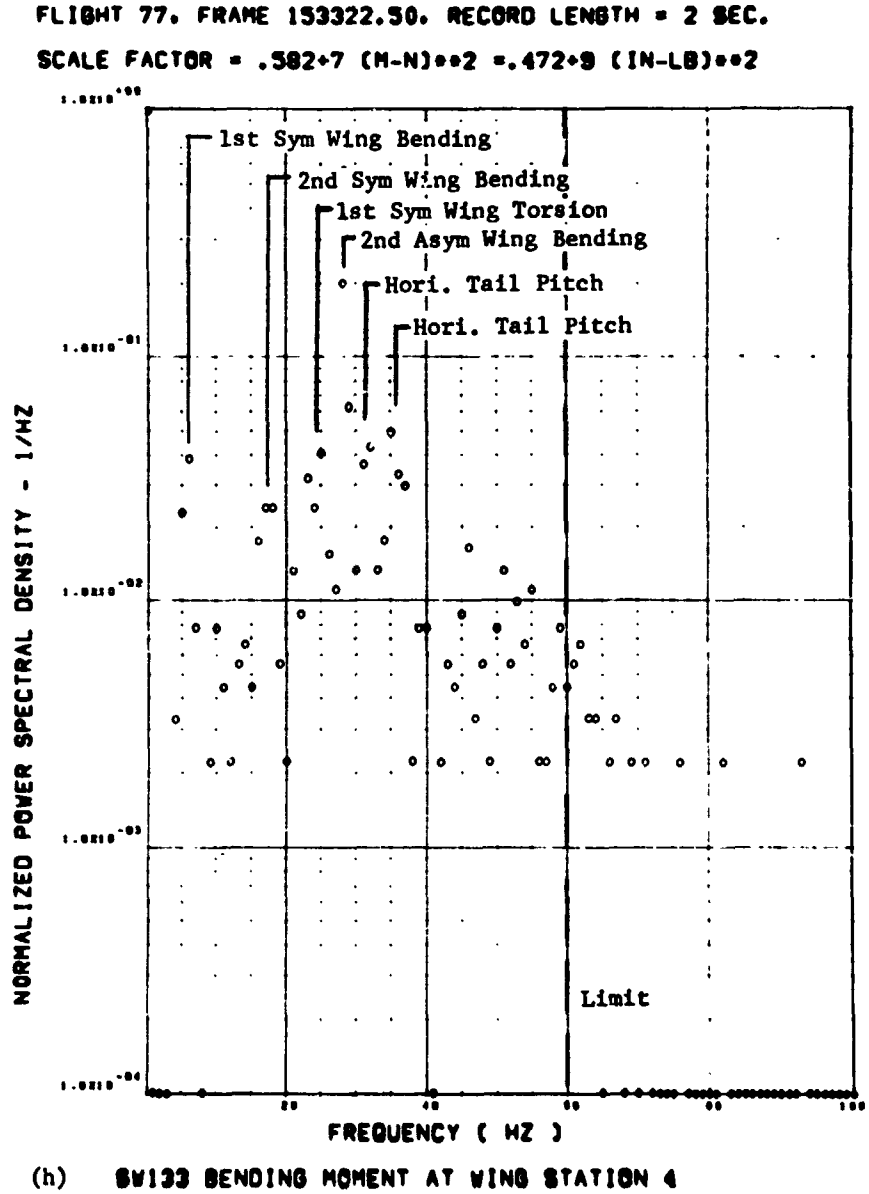

(h) SW133 BENDING MOMENT AT WING STATION 4

Figure 11. Continued

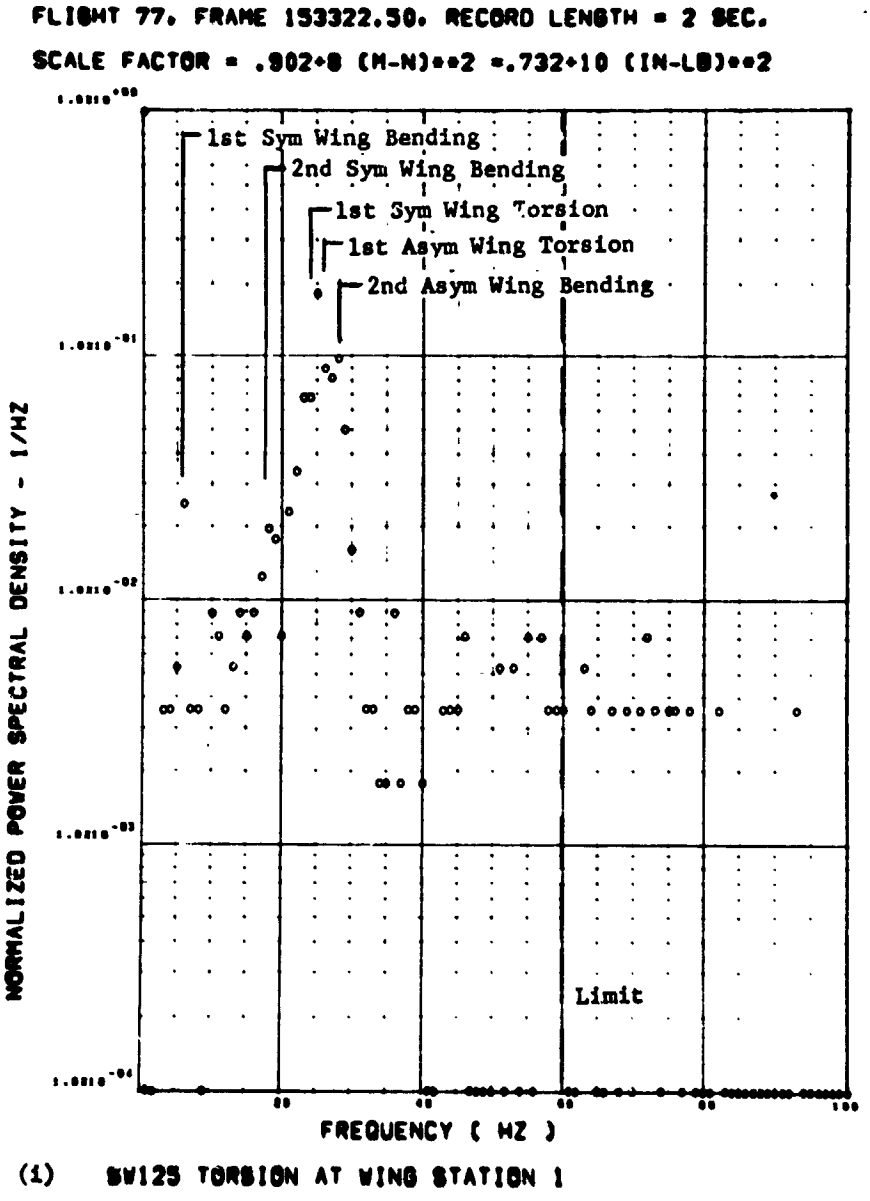

Figure 11. Continued

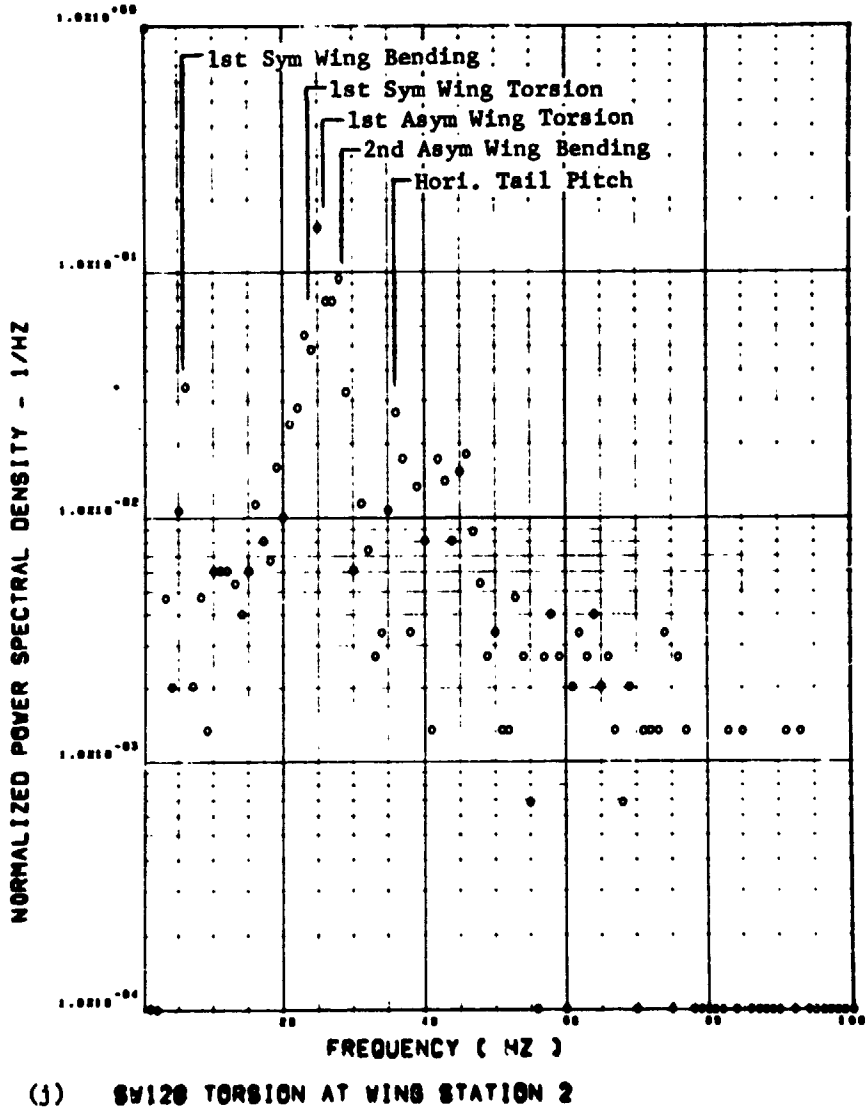

Figure 11. Continued

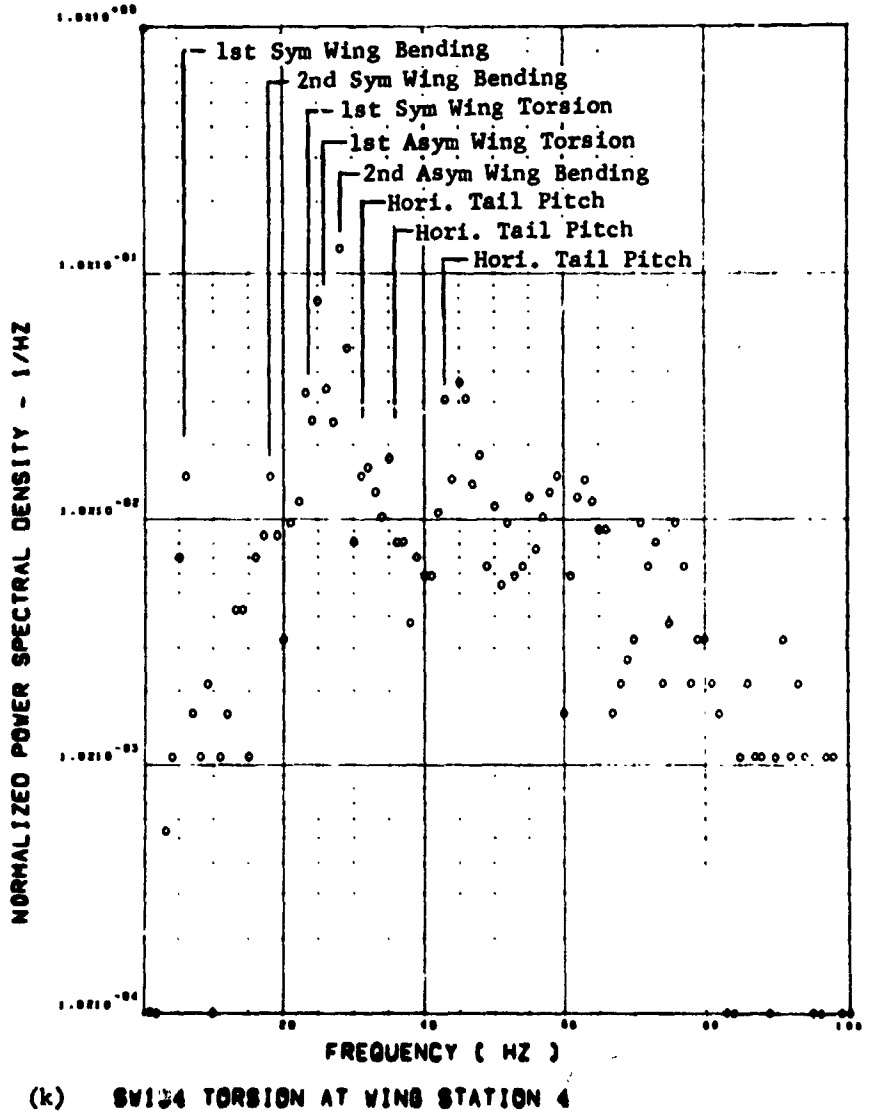

(k) SWING TORSION AT WING STATION 4

Figure 11. Continued

FLIGHT 77. FRAME 153322.50. RECORD LENGTH = 2 SEC.

SCALE FACTOR = .350+2 (G)**2

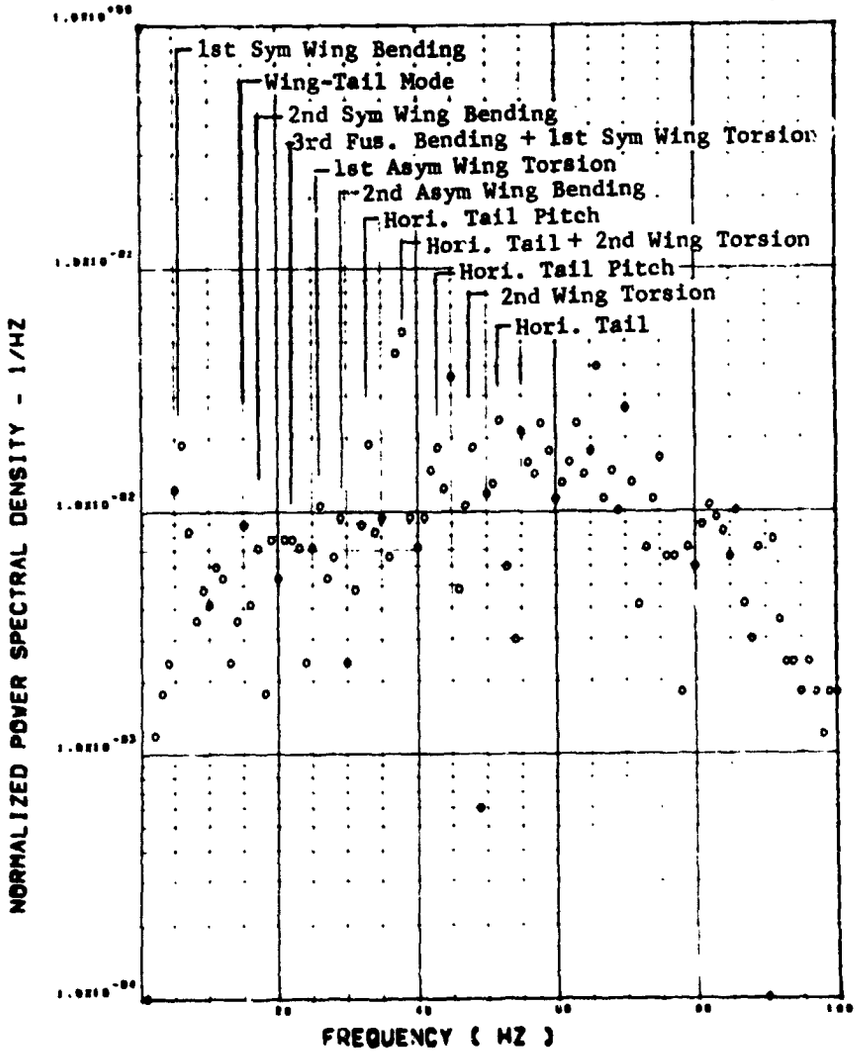

(1) AW001 L/H WING TIP VERTICAL ACCELEROMETER

Figure 11. Continued

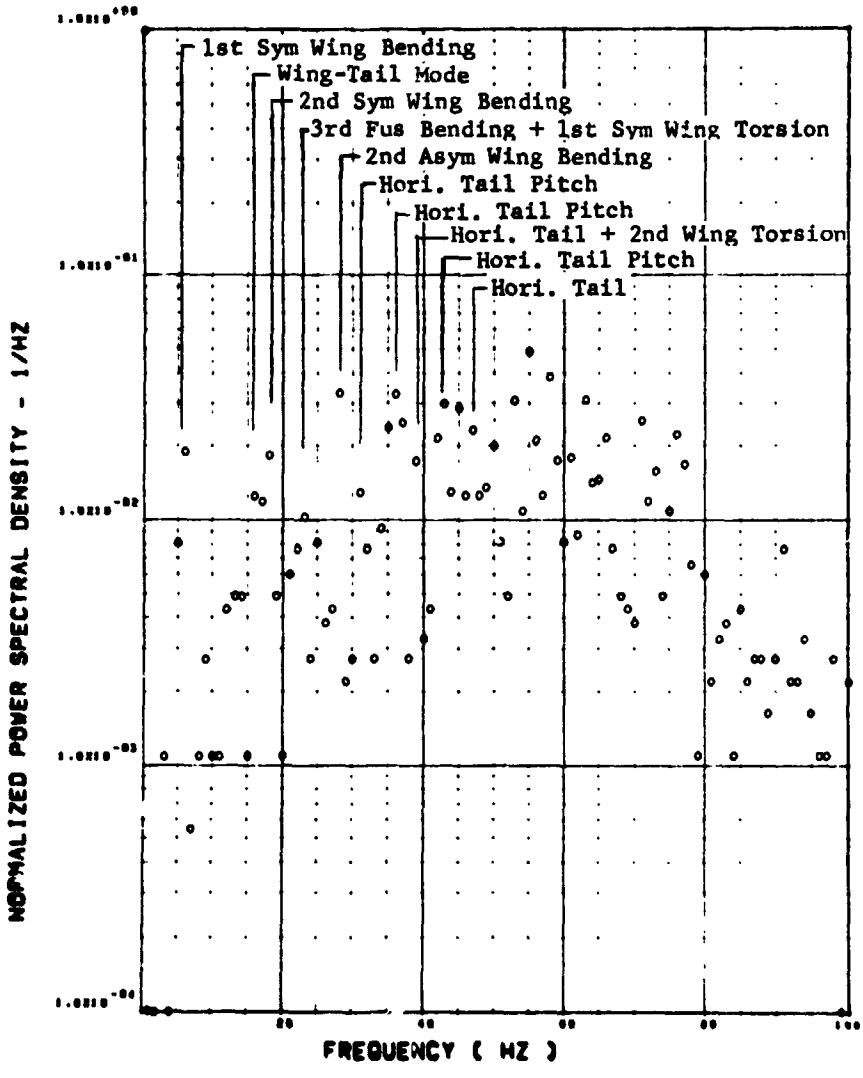

(m) AW002 R/H WING TIP VERTICAL ACCELEROMETER

Figure 11. Continued

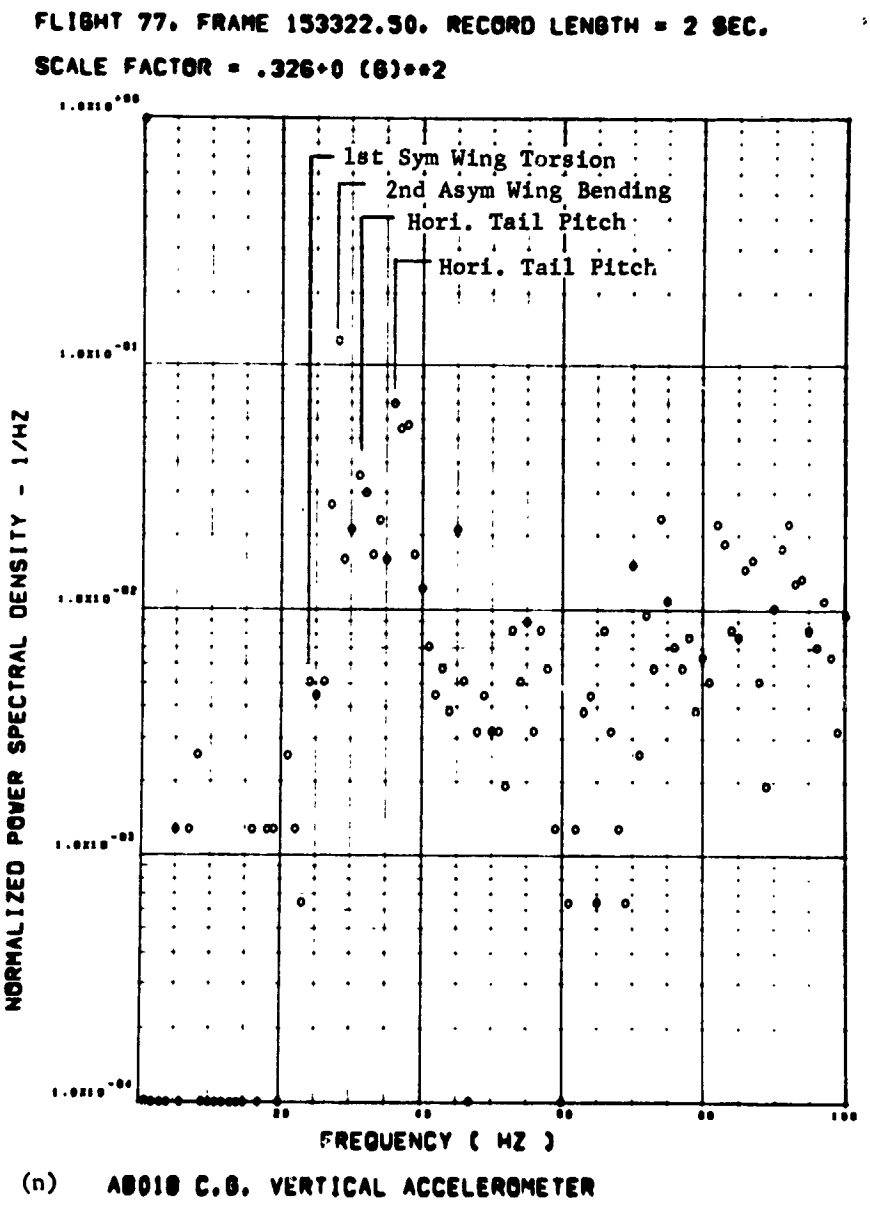

Figure 11. Continued

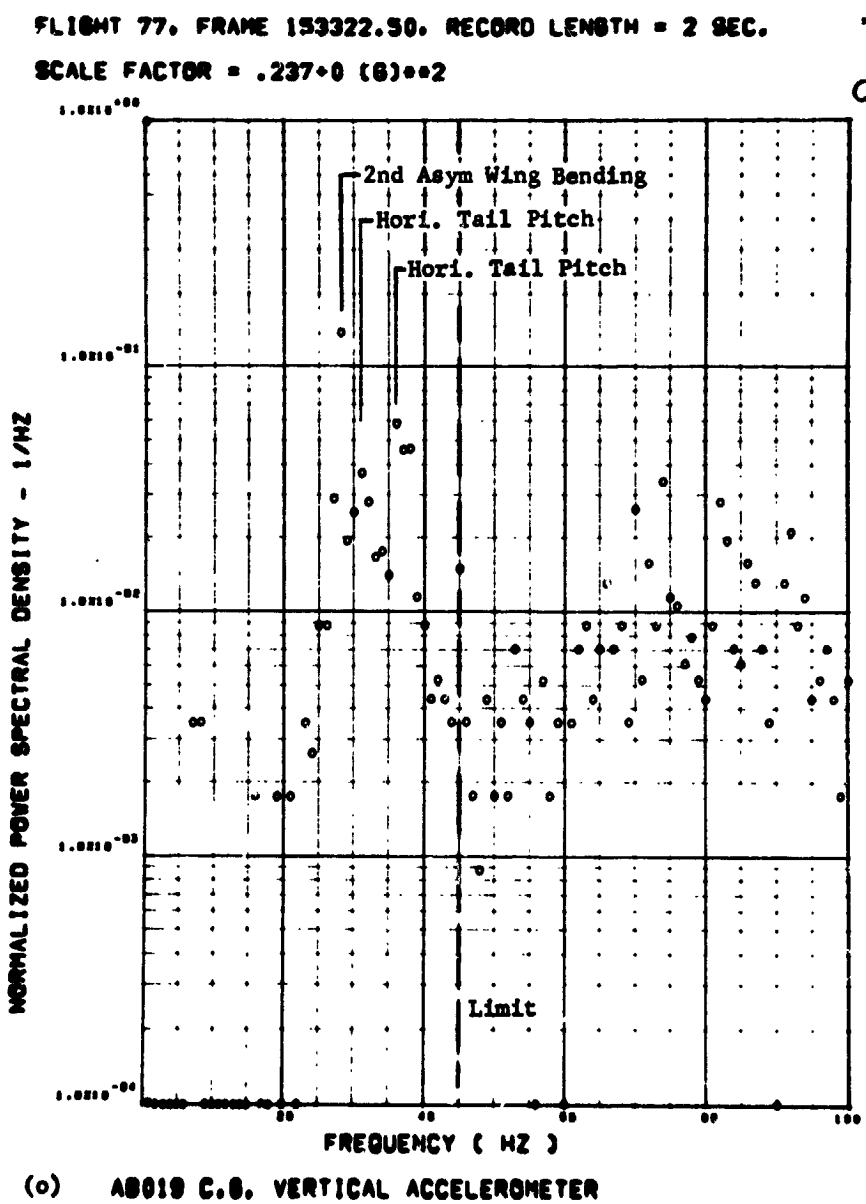

Figure 11. Continued

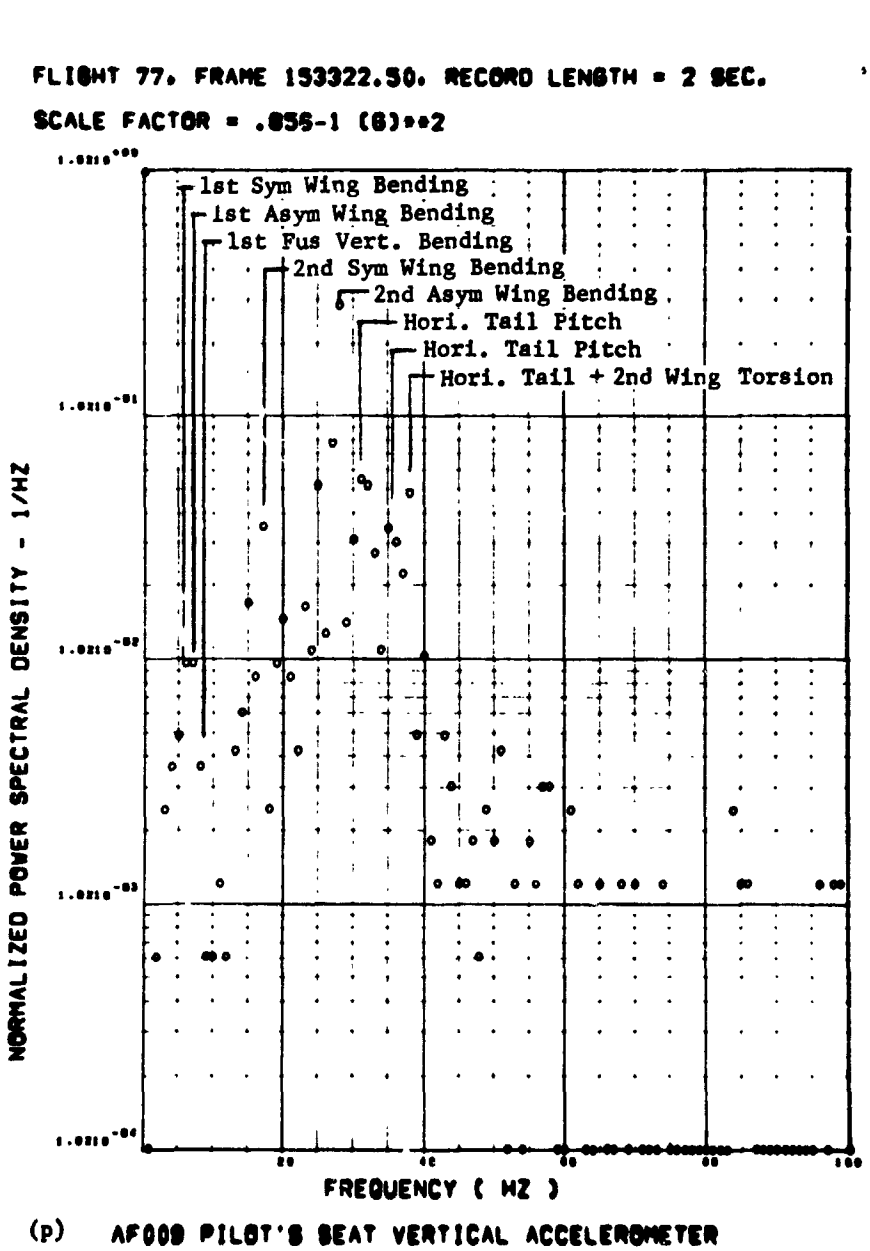

(p) AF009 PILOT'S SEAT VERTICAL ACCELEROMETER

Figure 11. Continued

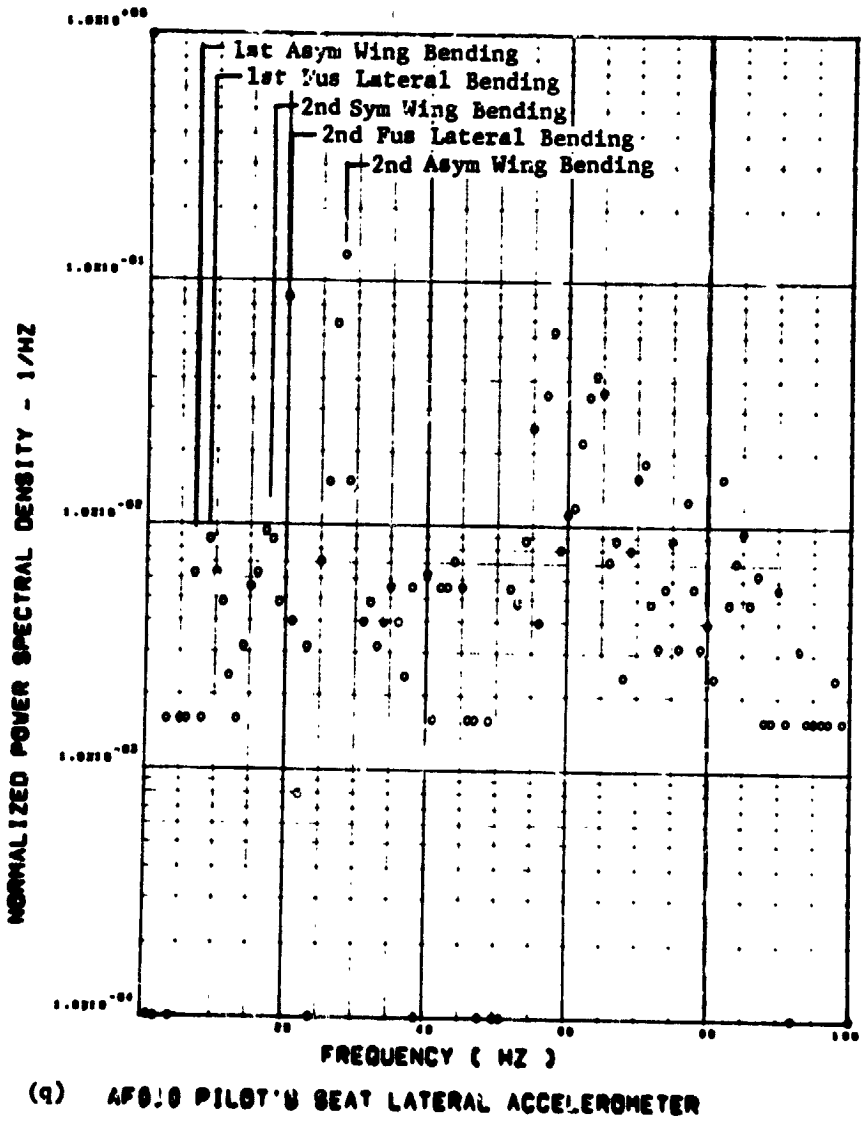

Figure 11. Continued

FLIGHT 77. FRAME 153322.50. RECORD LENGTH = 2 SEC.

SCALE FACTOR = .205-1 (G)**2

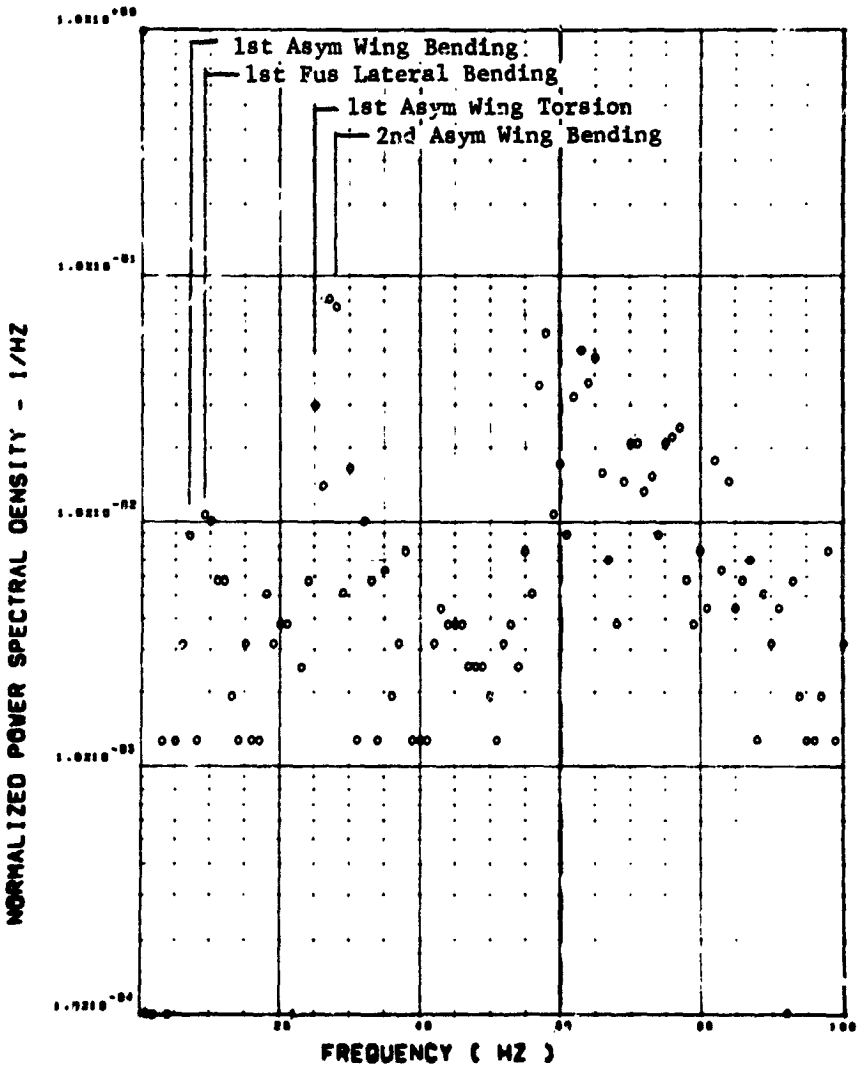

(r) AB020 C.G. LATERAL ACCELEROMETER

Figure 11. Concluded

first wing bending mode and the second antisymmetric wing bending mode predominate with significant response occurring in two horizontal tail pitch modes at higher frequencies. The response in the wing-tail and second wing bending modes are now small compared to the other modes. At Wing Station 3 the first wing bending response predominates with some response shown in wing second bending and higher order horizontal tail modes. Relatively small response is noted at the wing first torsion and the second wing antisymmetric bending frequencies. At Wing Station 4 the peak power value occurs at the second wing antisymmetric bending frequency with somewhat smaller responses in first wing bending, wing-tail, second wing bending, first wing torsion, and the horizontal tail pitch modes.

The wing bending gage data at the four wing stations show responses that are somewhat different from the shear gages. At Wing Station 1 the first wing bending mode predominates with small responses occurring in first wing torsion, second antisymmetric wing bending, and two horizontal tail pitch modes. At Wing Station 2, the first wing bending response is very strong and a small response is shown for second wing bending. Very little response is indicated at higher frequencies. At Wing Station 3, the first wing bending mode and the second antisymmetric wing bending mode responses are both large; and significant re-

sponses occur at second wing bending, first wing torsion, and the horizontal tail pitch modes. At Wing Station 4 the predominant mode is the second antisymmetric wing bending mode and smaller responses occur at first wing bending, second wing bending, first wing torsion, and the horizontal tail pitch mode frequencies.

A most significant finding of this study is indicated by the wing torsion responses. At Wing Stations 1, 2 and 4 a small response is noted in first wing bending, and the major response is in a broad band of frequencies varying from about 16 to 35 Hz with the major peak corresponding to first wing torsion at Wing Stations 1 and 2 and to second antisymmetric wing bending at Wing Station 4. This type of response is indicative of a very strong bending-torsion coupling. No torsion response data were available at Wing Station 3 for this flight, however, the response is expected to be similar in modal content to those at the other wing stations on the basis of responses noted for Flight 79, Run 9R.

The wing tip accelerometer responses for point 10 indicate that the left wing and right wing may not be receiving the same type of excitation. The left wing tip accelerometer shows a broad band of response between 40 and 80 Hz, a fairly large peak in a horizontal pitch mode at about 37 Hz and smaller peaks in the first wing bending mode and a lower order horizontal tail pitch mode. The right-hand wing tip accelerometer response shows

peaks in a wing-tail mode, second wing bending and second antisymmetric wing bending mode in addition to the peak in first wing bending and the broad band of responses between 40 and 80 Hz. The responses in first wing torsion are not large for either tip accelerometer which is somewhat surprising in view of the strong response indicated at Wing Station 4 on the right-hand wing.

The two vertical C.G. accelerometers show about the same responses with the major excitation occurring at the second antisymmetric wing bending mode and the horizontal tail pitch modes. Some significant response occurs at higher frequencies between 70 and 100 Hz. The pilot's seat vertical accelerometer shows a moderate response in a band including first wing bending and first fuselage vertical bending, and major responses in second wing bending, first wing torsion, second antisymmetric wing bending, and the horizontal tail pitch modes. The largest peak is at the second antisymmetrical wing bending frequency.

The lateral accelerometer at the pilot's seat has major responses at the second fuselage lateral bending, second antisymmetric wing bending, and a high order horizontal tail mode with only moderate responses in the first fuselage lateral bending mode and a wing-tail mode. The responses of the C.G. lateral accelerometer are similar in modal content to those at the pilot's seat except the wing-tail and second fuselage lateral bending mode responses are much smaller.

Interpretations

The right wing exhibits large responses in several modes and in particular undergoes a strong bending-torsion coupling. The C.G. and pilot seat accelerometers respond primarily at frequencies above 16 Hz despite the fact that large wing responses are noted at lower frequencies. A significant amount of the wing excitation occurs in antisymmetric modes despite the fact that the maneuver is nominally a symmetric maneuver. Further investigation brought out the fact that points 9 and 10 each include a brief roll disturbance and recovery. Figure 12 shows the roll-rate time history of the maneuver under study. After initial entry into the wind-up turn the roll-rate decays in a slightly oscillatory manner and just after 18 seconds a small spoiler input drives the roll rate positive. The rate decays rapidly to near zero and then just after 22 seconds another small spoiler input again drives the roll rate positive. Referring back to the other time histories in Figure 5(b)it can be seen that each spoiler input is preceded by a change in character of the torsion responses. This fact is particularly evident just before 22 seconds. In the sideslip angle trace in Figure 5(e)it can be seen that some oscillation occurs. All of these indications point to the occurrence of mild wing rock which possibly induces the antisymmetric responses noted in Figure 11.

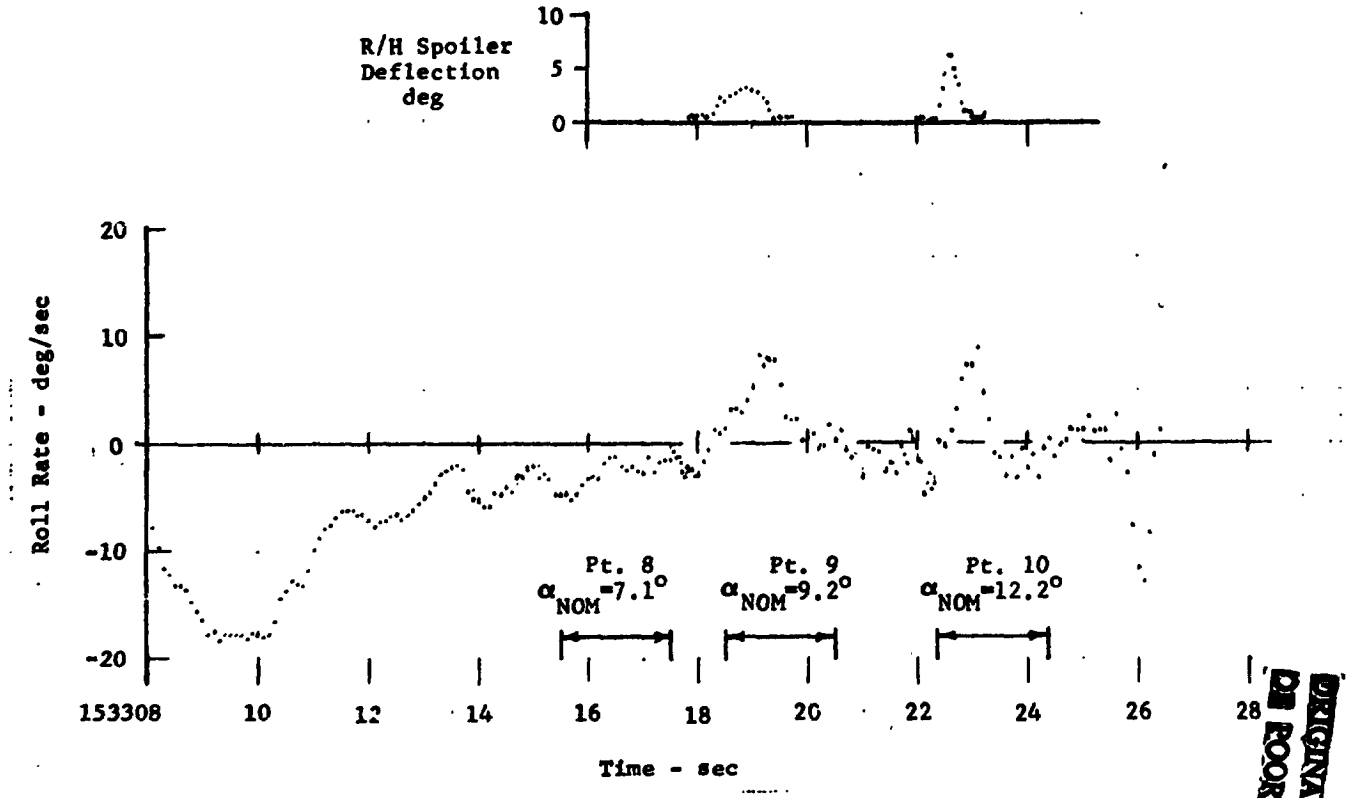

Figure 12. ROLL RATE TIME HISTORY, FLIGHT 77, RUN S&C-R

It is appropriate now to review information learned so far First, the structural responses during maneuver well into buffet are complex. Many of the natural vibration modes of the aircraft are excited and develop significant responses. Second, several different types of sensors and sensor locations are required to obtain an adequate description of the aircraft structural responses. Third, the modal content of the responses can change significantly as the penetration beyond buffet onset increases.

As a consequence of these three findings it appears unlikely that a simplified prediction method will produce accurate estimates of buffet loads and accelerations, but there is a need to assess how severe the buffet loads and accelerations are before making any judgment on what degree of accuracy may be needed.

Magnitudes of the Structural Responses

The complexity of the modal responses makes it difficult to comprehend the variations in magnitude of the structural responses by attempts to compare mode by mode. Therefore, the concept of root-mean-square (rms) values is used for this purpose. By summing the magnitudes of the power spectra over a range of frequencies and taking the square root of the sum, a measure of the total response for each item of instrumentation is achieved.

In the following discussion the rms values are evaluated over the frequency ranges from 1 to 50 Hertz or from 1 to the limit of

recorder response if less than 50 Hertz for a particular item. If rms values over a different frequency range are desired they can be calculated using the tabulated PSD data presented in NASA CR 152111.

One purpose of the rms analysis was to investigate effects of Mach number and altitude on the magnitudes of the responses. To do so, first the results of the wind up turn at M=0.70 are examined, followed with comparisons of the data for the three M=0.80 maneuvers, and lastly, with comparisons of the three maneuvers at M=0.87.

M=0.70 Results

Figures 13 through 15 present the wing strain gage responses at each of the four instrumented wing stations. The rms values are plotted at the nominal angles of attack previously assigned in Table 7 (remember, however, that each data point represents data taken over a discrete interval of time and therefore a range of angles of attack). The curves shown in Figures 13 through 15 show a remarkable consistency in the variations. In every case the trend with angle of attack is similar. In particular an inflection occurs between 11 and 12 degrees nominal angle of attack. Referring back to Figure 6(a) it can be seen that an inflection also occurs in the variation of angle of attack with time. The implication is that a wing panel leading-edge stall

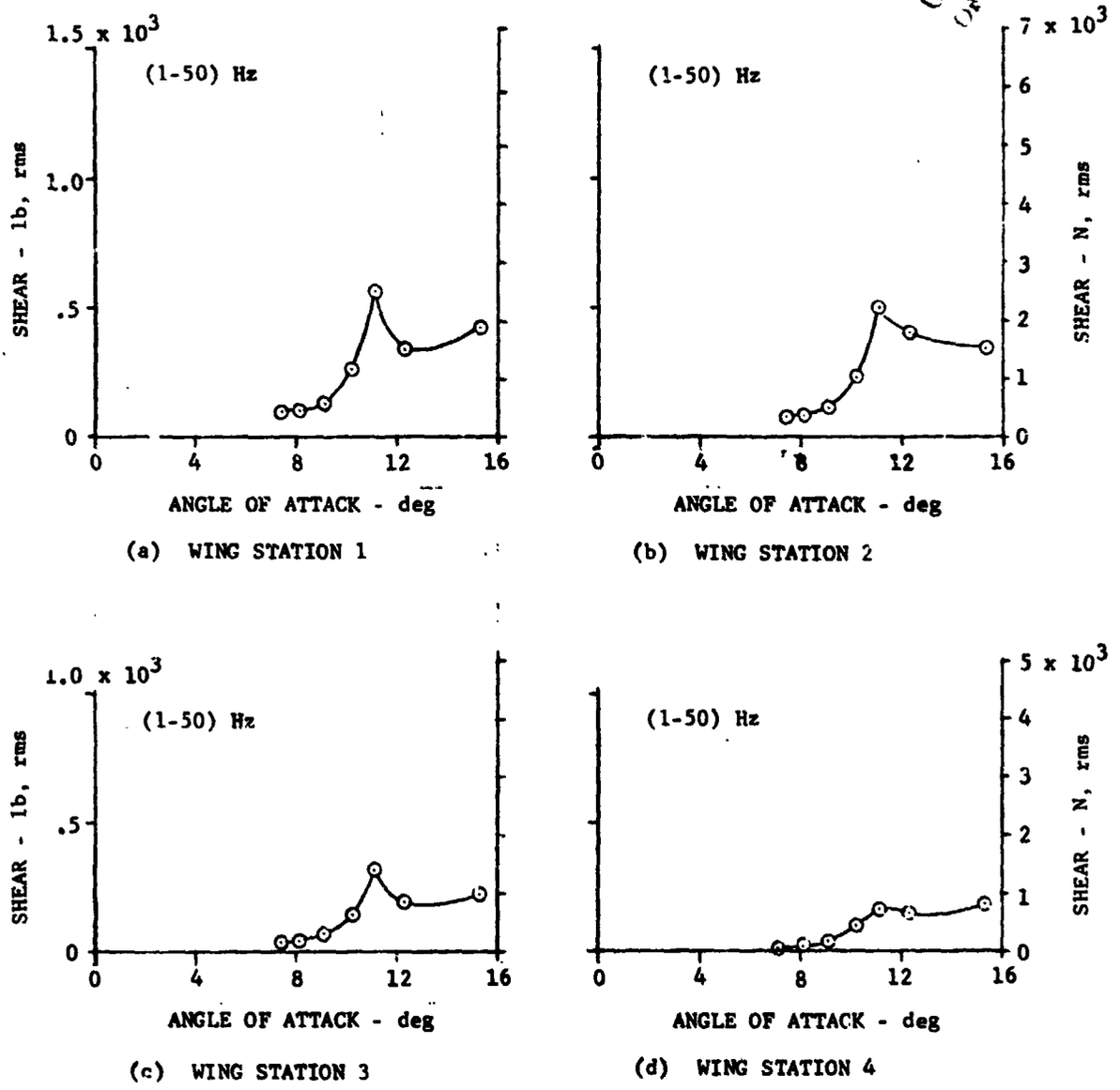

Figure 13. ROOT MEAN SQUARE VALUES OF WING SHEAR RESPONSES FOR NOMINAL MACH NUMBER = 0.70

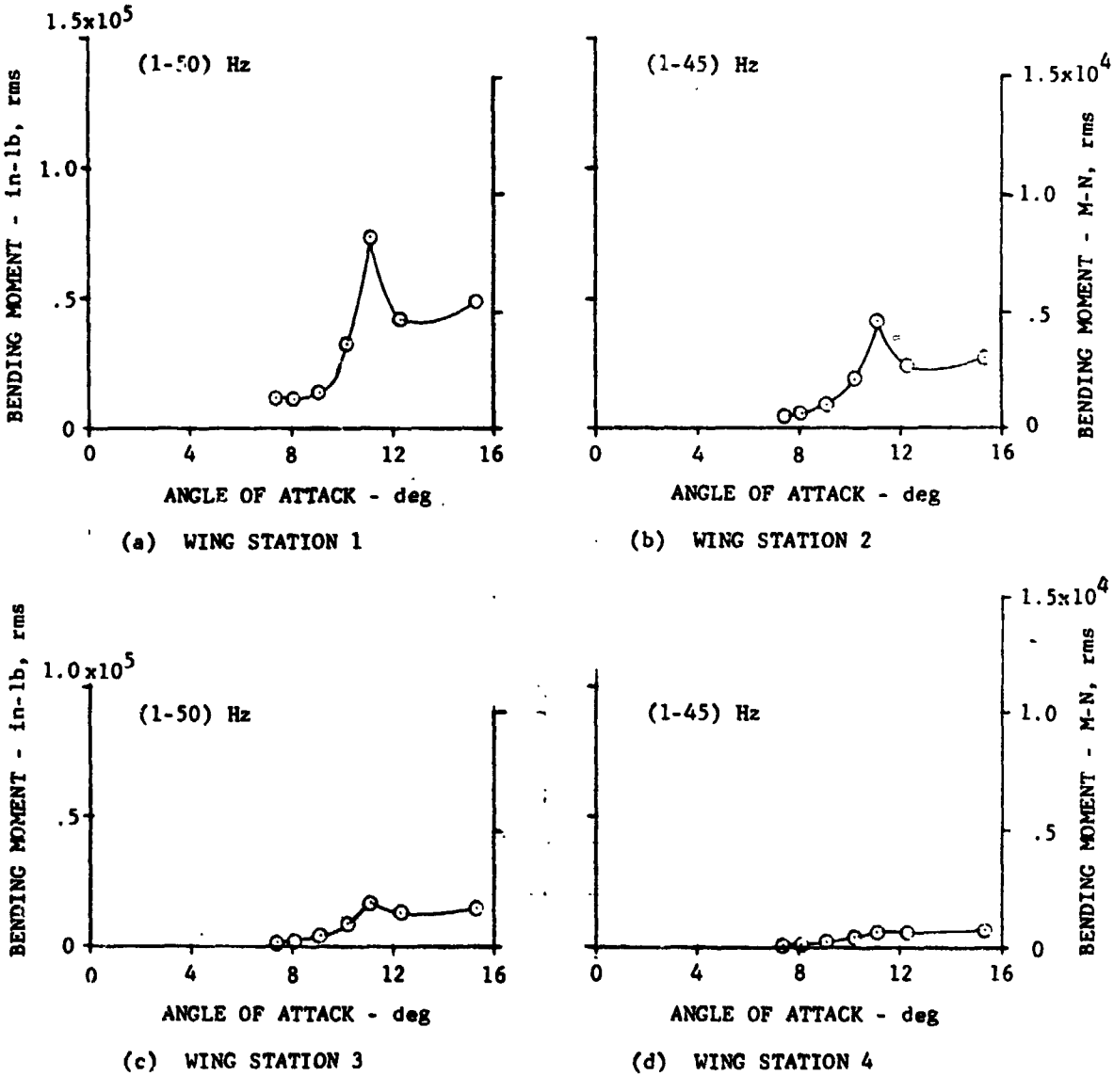

FIGURE 14. ROOT MEAN SQUARE VALUES OF WING BENDING MOMENT RESPONSES FOR NOMINAL MACH NUMBER = 0.70

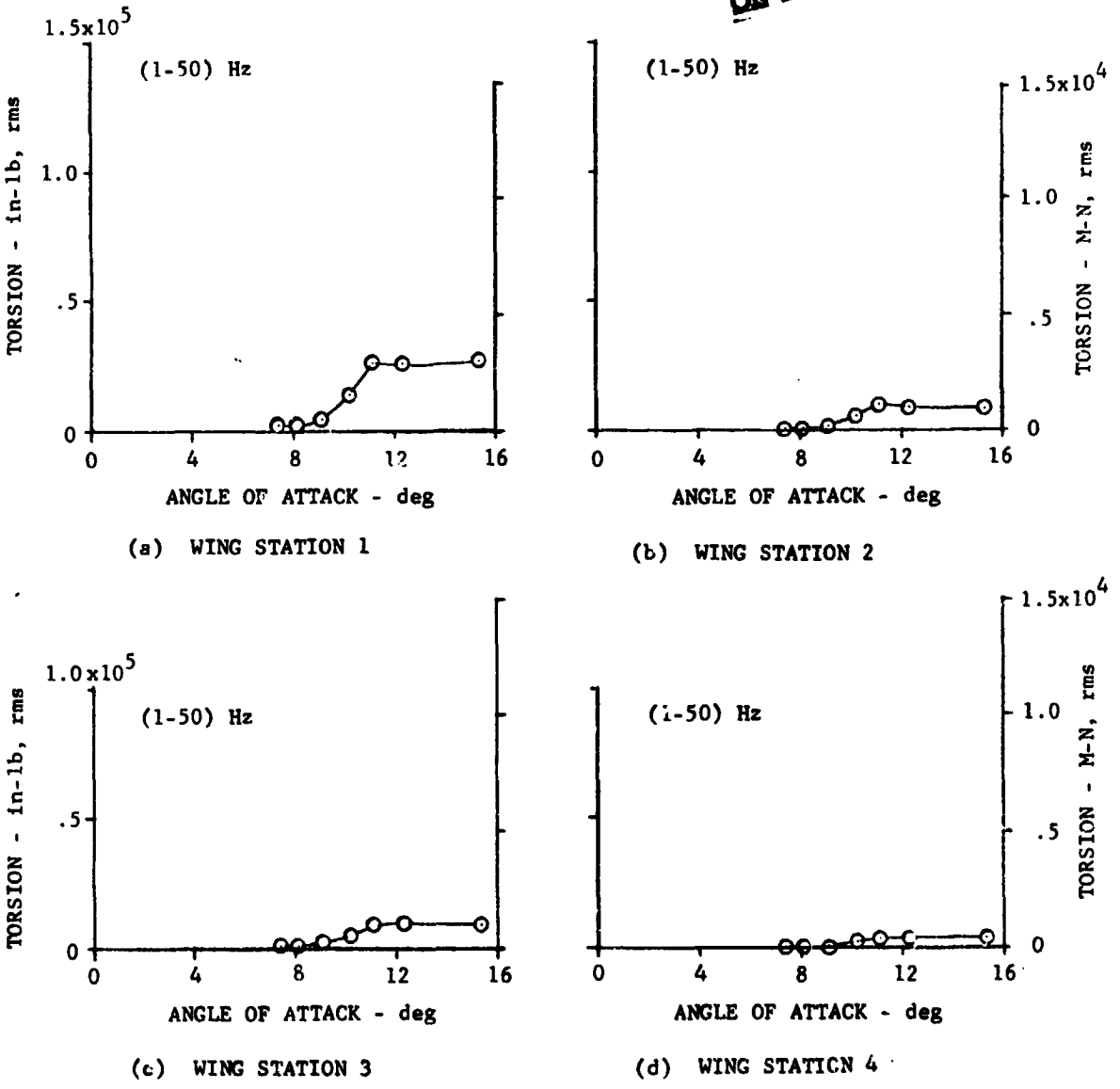

Figure 15. ROOT MEAN SQUARE VALUES OF WING TORSION RESPONSES FOR NOMINAL MACH NUMBER = 0.70

has occurred. Figures 13 and 14 show that the rms values of shear and bending moment decrease rather abruptly beyond 11 degrees and then rise again somewhat. Figure 15 shows that the torsion values tend to remain nearly constant above 11 degrees. Inspection of the PSD data for this maneuver (NASA CR-152110) revealed that between 11 and 12 degrees there is a shift in bending moment response from the first wing bending mode to higher frequency bending modes, particularly outboard on the wing. Finally the time histories for the right-hand wing spoilers presented in the Appendix show that a small and short duration spoiler deflection occurs just after the time sample associated with the data point represented at 11 degrees angle of attack. All this evidence points to a mild wing rock occurring during development of the leading-edge stall.

Figure 16 presents the accelerometer responses obtained during the wind up turn maneuver of Flight 48, Run 6. Figures 16(a) through 16(d) show the vertical accelerometer responses at the right-hand wing tip, the center of gravity and the pilot's seat. The similarity of the trends in variations of the responses with angle of attack is again noted. All the vertical accelerometers show an inflection occurring between 11 and 12 degrees just as the wing strain gage responses did. The structural characteristics of the aircraft are such that a significant

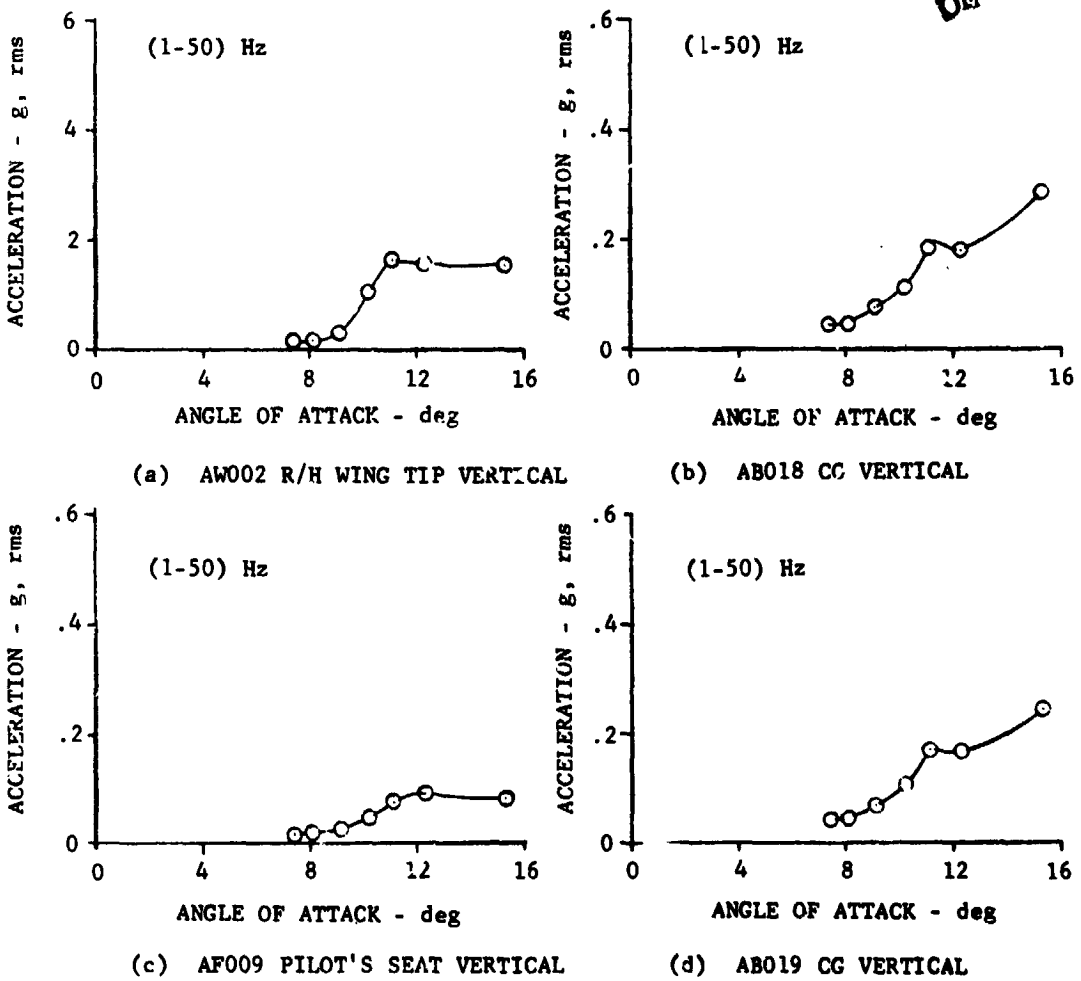

Figure 16. ROOT MEAN SQUARE VALUES OF ACCELEROMETER RESPONSES FOR NOMINAL MACH NUMBER = 0.70

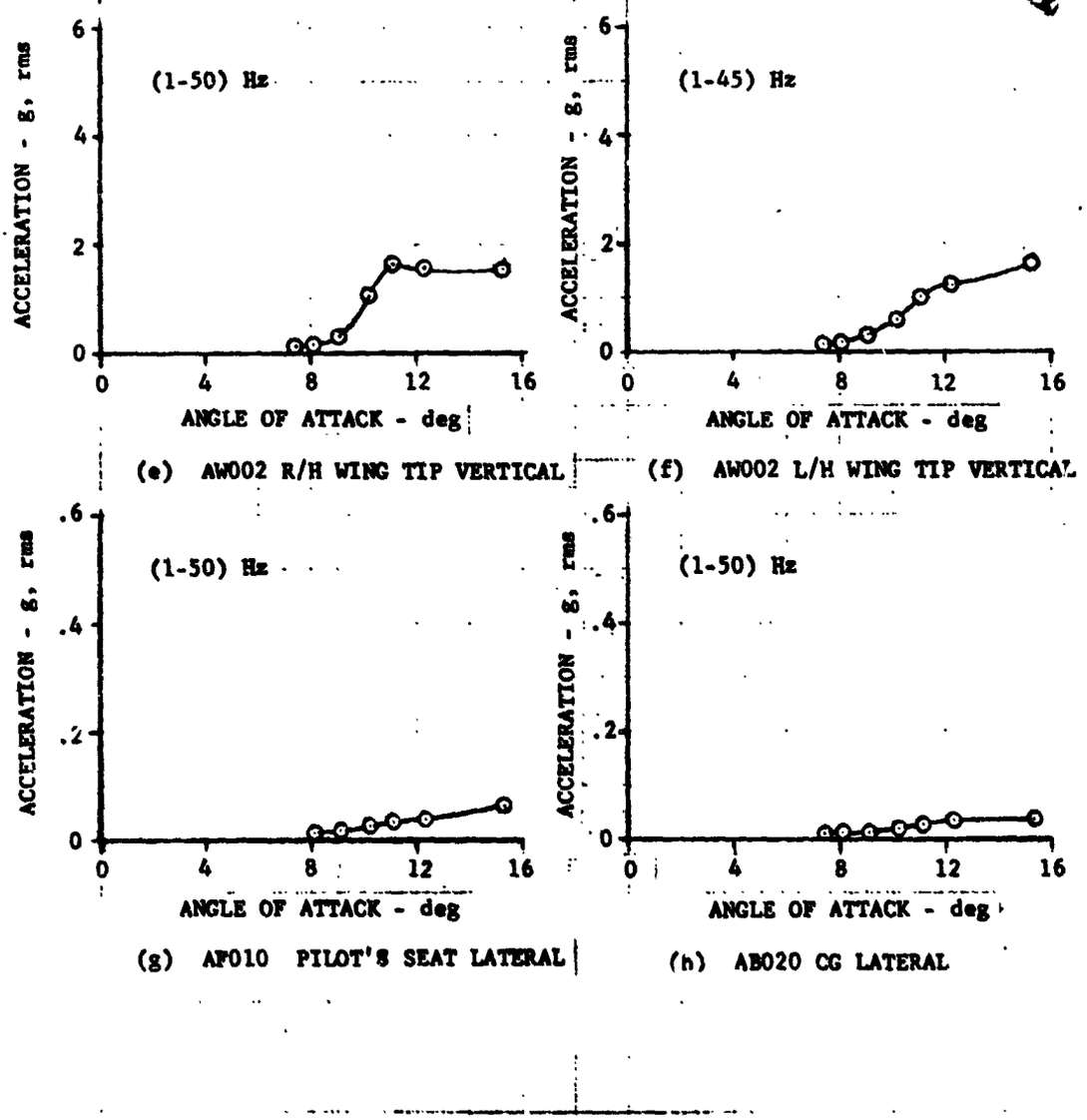

Figure 16. CONCLUDED

reduction in rms magnitudes of the response occurs between the wing tip and the center of gravity and a further reduction occurs between the center of gravity and the pilot's seat.

Figures 16(e) through 16(h) present the vertical accelerometer responses for both the right and left hand wing tip and the lateral accelerometer responses at the pilot's seat and the center of gravity. Comparing Figures 16(e) and 16(f) it is seen that the responses at the two wing tips are similar at the lower angles of attack and then differ somewhat at the higher angles of attack. The differences may be attributed to a slightly different progression of flow separation on the two wings which is accentuated by the spoiler deflection on the right hand wing between the data points shown for 11 and 12 degrees angle of attack.

Figures 16(g) and 16(h) show that the lateral accelerations are small at the pilot's seat and particularly so at the center of gravity.

M = 0.80 Results

Figures 17, 18, and 19 present the wing strain gage responses and Figure 20 the accelerometer responses for the three maneuvers performed at approximately M = 0.80 but at different altitudes. Four sets of data are shown because both one-second and two-second samples were analyzed for the wind up turn maneu-

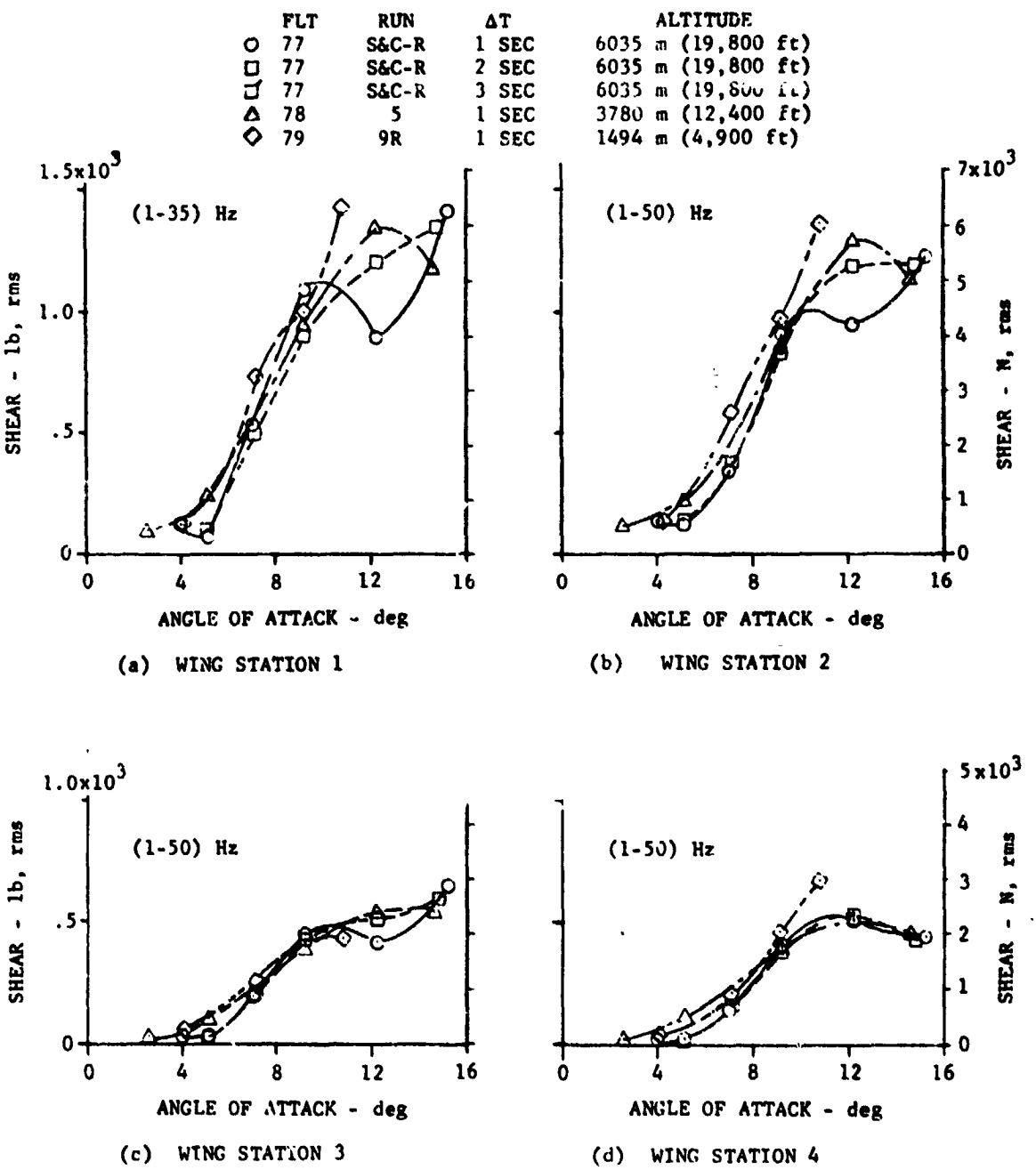

Figure 17. ROOT MEAN SQUARE VALUES OF WING SHEAR RESPONSES FOR NOMINAL MACH NUMBER = 0.80

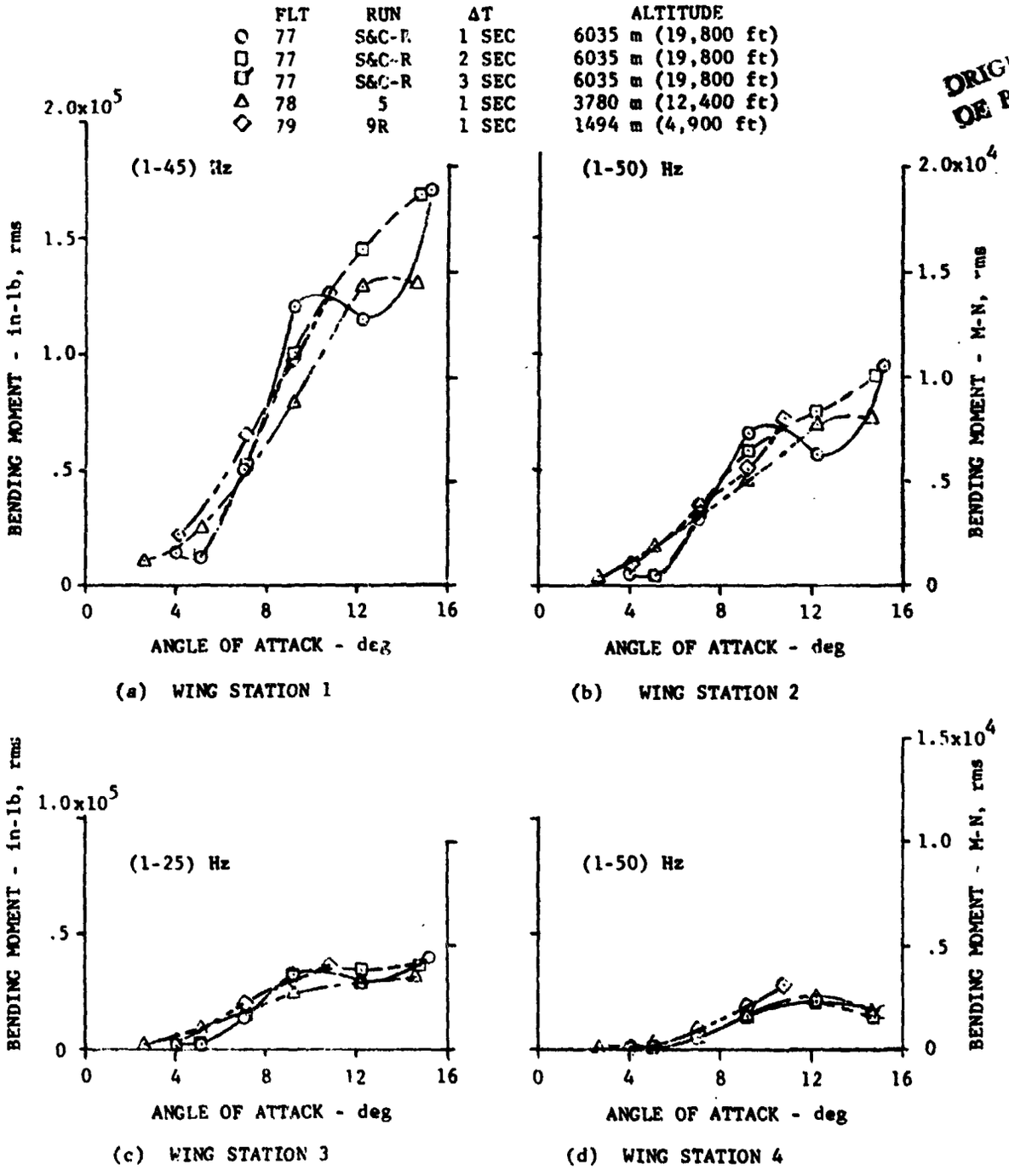

Figure 18. ROOT MEAN SQUARE VALUES OF WING BENDING MOMENT RESPONSES FOR NOMINAL MACH NUMBER = 0.80

	FLT	RUN	ΔT	ALTITUDE
○	77	S&C-R	1 SEC	6035 m (19,800 ft)
□	77	S&C-R	2 SEC	5035 m (19,800 ft)
▽	77	S&C-R	3 SEC	6035 m (19,800 ft)
△	78	5	1 SEC	3780 m (12,400 ft)
◇	79	9R	1 SEC	1494 m (4,900 ft)

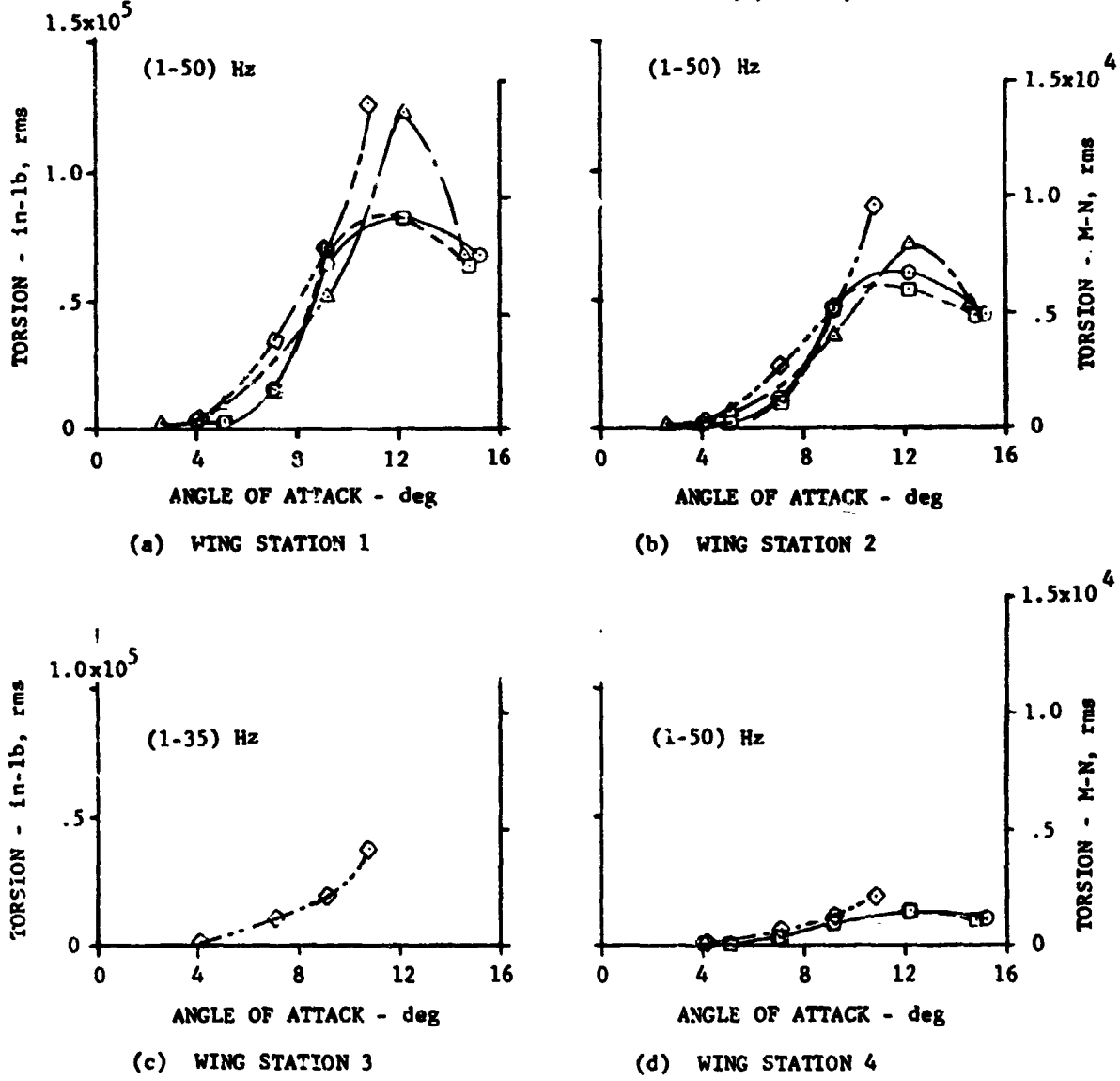

Figure 19. ROOT MEAN SQUARE VALUES OF WING TORSION RESPONSES FOR NOMINAL MACH NUMBER = 0.80

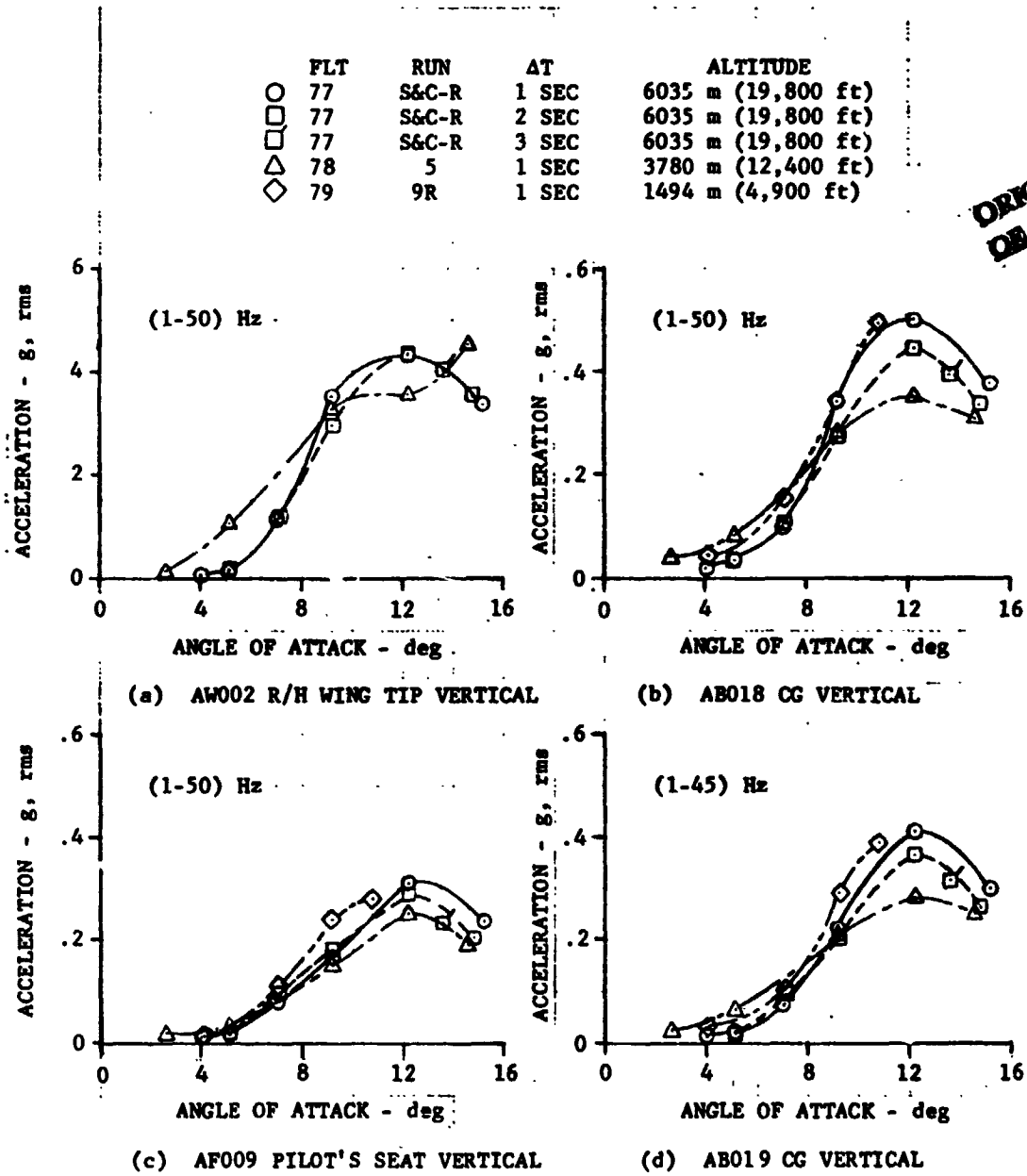

Figure 20. ROOT MEAN SQUARE VALUES OF ACCELEROMETER RESPONSES FOR NOMINAL MACH NUMBER = 0.80

	FLT	RUN	ΔT	ALTITUDE
○	77	S&C-R	1 SEC	6035 m (19,800 ft)
□	77	S&C-R	2 SEC	6035 m (19,800 ft)
□	77	S&C-R	3 SEC	6035 m (19,800 ft)
△	78	5	1 SEC	3780 m (12,400 ft)
◇	79	9R	1 SEC	1494 m (4,900 ft)

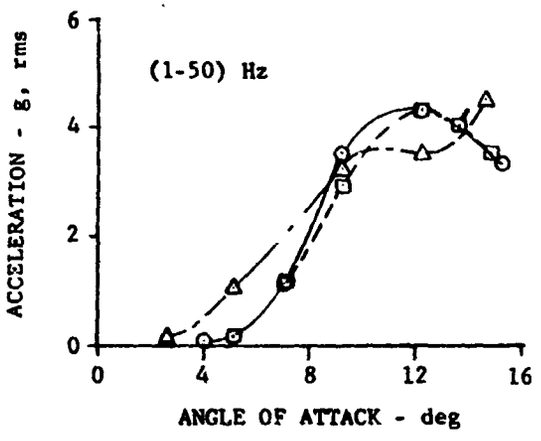

(e) AW002 R/H WING TIP VERTICAL

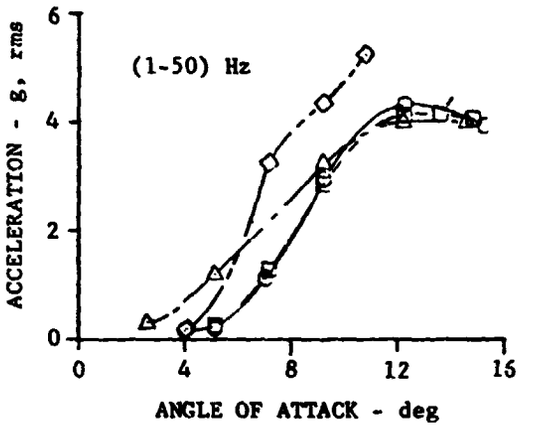

(f) AW001 L/H WING TIP VERTICAL

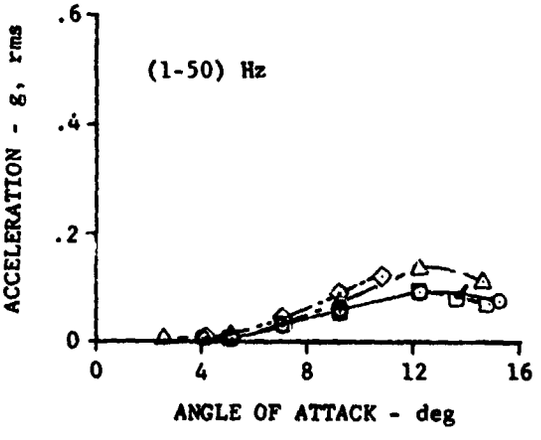

(g) AF010 PILOT'S SEAT LATERAL

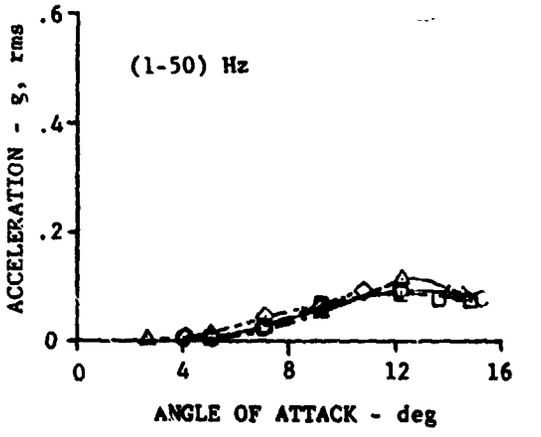

(h) AB020 CG LATERAL

Figure 20. CONCLUDED

ver of Flight 77, Run S&C-R. These are shown on the plots as the circles and squares, respectively. These results will be discussed first before considering the responses for the other maneuvers. While the one-second and two-second data are generally similar in magnitude, some differences do exist particularly in the high angle of attack region at about 12 degrees for the shear and bending moments. The fact that a mild wing rock occurs during this maneuver has previously been discussed under the power spectral density analysis. It is apparent that the two-second samples tend to smooth the variation of response with angle of attack for Wing Stations 1, 2, and 3, but there is little difference at Wing Station 4. The torsional responses tend to be more nearly the same for the one-second and two-second sample data at each angle of attack.

The general trends of the variations in response with angle of attack are different from the trends at M = 0.70 in two ways. First buffet onset occurs at lower angle of attack (about 5 degrees) which is expected for this particular wing leading-edge sweep. The initial flow separation is shock-induced at this condition. Second, the increase in the responses with angle of attack is generally more gradual even though the maximum measured rms values are much larger than those at M = 0.70. Comparison of the shear and bending moment response magnitude variations

with wing station indicate that the flow separation is primarily outboard of Wing Station 2, since there is little change in rms values of shear between Stations 1 and 2 but a large change in rms values of bending moment between those stations. The torsion responses at Wing Stations 1, 2, and 4 all have maximums at about 12 degrees angle of attack and then decrease, whereas at M = 0.70 the torsion data indicated a nearly constant response level at high angle of attack. Torsion data are not available at Wing Station 3 for Flight 77.

The vertical accelerometer responses shown in Figures 20(a) through 20(d) show little difference in the right-hand wing tip accelerations for the one- and two-second samples, fairly significant differences for the center of gravity measurements and smaller differences for the pilot's seat measurements.

The wing tip responses are three times larger at M = 0.80 than they were at M = 0.70, whereas the center of gravity responses and the pilot seat responses are about twice larger. The variations with angle of attack are similar to each other with peak magnitudes occurring at about 12 degrees.

Figures 20(e) and 20(f) show the accelerations at the right-hand and left-hand wing tips in a side-by-side presentation to allow comparison by inspection. Note that the variations with angle of attack and the peak magnitudes are generally similar for

both wing tips for Flight 77, Run S&C-R, but the left-hand wing shows somewhat more response than the right-hand wing at the highest angle of attack.

Figures 20(g) and 20(h) present the lateral acceleration responses at the pilot's seat and the center of gravity, respectively. For this maneuver the responses show similar trends with angle of attack and the magnitudes are nearly the same at the two locations. The lateral accelerations also peak at about 12 degrees angle of attack, and are about one-fourth of the value of the vertical acceleration at the center of gravity and one-third the values of vertical accelerations at the pilot's seat. The peak magnitudes of the lateral accelerations are about 3 times the values at M = 0.70.

Summarizing the differences between responses obtained during the wind up turn maneuvers at M=0.70 and M=0.80 it was found that the differences in flow separation conditions leads to buffet onset at lower angle of attack at M = 0.80, and more gradual increases in the responses with angle of attack. The minimum measured responses, however, are much larger than those measured at M = 0.70 and cannot be explained solely on the basis of the increase in dynamic pressure.

Next, the effects of altitude (or dynamic pressure) on the responses are examined. Figures 17 through 19 also present

wing strain gage data and Figure 20 the accelerations for two pull up maneuvers performed at approximately M = 0.8 — one at about 3800 m and the other at about 1500 m. Data for these maneuvers are shown as triangles and diamonds, respectively. In general the responses for the lower altitude maneuvers are higher for a given angle of attack. A cursory examination of the bending moment and torsion responses indicates the magnitudes are approximately related between the two pull up maneuvers by the dynamic pressure values. Since the power spectra indicate the bending moment responses for the two inboard stations are predominantly in the first wing bending mode, one can apply the simple linear elastic system analysis described in Reference 20. That analysis indicates that damping is (1) primarily structural if the response relationship is a direct function of dynamic pressure or (2) primarily aerodynamic if the relationship is a square root function of dynamic pressure. The measurements discussed above would indicate that structural damping predominates in the first wing bending mode for the two high-g pull up maneuvers at M = 0.80.

It is obvious that the response data for the wind up turn do not belong to the same family of curves as the data for the two pull up maneuvers. There are several pertinent factors which can alter the response such that the expected relationship did not

apply. First the difference in pitch rate between the wind-up turn and the pullups is a possible cause. Second, the gross weight for the wind-up turn was much lower than those for the pullups. Third is the fact that the wing has a different aeroelastic shape (twist distribution) for each maneuver altitude and the progression of flow separation can be significantly different. This aspect of the problem will be explored further as we examine the higher Mach number results.

M ~ 0.87 Results

Figures 21 through 24 present the wing strain gage and accelerometer responses for the three maneuvers performed at Mach numbers of about 0.87. Because these maneuvers were all rather abrupt, the rms magnitudes of response were expected to be similar in trend with angle of attack and to correlate with altitude. However, that did not happen. The results of the roller coaster maneuver performed at high altitude will be examined first, followed by further examination of the effect of Mach number on the variations of response with angle of attack.

The maximum magnitudes of shear and bending moment response are about the same as those measured at M=0.80 but the values for torsion response are somewhat lower. There is an indication that a peak might occur in some of the responses just above the

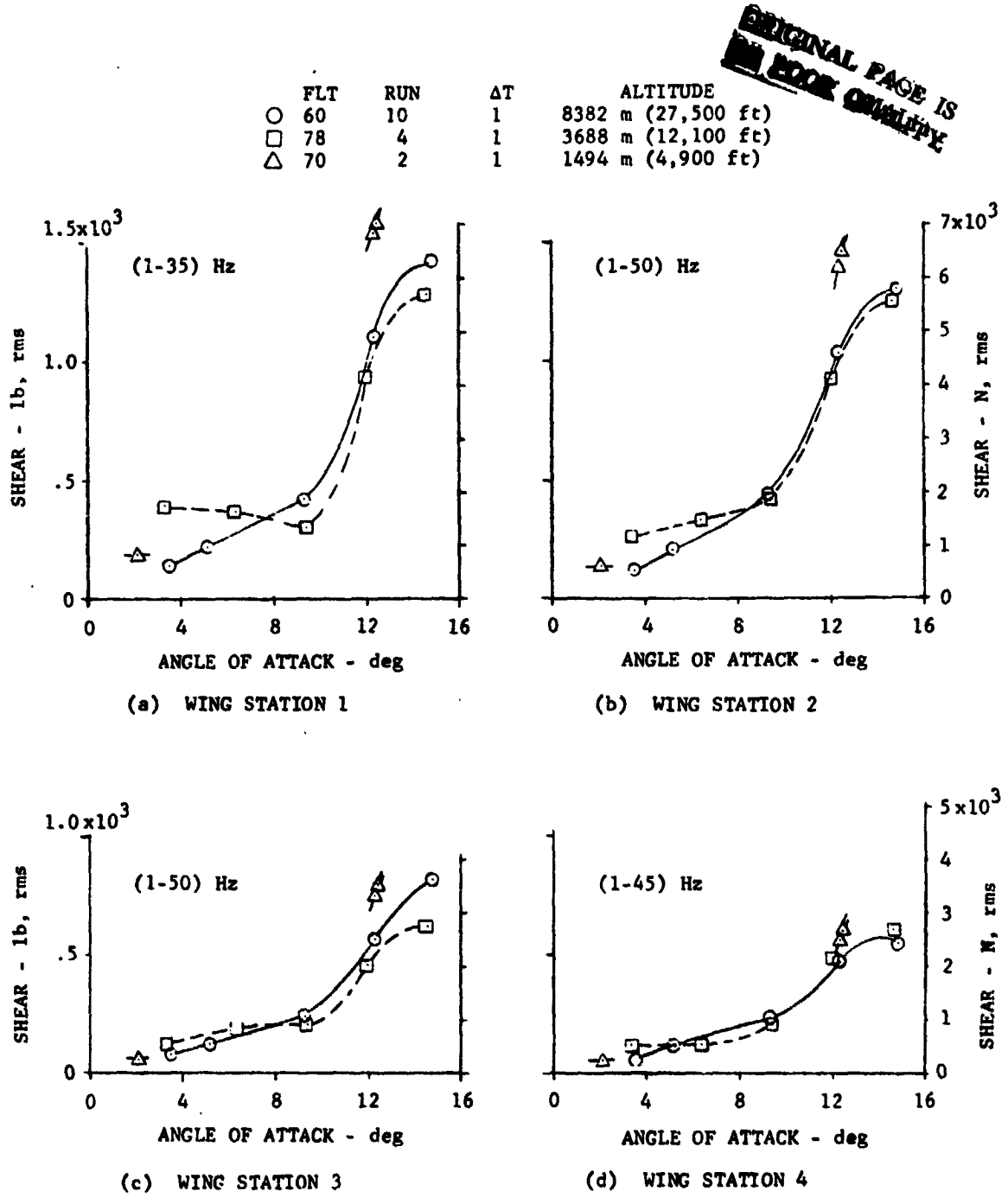

Figure 21. ROOT MEAN SQUARE VALUES OF WING SHEAR RESPONSES FOR NOMINAL MACH NUMBER = 0.87

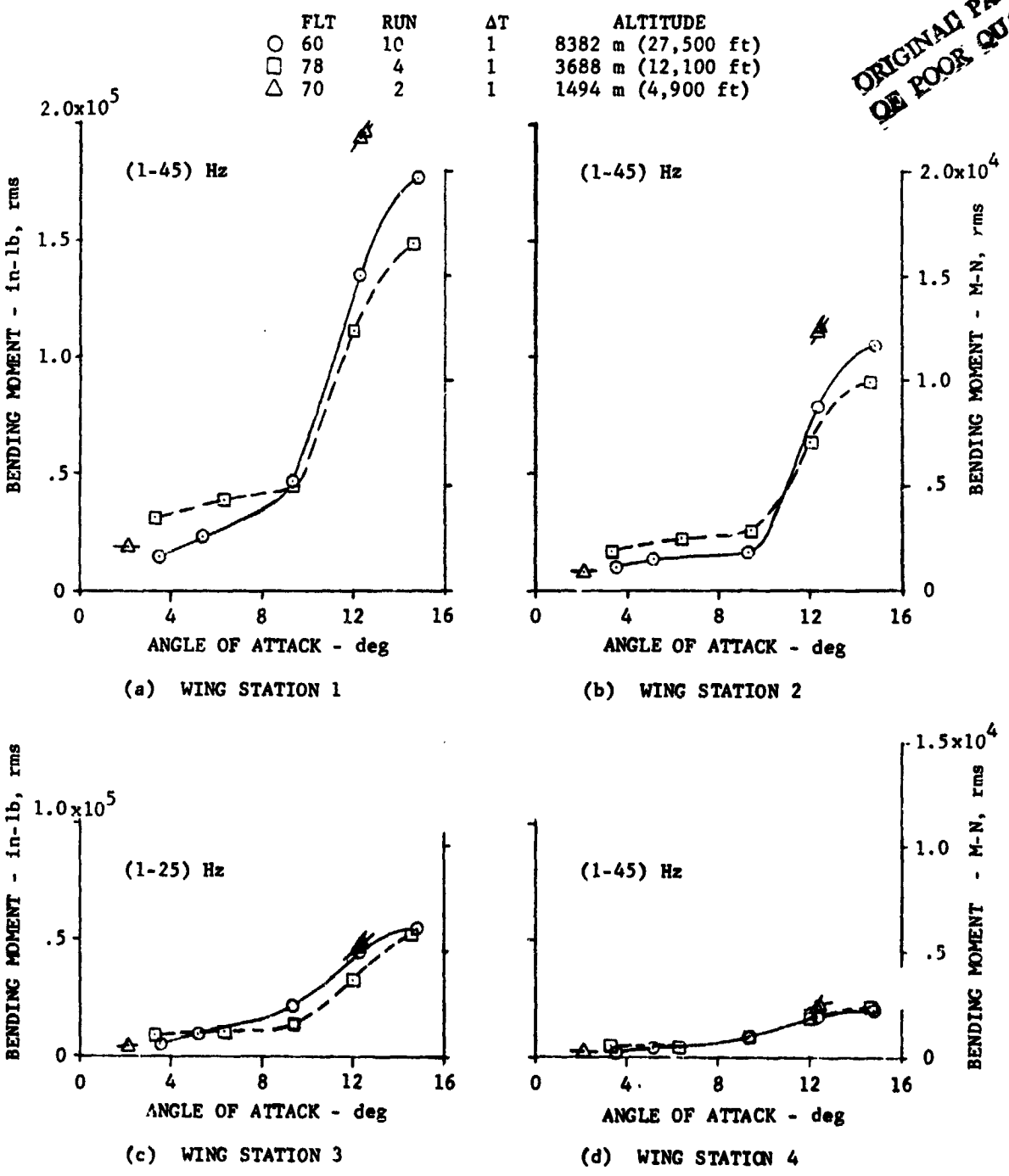

Figure 22. ROOT MEAN SQUARE VALUES OF WING BENDING MOMENT RESPONSES FOR NOMINAL MACH NUMBER = 0.87

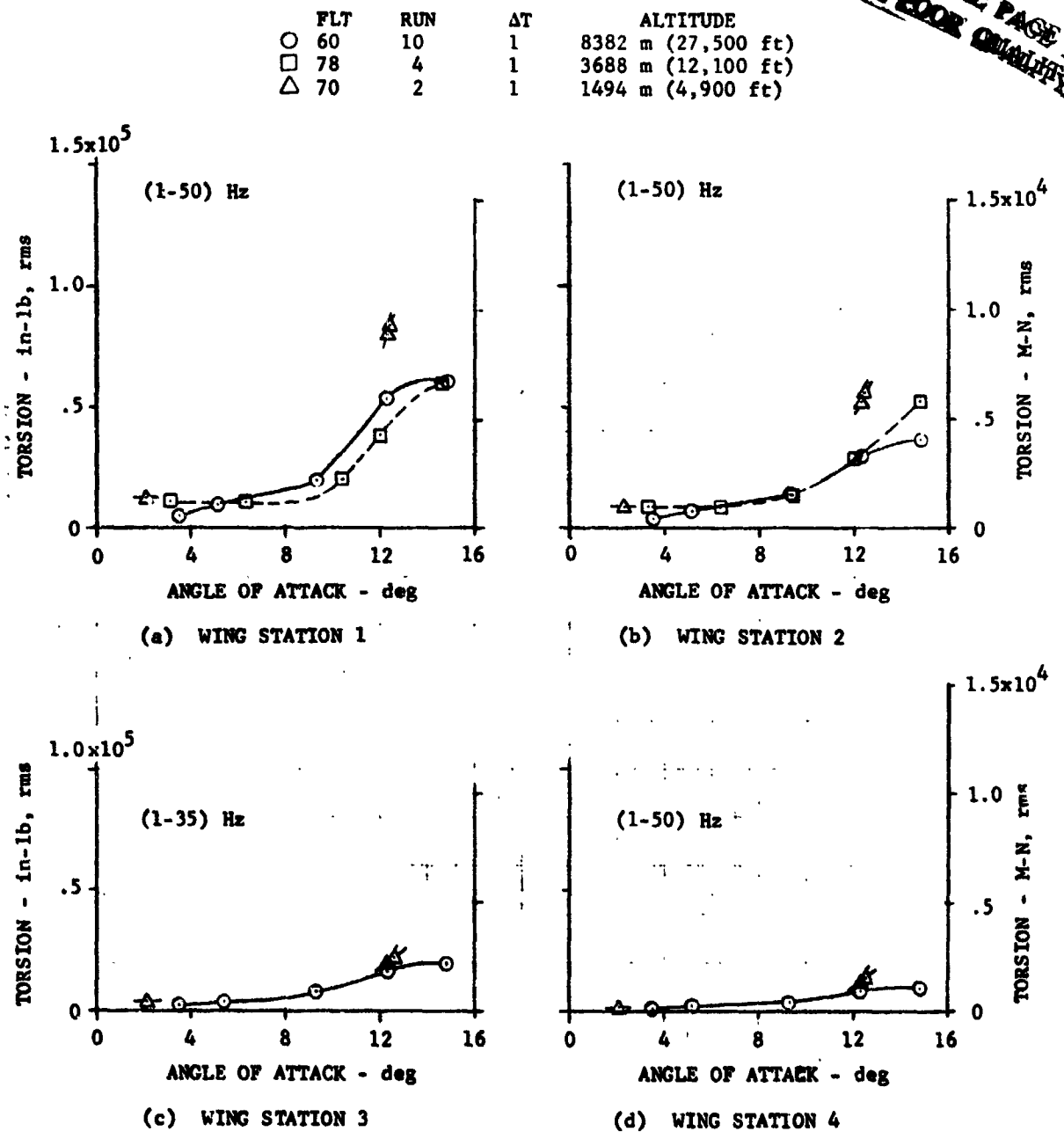

Figure 23. ROOT MEAN SQUARE VALUES OF WING TORSION RESPONSES FOR NOMINAL MACH NUMBER = 0.87

	FLT	RUN	ΔT	ALTITUDE
○	60	10	1	838? m (27,500 ft)
□	78	4	1	368 m (12,100 ft)
△	70	2	1	149 m (4,900 ft)

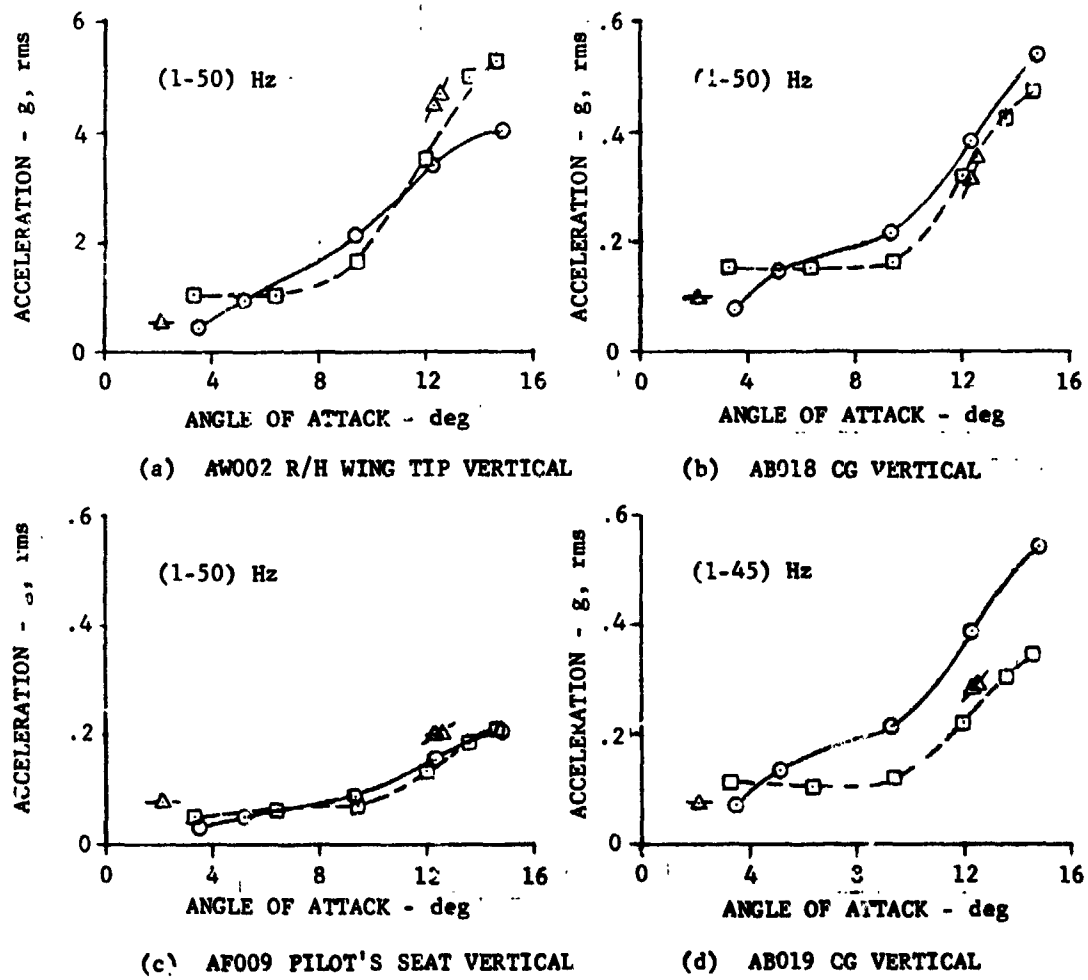

Figure 24. ROOT MEAN SQUARE VALUES OF ACCELEROMETER RESPONSES FOR NOMINAL MACH NUMBER = 0.87

	FLT	RUN	ΔT	ALTITUDE
○	60	10	1	8382 m (27,500 ft)
□	78	4	1	3688 m (12,100 ft)
△	70	2	1	1494 m (4,900 ft)

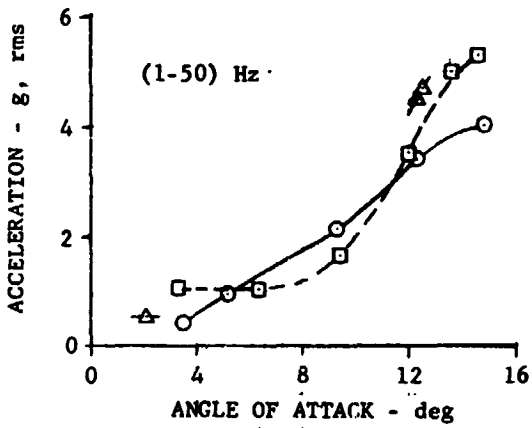

(e) AW002 R/H WING TIP VERTICAL

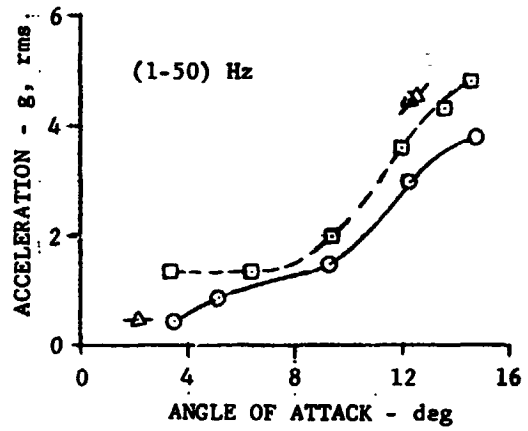

(f) AW001 L/H WING TIP VERTICAL

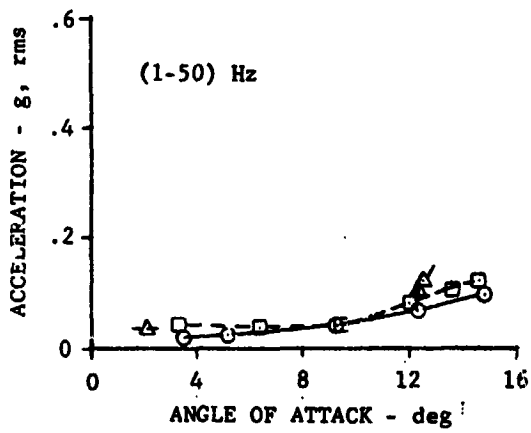

(g) AF010 PILOT'S SEAT LATERAL

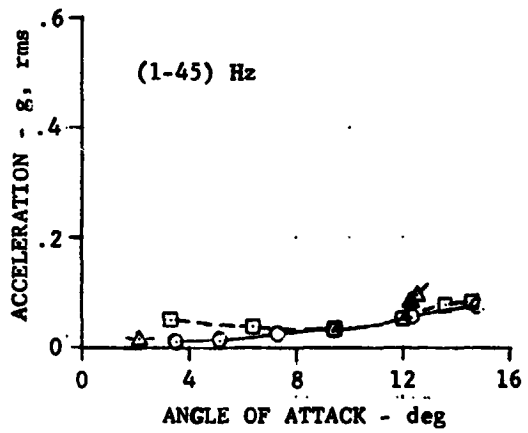

(h) AB020 CG LATERAL

Figure 24. CONCLUDED

last data point or at about 15 degrees angle of attack. The accelerations are in general lower than at M = 0.80 and do not peak in the angle of attack range measured.

Turning now to the data for the pullup performed at about 3700 m which are represented by square symbols in Figures 21 through 24, it can be seen that, in general, the variations in response are similar to those for the roller coaster maneuver. The higher initial levels of response are caused by the fact that the wing was in buffet even at trim conditions for 1-g flight. It is interesting that the change in slope of the responses still occurs above 9.3 degrees angle of attack. At the higher angles of attack the magnitudes of response for the shear and bending moments are slightly smaller than those for the roller coaster maneuver despite the fact that the dynamic pressure is much larger. The fuselage vertical accelerations follow a similar trend but the wing tip accelerometer responses are slightly higher than those for the roller coaster maneuver.

Data for the pullup maneuver performed at 1500 m are presented as triangles in Figures 21 through 24. Because this maneuver was so abrupt only three points are shown, one at 1-g trim conditions and two at high angle of attack. The wing strain gage responses at high angle of attack are larger than can be accounted for by a dynamic pressure effect. The probable cause

is the fact that the Mach number is about 0.04 lower than the other maneuvers at this angle of attack. The accelerometer responses are only slightly higher than those for the other pullup maneuver.

When the responses for the three maneuvers are compared, it is again obvious that they do not correlate with altitude. In this comparison, two of the three factors mentioned in the discussion of the M=0.80 comparisons have been minimized. The pitch rates are more nearly the same for the present comparison and the gross weights are also nearly the same. As a consequence we must attribute the anomalous trends with altitude primarily to differences in aeroelastic deformation of the wing which can cause significantly different shock patterns and thus differences in the progression of flow separation with angle of attack.

Summary Analyses

Before moving on to a discussion of the significance of the measured responses with respect to design loads, a brief review of what has been learned about the effects of Mach number is in order. Figure 25 presents comparisons of the shear, bending moment and torsion responses at Wing Station 1 and the pilot's seat vertical accelerometer responses as functions of angle of attack for each of the three high altitude maneuvers. Three features of these comparisons are of particular interest.

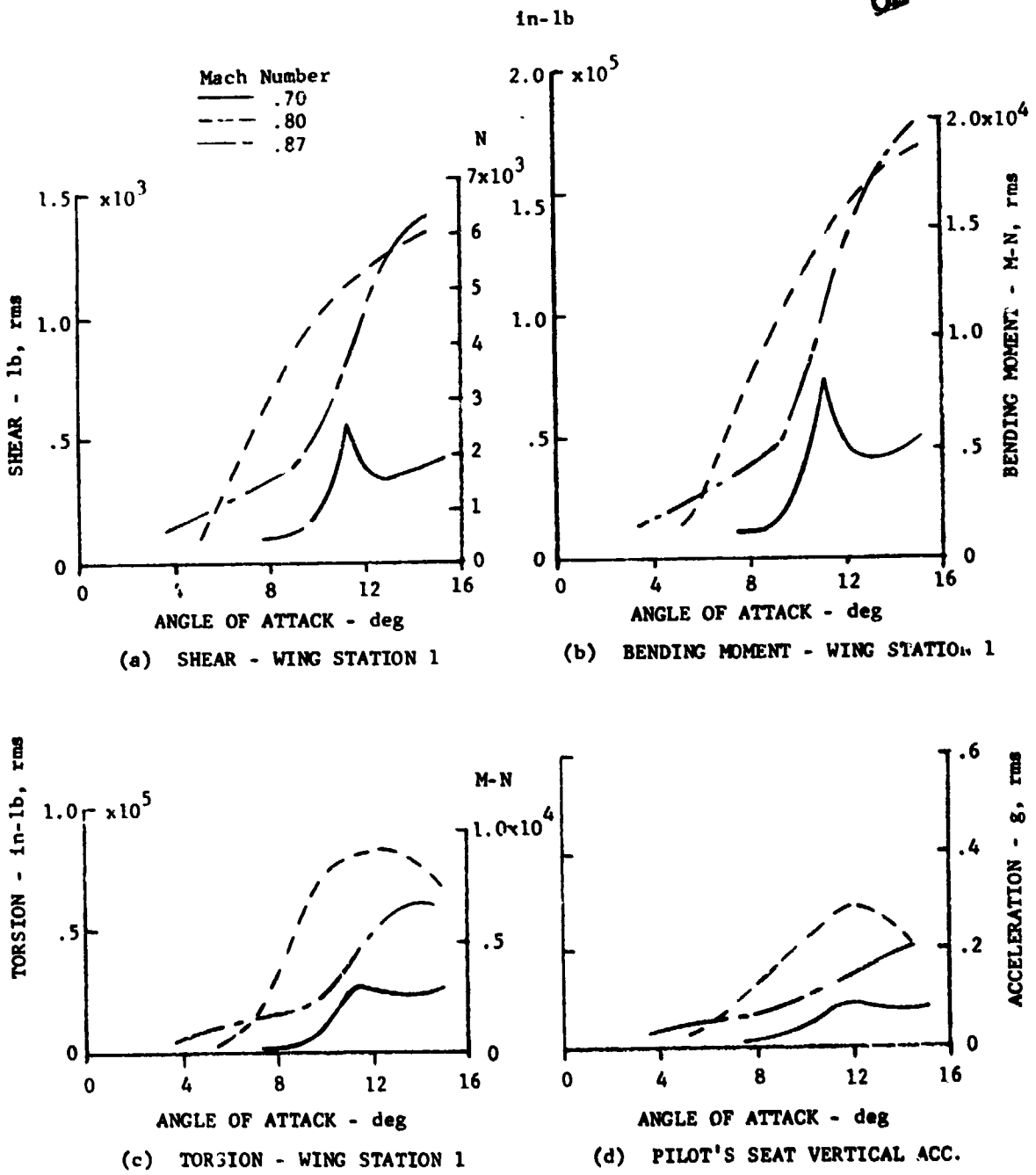

Figure 25. TYPICAL EFFECTS OF MACH NUMBER ON WING AND PILOT'S SEAT RESPONSES

First is the different response variations with angle of attack as Mach number increases. At M = 0.70 the variation is typical of that produced by leading-edge flow separation, which starts outboard on the wing and then progresses rapidly across the wing as angle of attack is increased. The peak response apparently occurs when the progression is completed. At M = 0.80 the variation is representative of shock-induced separation under conditions where the outboard shock is located very near the crest of the airfoil and moves ahead of the crest as angle of attack is increased. At M = 0.87 the variation is representative of a shock induced separation in which the outboard shock is well aft of the crest at low angle of attack and then moves forward slowly with angle of attack until the shock passes forward of the crest.

Second is the fact that the torsional responses tend to peak and the angle of attack for the peak increases as Mach number increases. This behavior may be a manifestation of the breakdown of the flow from a shock-induced separation to a leading-edge separation at the higher Mach numbers as described by Pearcey in Reference 21.

Third is the fact that the pilot's seat vertical accelerometer response tends to track the wing torsion response more so than it does wing shear or bending responses both in terms of

curve shape and relative magnitudes. This finding could lead to a whole new approach to predicting pilot's seat response if the same trends continue for other wing sweep angles. In any event, it indicates that scaling of the first wing torsion frequency, in addition to the first wing bending frequency, may lead to more accurate predictions of full-scale responses from small-scale wind tunnel model measurements.

Normalized Accelerometer Responses

In order to gain a perspective of the relative magnitudes of the accelerometer responses during buffet, the maximum measured responses were normalized by the maximum maneuver load factor for each maneuver. The normalized responses are presented in Figure 26. The various symbols designate nominal values of altitude and the Mach number values represent the average Mach number for each particular data sample. The analysis shows three pertinent results.

First, the relative responses at high altitude are larger than those at lower altitudes. This result was expected since the aircraft must operate at higher angle of attack for a given load factor and therefore penetrates farther above buffet onset at high altitude than it does at low altitude.

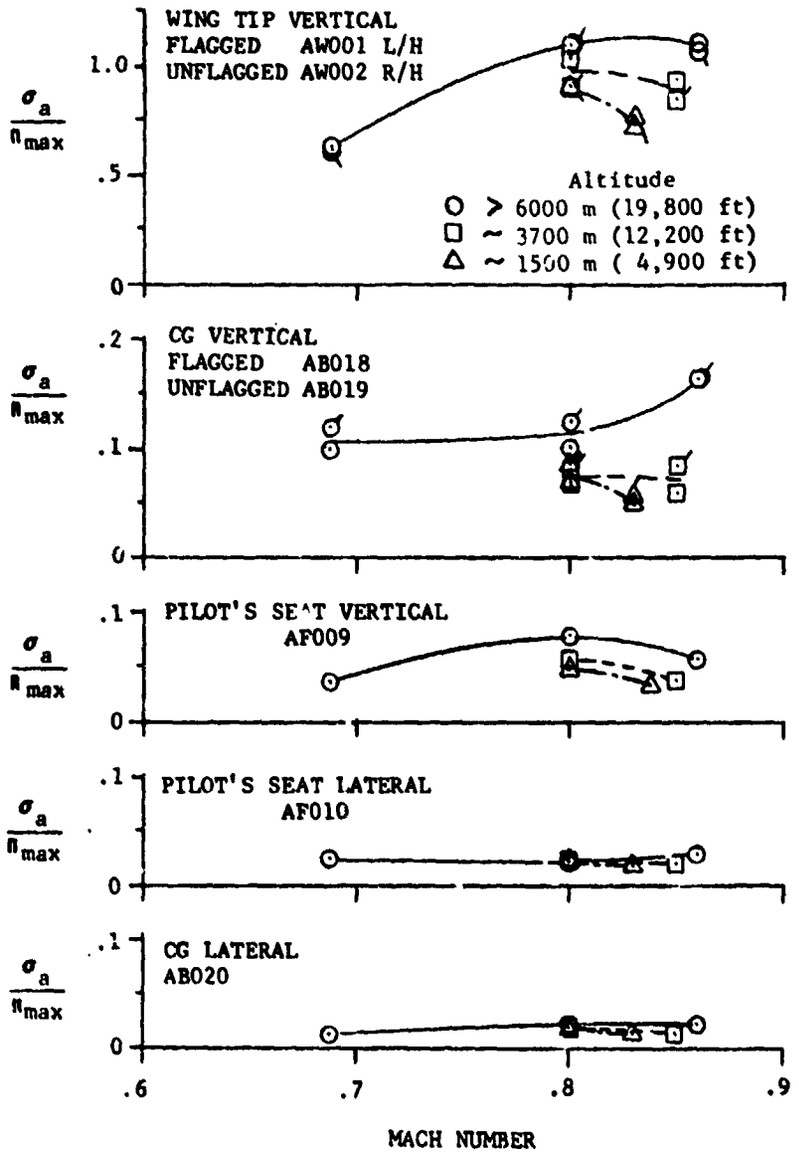

Figure 26. PEAK ACCELEROMETER RESPONSES NORMALIZED BY MANEUVER MAXIMUM LOAD FACTOR

Second, the maximum relative response for the wing tip and pilot's seat vertical accelerometers increases with Mach number, reaches a peak between 0.80 and 0.85 Mach number and then decreases again whereas the center of gravity response continues to increase at high altitude. As a consequence, the center of gravity response is probably not the best measurement to use as an indicator of buffet intensity effects.

Third, the structural arrangement of the aircraft is such that response levels attenuate considerably between the wing tips and center of gravity and also attenuate between the center of gravity and the pilot's seat. A major factor contributing to the attenuation is the fact that very little response is excited at those two fuselage locations at the low frequencies associated with the first symmetric and first antisymmetric wing bending modes with the wing sweep set at 26 degrees.

Normalized Wing Buffet Loads

One of the key questions that was to be answered by this investigation was just how significant are the buffet loads encountered in high-g maneuvers. It was possible to obtain an answer to this question for the wing shear and wing bending loads because M=.88, Λ_{LE}=26 was one of the anticipated limit loading conditions for the structural design of the aircraft and detailed

analyses of the "steady" (mean) loads produced during the Loads Demonstration Program for the F-111A aircraft. The wing torsional moment at this same condition is not a critical loading for the F-111A aircraft. The maximum rms values of shear and bending moment measured at each wing station during the three maneuvers performed at about M=0.86 have been normalized on the basis of the design load factor "steady" airloads for the specific dynamic pressure values associated with the measured buffet loads. The "steady" airloads were obtained from an analysis presented in Reference 22 in which values of shear and bending moment per unit dynamic pressure were plotted against dynamic pressure for $\Lambda=26^{o}$, $M \approx 0.88$.

The results of this analysis are presented in Figure 27 which shows the spanwise variations of normalized maximum shear and bending moment buffet loads. The symbols designate the different maneuvers. The plots show that there is an important spanwise variation of buffet loading and that the highest relative values occur at the most outboard measuring station. The effect of altitude is essentially similar to that for the accelerometer responses. At high altitude the dynamic response is a larger percentage of the "steady" airload than at lower altitudes. While the relative buffet loads are small they are not insignificant.

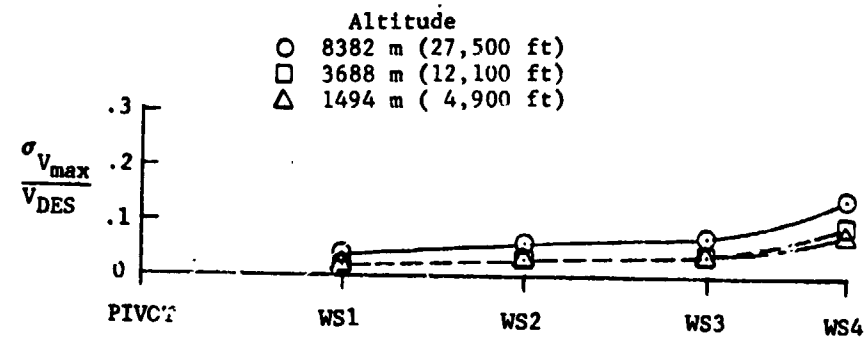

(a) SHEAR

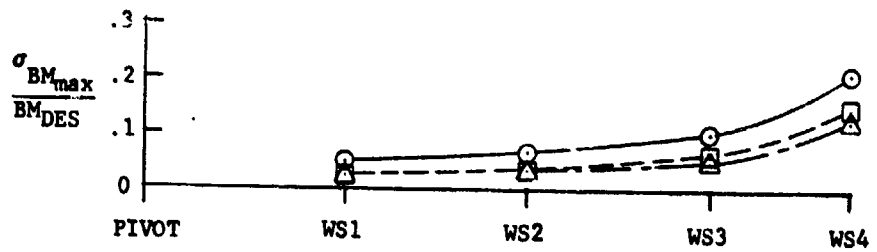

(b) BENDING MOMENT

Figure 27. SPANWISE VARIATION OF NORMALIZED BUFFET LOADS — $M \approx 0.86$

SECTION 8

CONCLUDING REMARKS

This investigation has provided some valuable new information about aircraft structural response to aerodynamic buffet at subsonic and transonic speeds. In particular,it was found that the structural response to buffet during moderate-to-high-g maneuvers is very complex. Nearly all the natural vibration modes of the aircraft,both symmetric and antisymmetric,are excited during a maneuver. As a consequence, an extensive array of instrumentation is needed to obtain an adequate description of the structural responses. As the penetration (angle of attack) beyond buffet onset increases, significant changes in the modal contributions to the total root-mean-square responses can occur. Therefore, no single vibration mode can be selected as an indicator of the variation of buffet intensity during a maneuver.

In general, the fluctuating shear and bending moments on the wing are small except near the wing tip where the rms values approach 15 to 20 percent of the design "steady" loads. The rms values of torsion response are higher than expected on the basis of previous buffet studies and amount to between 1/3 and 1/2 of the corresponding wing-bending response values. Some evidence of strong wing bending-torsion coupling was obtained at high

angle of attack at transonic flow conditions.

The effects of Mach number on the variations of wing responses with angle of attack were about as expected from previous buffet studies. At M = 0.70 the progression of response intensity with angle of attack is quite rapid and reaches a peak about four degrees after onset and then decreases. At M = 0.80 onset occurs at a lower angle of attack than at 0.70. The progression is somewhat less with angle of attack but the maximum measured values are significantly larger and occur at the highest angle of attack. At M ≈ 0.87 onset occurs at a still lower angle of attack than at 0.80. The initial rate of increase of response is low for several degrees and is followed by a larger rate of increase such that the maximum measured values are about the same as those measured at M = 0.80.

Attempts to correlate the responses at the various altitudes as functions of dynamic pressure generally failed. There is an indication that damping in the first wing bending mode is primarily structural at low altitude but not at high altitude where the "steady" air loads are much smaller in absolute magnitude. On the basis of the limited data available it was concluded that the differences in "steady" aeroelastic deformation (twist) of the wing alter the progression of flow separation as angle of attack is increased at the different altitudes.

J. G. Jones has shown in Reference 23 that the "apparent damping" in the first wing bending mode is highly nonlinear with angle of attack for a small fighter aircraft. It is possible then that the variations in the aerodynamic damping with angle of attack are different for the F-111 wing at different altitudes due to the differences in twist distribution. That situation could account for the inability to correlate the effects of altitude with functions of dynamic pressure.

It is now appropriate to review what impact the results of this investigation might have on future flight programs to investigate buffet characteristics and also on the development of methods to predict structural responses to aerodynamic buffet.

First, with respect to future flight programs, it is clear that a significantly larger array of instrumentation is needed to adequately assess aircraft structural response than has been used on most previous flight programs. In addition the sensitivities of strain-gage-bridges used to measure buffet loads should be significantly larger than those used to measure total aircraft loads in order to obtain an optimum signal-to-noise ratio for processing the dynamic data. In-flight measurement of the

fluctuating pressures and the aeroelastic deformations of the wing could considerably enhance the value of flight measurements of buffet characteristics that are to be compared with predictions. The twist distributions are of primary interest although chordwise deflections at several span stations would be of significant value if fluctuating pressure measurements are obtained in addition to loads and accelerations.

All measurements that are pertinent to a buffet analysis should be recorded on FM tape recorders and subchannel recording frequency limits should be no lower than the second wing torsion frequency. If leading and/or trailing edge flaps are a part of the configuration, frequencies associated with flap modes should also be within the recorder frequency limits. Finally, it is recommended that very gradual windup turn maneuvers be used to acquire buffet measurements so that sample times will be adequate for statistical analyses.

Second, with respect to development of prediction methods, one must consider the objective of the prediction. If it is desired to obtain detailed estimates of the aircraft vibrational environment due to buffet, i.e., loads, accelerations, and displacements, then the prediction method should probably include considerations of all aircraft symmetric and antisymmetric vibration modes up to and including that associated with second wing

torsion. If the objective is to obtain comparative rms accelerations at the pilot's seat at different flight conditions, it would probably be sufficient to consider symmetric and antisymmetric modes up to and including first wing torsion and symmetric and antisymmetric wing-fuselage-horizontal tail modes in the range of frequencies covered by the wing modes. The horizontal tail modes appear to be particularly important with respect to damping of the fuselage motions.

REFERENCES

1. Coe, C. F., "The Effect of Model Scale on Rigid-Body Unsteady Pressures Associated with Buffeting," Proceedings of Symposium on Aeroelastic and Dynamic Modeling Technology, USAF (RTD TDR-63-4197, Part II), March 1964.

2. Ray, E. J., and Taylor, R. T., Buffet and Static Aerodynamic Characteristics of a Systematic Series of Wings Determined from a Subsonic Wind Tunnel Study, NASA TN D 5805, 1970.

3. Ray, E. J., Techniques for Determining Buffet Onset, NASA TM X-2103, November 1970.

4. Hanson, P. W., Evaluation of An Aeroelastic Model Technique for Predicting Airplane Buffet Loads, NASA TND 7066, February 1973.

5. Friend, E. L., and Monaghan, R. C., Flight Measurements of Buffet Characteristics of the F-111A Variable Sweep Airplane, NASA TM X-1876, 1969.

6. Fischel, J., and Friend, E. L., Preliminary Assessment of Effects of Wing Flaps on High Subsonic Flight Buffet Characteristics of Three Airplanes, NASA TM X-2011, 1970.

7. Friend, E. L., and Sefic, W. J., Flight Measurements of Buffet Characteristics of the F-104 for Selected Wing-Flap Deflections, NASA TN D 6943, August 1972.

8. DeAngelis, M. V., and Banner, R. D., "Buffet Characteristics of the F-8 Supercritical Wing Airplane," Paper 7 in Supercritical Wing Technology. A Progress Report on Flight Evaluations, NASA SP-301, 1972.

9. Margolin, M., and Chung, J. G., "F-105F Transonic Buffet Study and Effect of Maneuvering Flaps, Air Force Flight Dynamics Lab, Technical Report AFFDL-TR-69-37, July 1969.

10. Titiriga, A., Jr., F-5A Transonic Buffet Flight Test, Air Force Flight Dynamics Lab, Technical Report AFFDL TR-69-110, December 1969.

11. Cohen, Marshall, Buffet Characteristics of the Model F-4 Airplane in the Transonic Flight Regime, Air Force Flight Dynamics Lab, Technical Report AFFDL-TR-70-56, April 1970.

12. Emerson, E. R., F-106A Transonic Buffet Flight Test, Air Force Flight Dynamics Lab, Technical Report AFFDL-TR-70-87, June 1970.

13. Mullans, R. E., and Lemley, C. E., Buffet Dynamic Loads During Transonic Maneuvers, Air Force Flight Dynamics Lab, Technical Report AFFDL-TR-72-46, September 1972.

14. Anon., Turbulence Study of A Transonic Wind Tunnel and an Analysis and Tests of Aircraft Response to Turbulence, North American Aviation, Inc., Columbus Division, Report NA 63H-636, 1 October 1964.

15. Mayes, J. F., Lores, M. E., and Barnard, H. R., Transonic Buffet Characteristics of a 60 Degree Swept Wing with Design Variations, AIAA Paper No. 69-793.

16. Damstrom, E. K., and Mayes, J. F., Transonic Flight and Wind Tunnel Buffet Onset Investigation of the F-8D Aircraft — Analysis of Data and Test Techniques, AIAA Paper No. 70-341.

17. Post, J. P., Botman, M., and Bennett, R. V., An Analytical and Experimental Study of Aircraft Response to Buffeting, North American Aviation, Inc., Columbus Division, Report NA 60H-742, 6 September 1961.

18. Nevius, H. E., F-111A Ground Vibration Test No Wing Stores (Airplane 12), General Dynamics' Fort Worth Division Report FZS-12-167, 5 August 1966, and Supplement 1, 1 August 1967.

19. Nevius, H. E., F-111A Ground Vibration Tests No Wing Stores (Airplane 1-11), General Dynamics' Fort Worth Division Report FZS-12-060, 1 March 1965.

20. Huston, W. B., Rainey, A. G., and Baker, T. F., A Study of the Correlation Between Flight and Wind Tunnel Buffeting Loads, NACA RM L55E16b, July 1955.

21. Pearcy, H. H., "Some Aspects of the Physical Nature of Transonic Flow Past Aerofoils and Wings," Symposium Transonicum, Springer-Verlag, Berlin, 1962, pp. 264-275.

22. Kerr, G. W., and Gish, S. K., F-111A 100% Flight Loads Program Results: Volume I – Balanced Symmetric Maneuver and Miscellaneous Component Loads Without External Stores, General Dynamics' Convair Aerospace Division, Fort Worth operation Report FZS-12-1039, Volume I, 13 March 1973.

23. Jones, J. G., A Survey of the Dynamic Analysis of Buffeting and Related Phenomena, Royal Aircraft Establishment (Farnborough, England) Report TR 72197, February 1973.

APPENDIX

TIME HISTORIES OF INSTRUMENTATION OUTPUT

In this Appendix time histories of the instrumentation output are displayed in analog form for the following maneuvers:

Figure	Flight	Run	Maneuver
A-1	48	6	Windup Turn
A-2	78	5	Pullup
A-3	79	9R	Pullup
A-4	60	10	Roller Coaster
A-5	78	4	Pullup
A-6	70	2	Pullup

The time histories for the Flight 77, Run S&C-R windup turn maneuver are presented in the main body of the report.

Each set consists of several records and each record contains the output from several instrumentation channels. The top channel on each record shows the output for the same item - AW002, the R/H wing tip accelerometer (except Figure A-3 which has DH001C, angle of attack). The particular groupings of items presented are those used in the study and some items appear more than once. The flight time (actually frame number) which is the correlating item appears at the lower boundary of each record. Each second is indicated by a tick in the time trace.

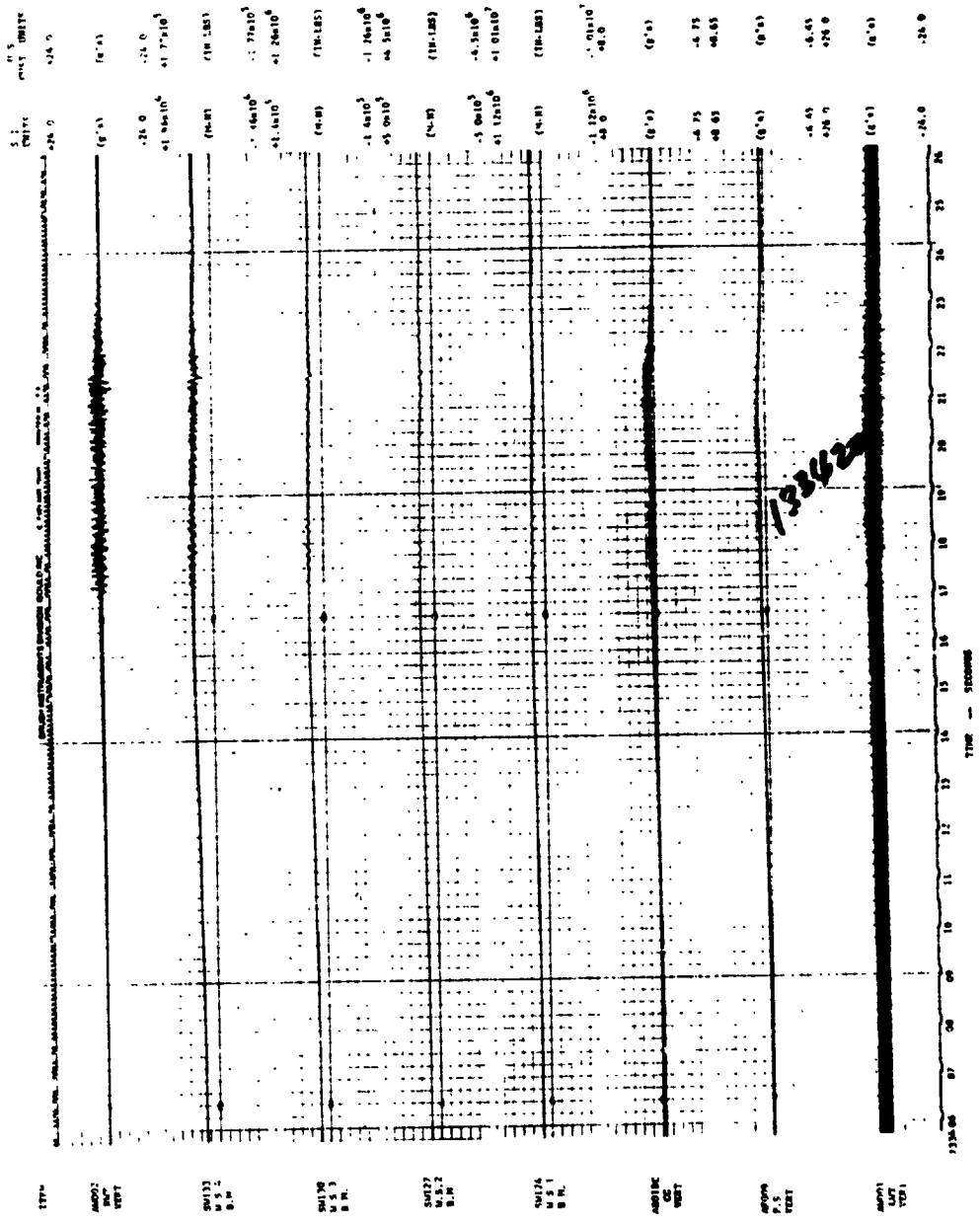

(a)

Figure A-1. TIME HISTORIES OF INSTRUMENTATION OUTPUT FOR WINDUP TURN, FLIGHT 48, RUN 6

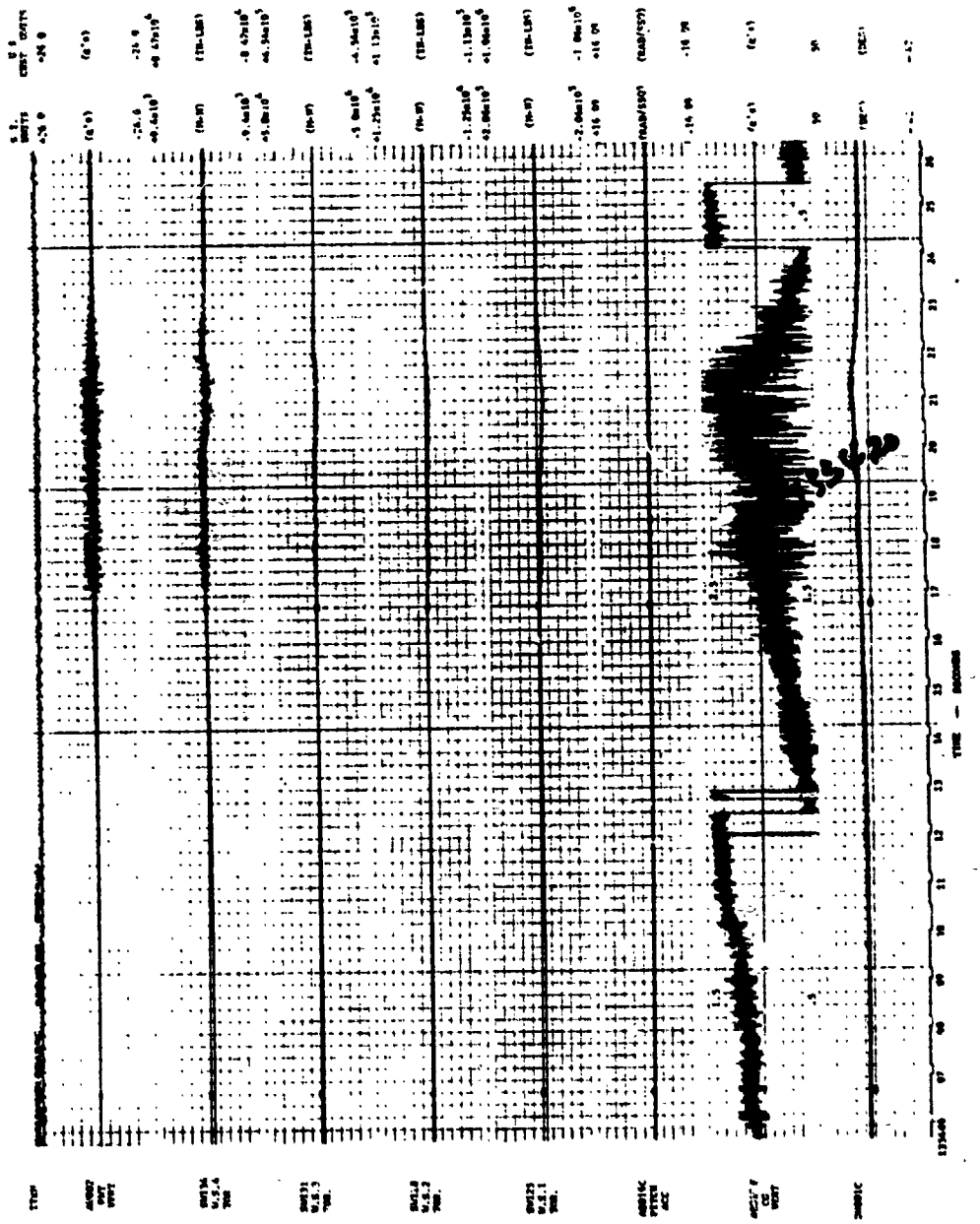

(b)

Figure A-1. Continued

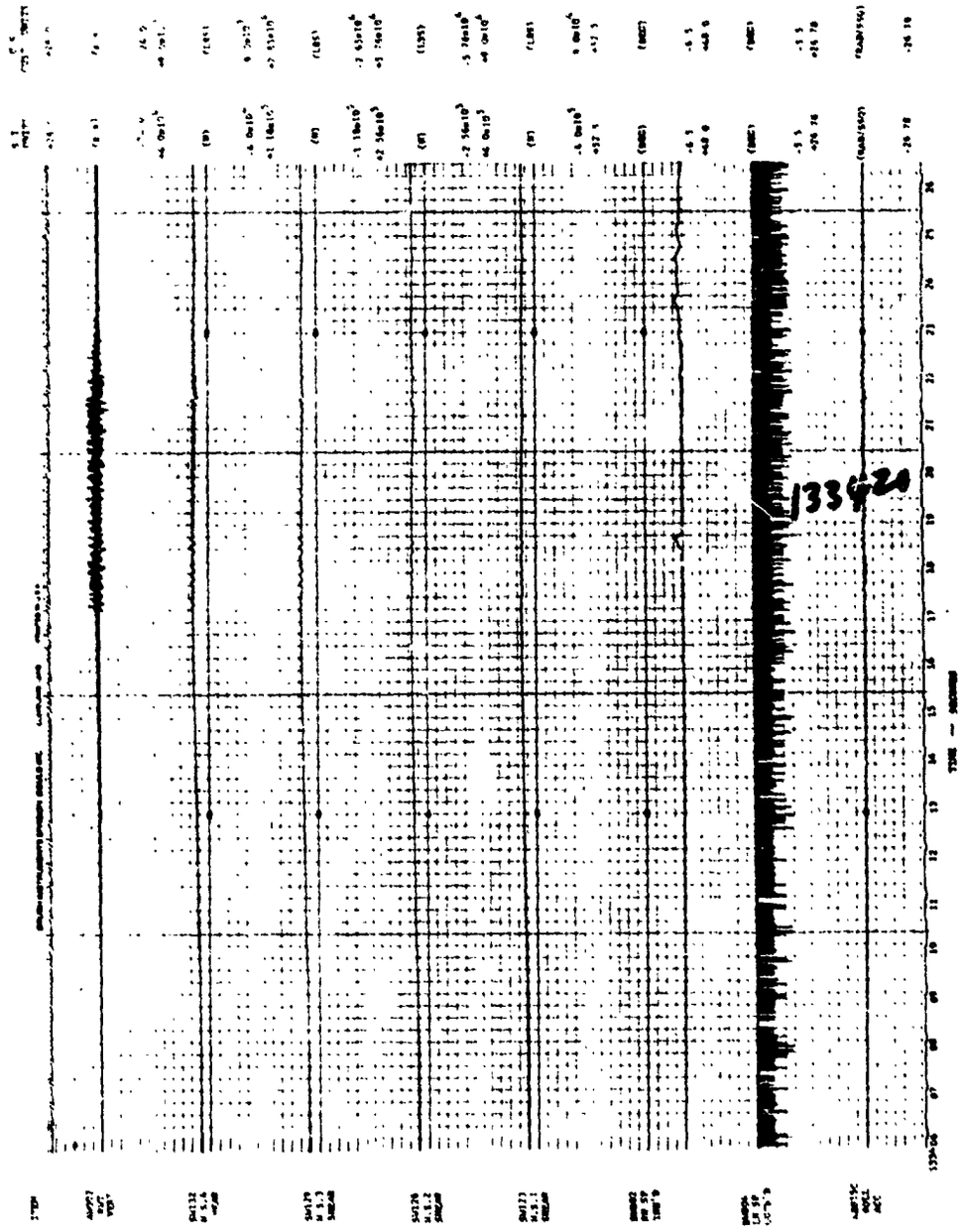

(c)

Figure A-1. Continued

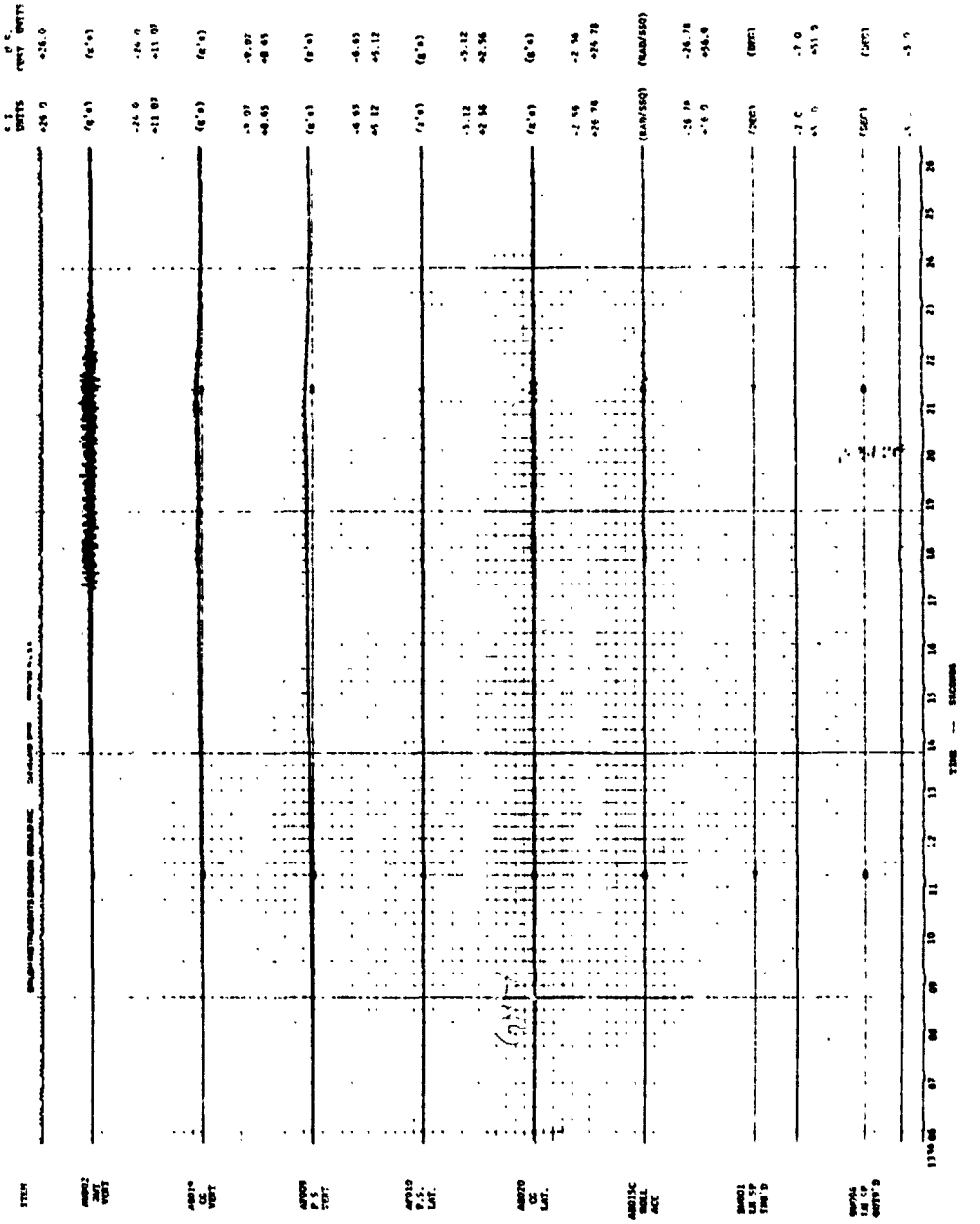

(d)

Figure A-1. Continued

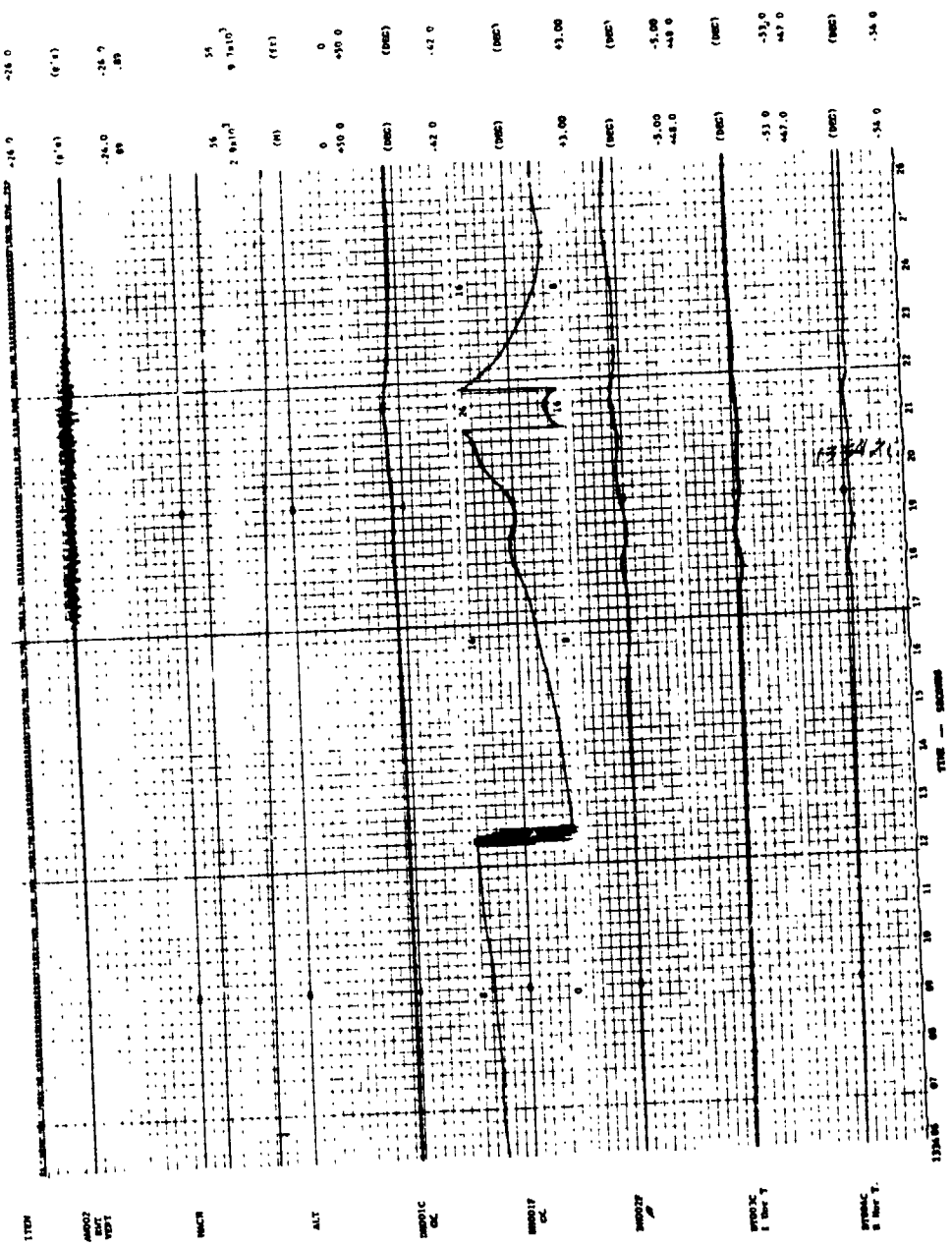

(e)

Figure A-1. Concluded

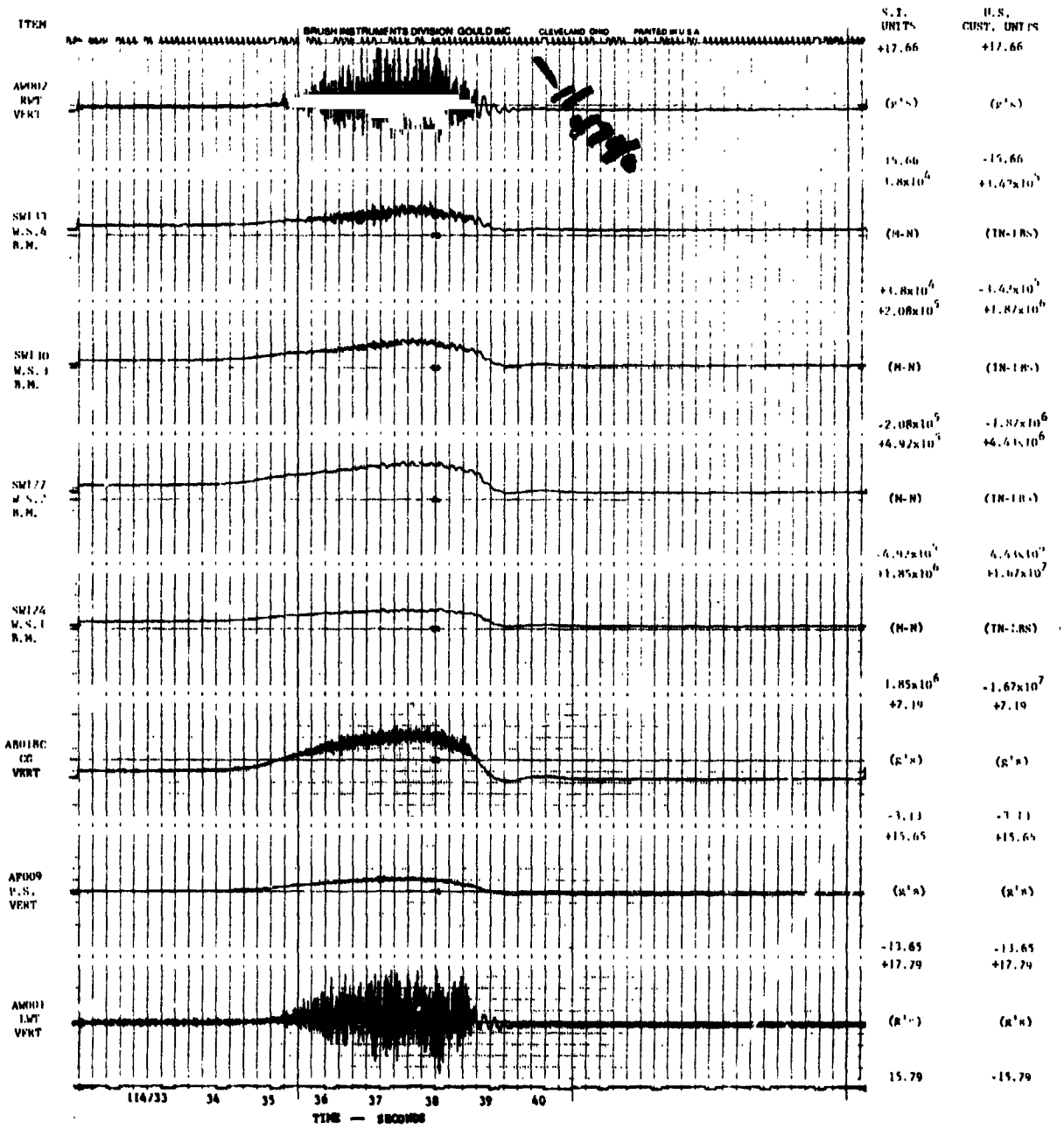

(a)

Figure A-2. TIME HISTORIES OF INSTRUMENTATION OUTPUT FOR PULLUP, FLIGHT 78, RUN 5

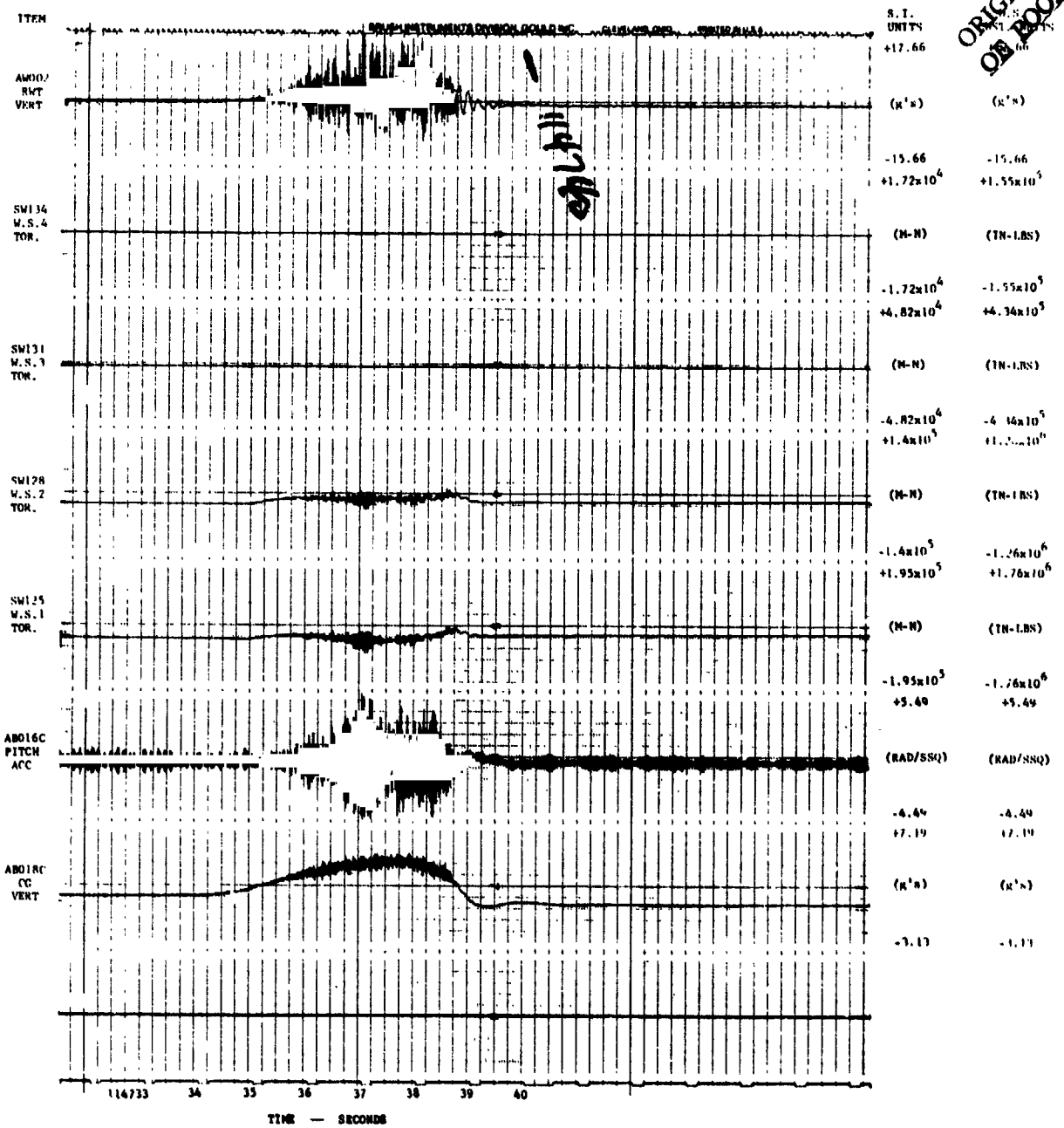

(b)

Figure A-2. Continued

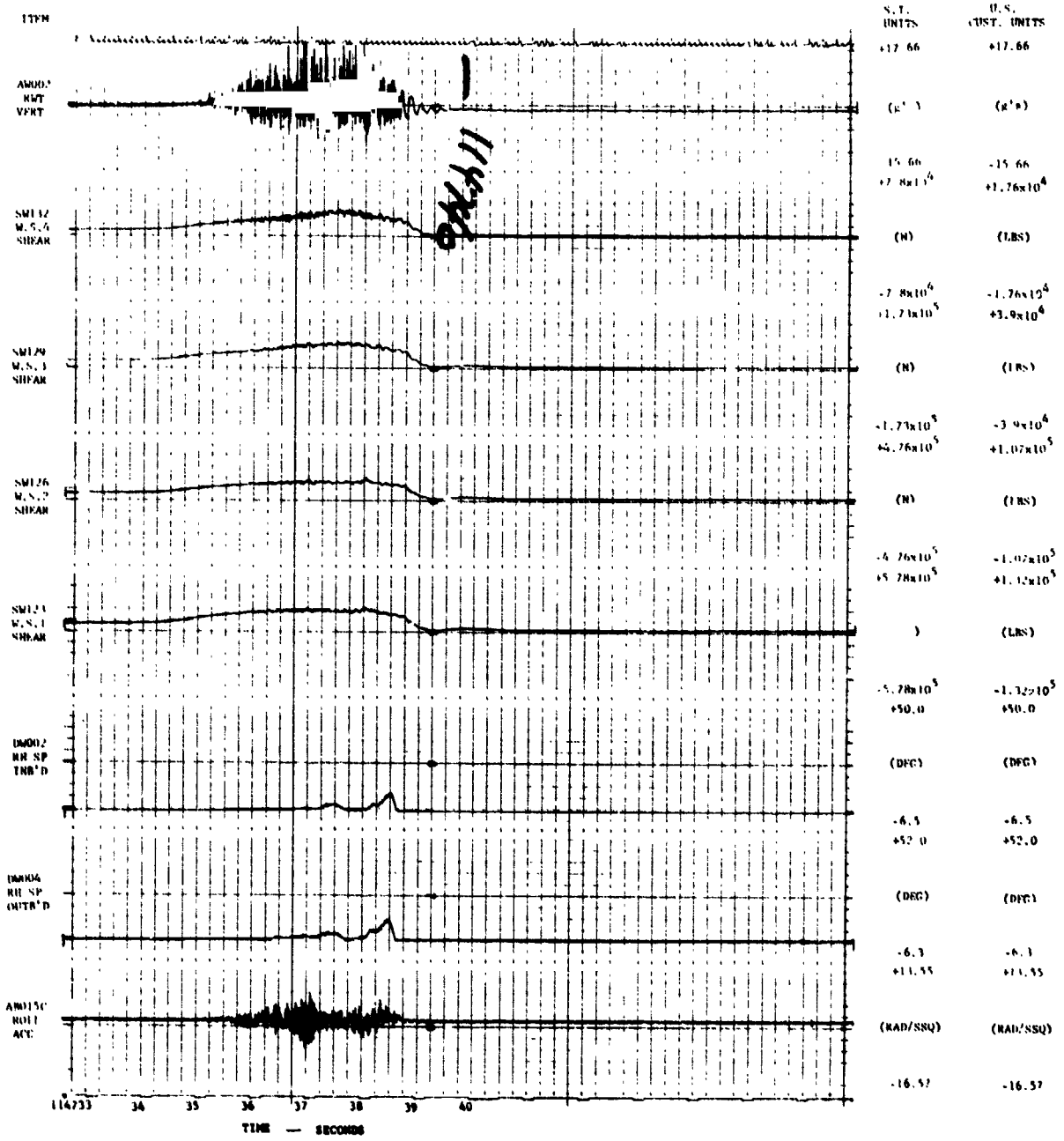

(c)

Figure A-2. Continued

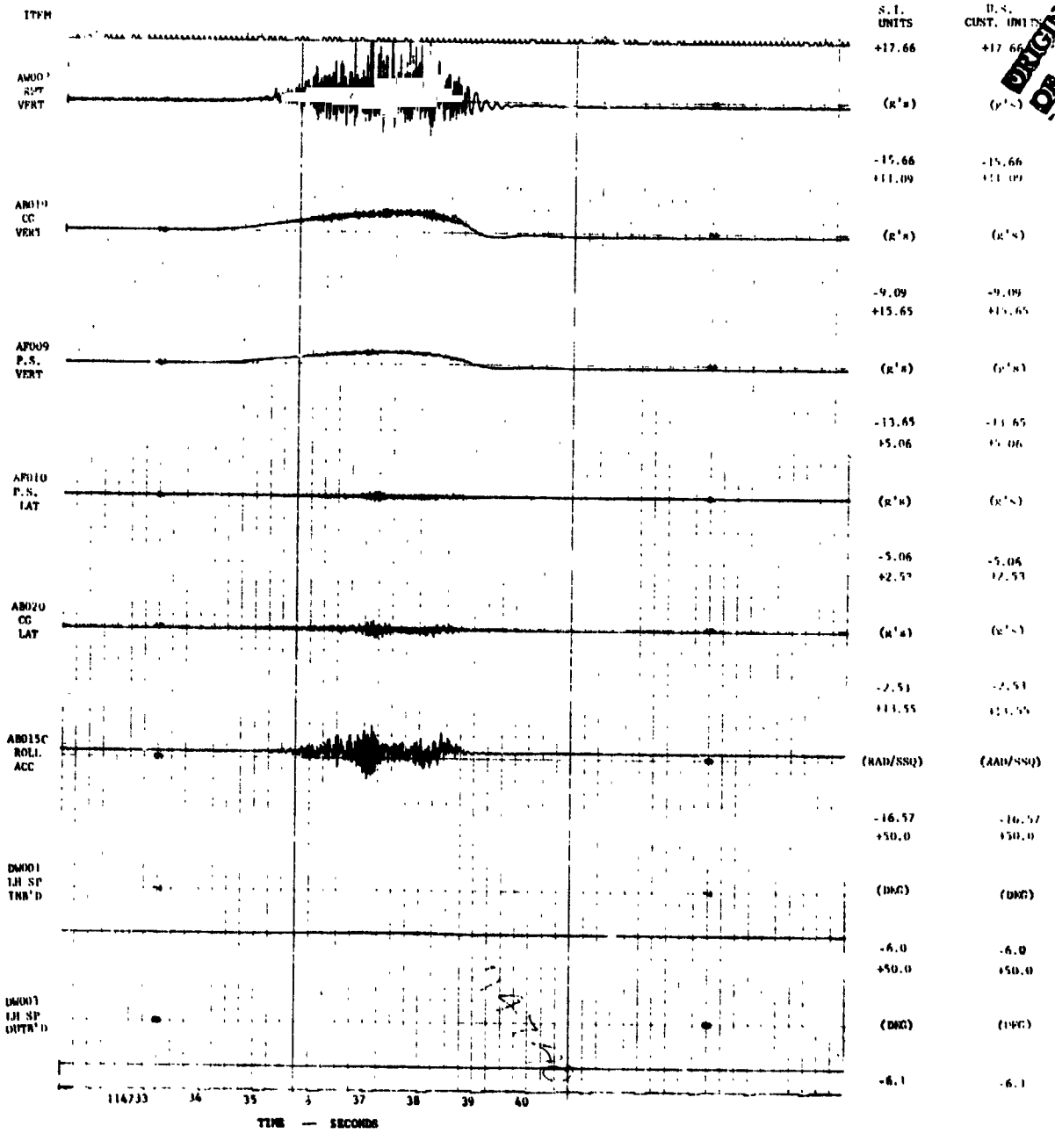

(d)

Figure A-2. Continued

ORIGINAL PAGE IS
OF POOR QUALITY

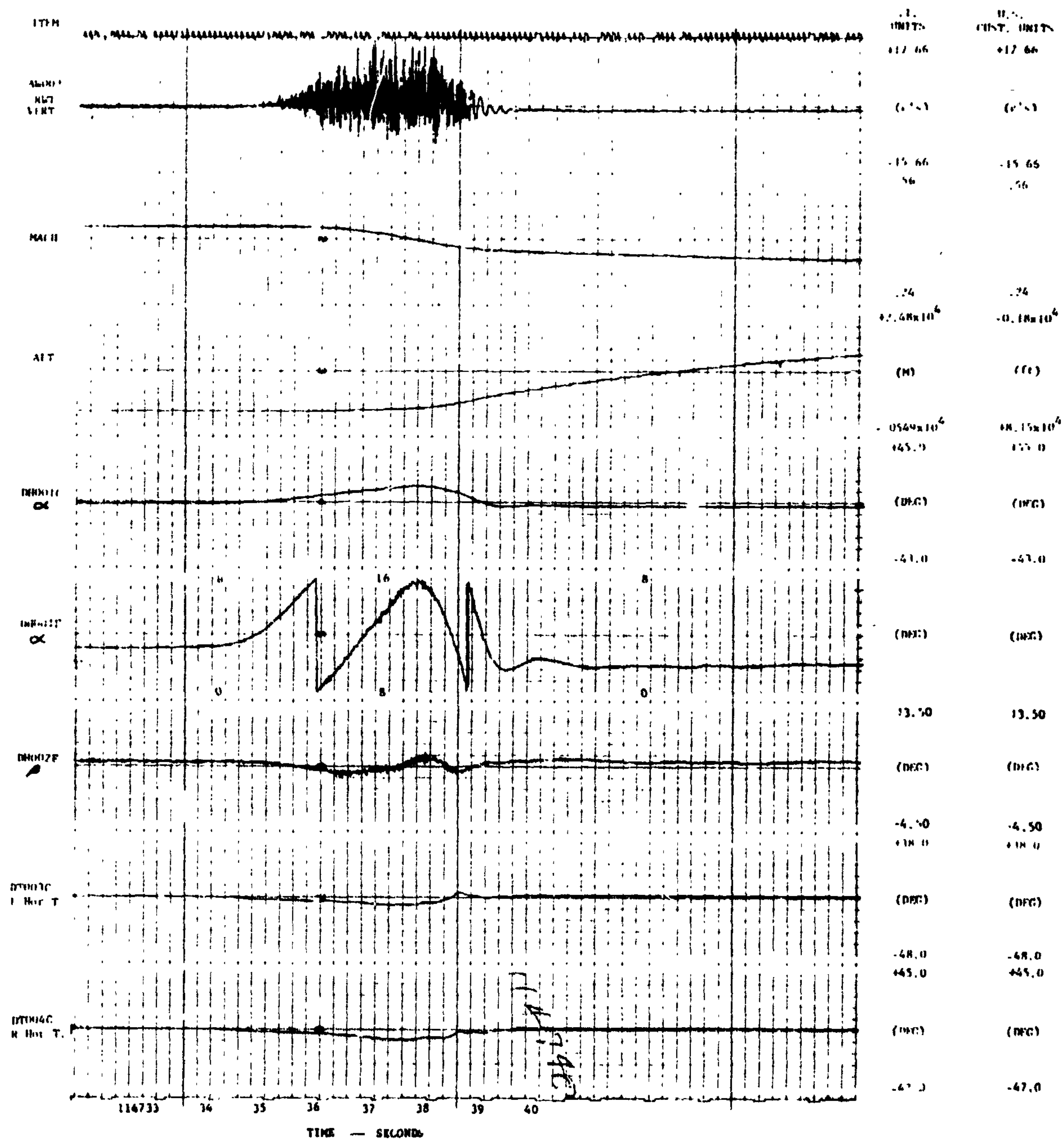

(e)

Figure A-2. Concluded

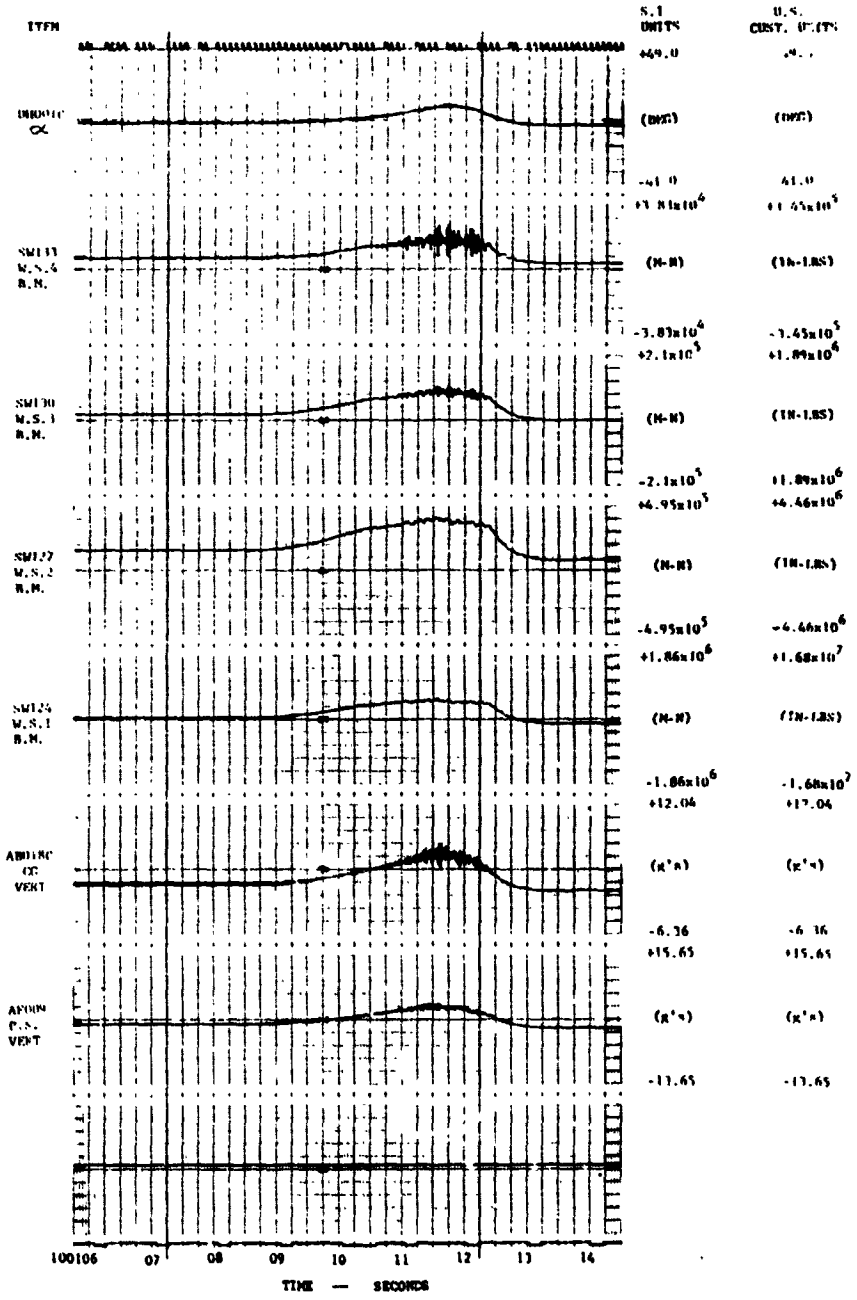

(a)

Figure A-3. TIME HISTORIES OF INSTRUMENTATION OUTPUT FOR PULLUP, FLIGHT 79, RUN 9R

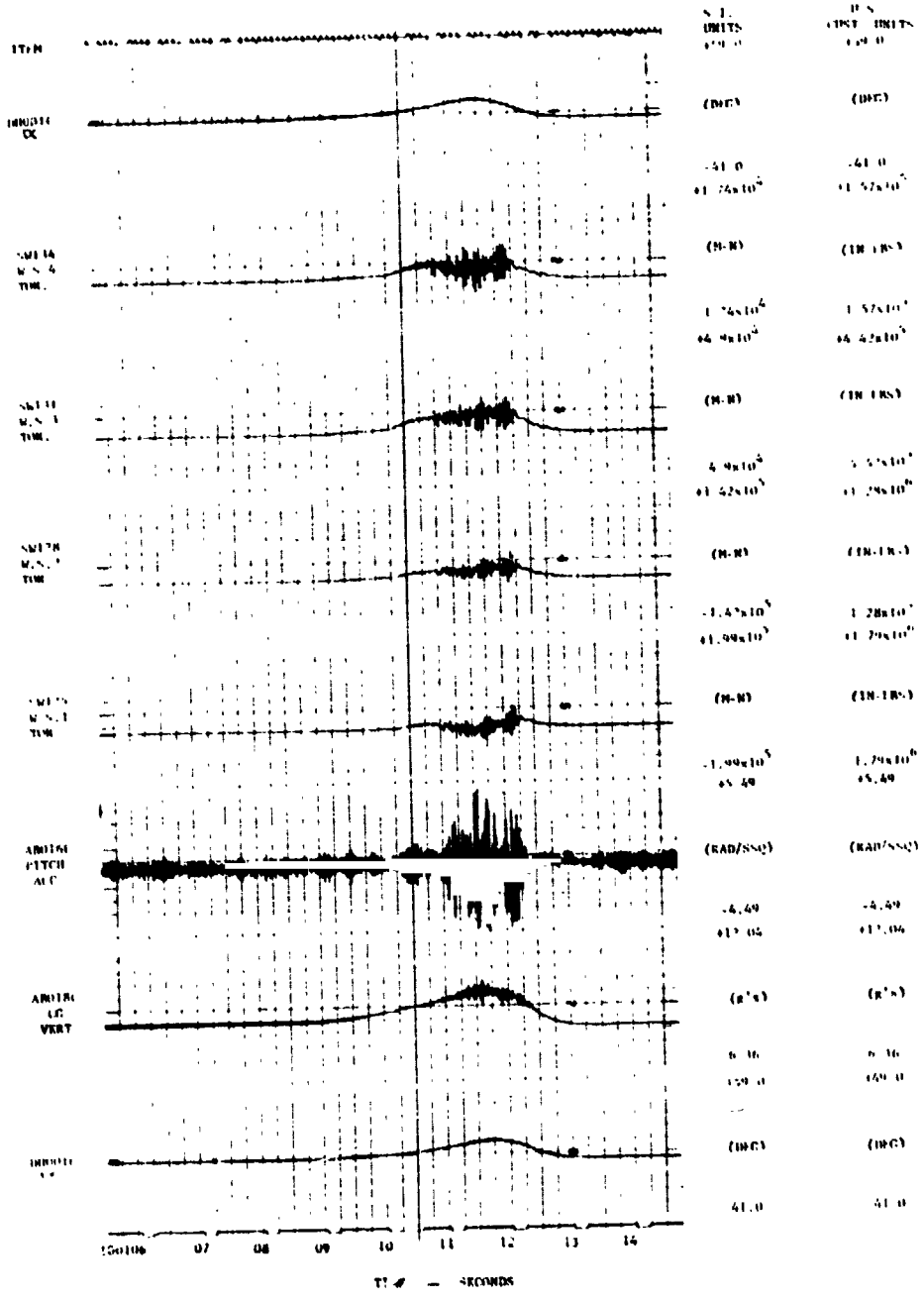

(b)

Figure A-3. Continued

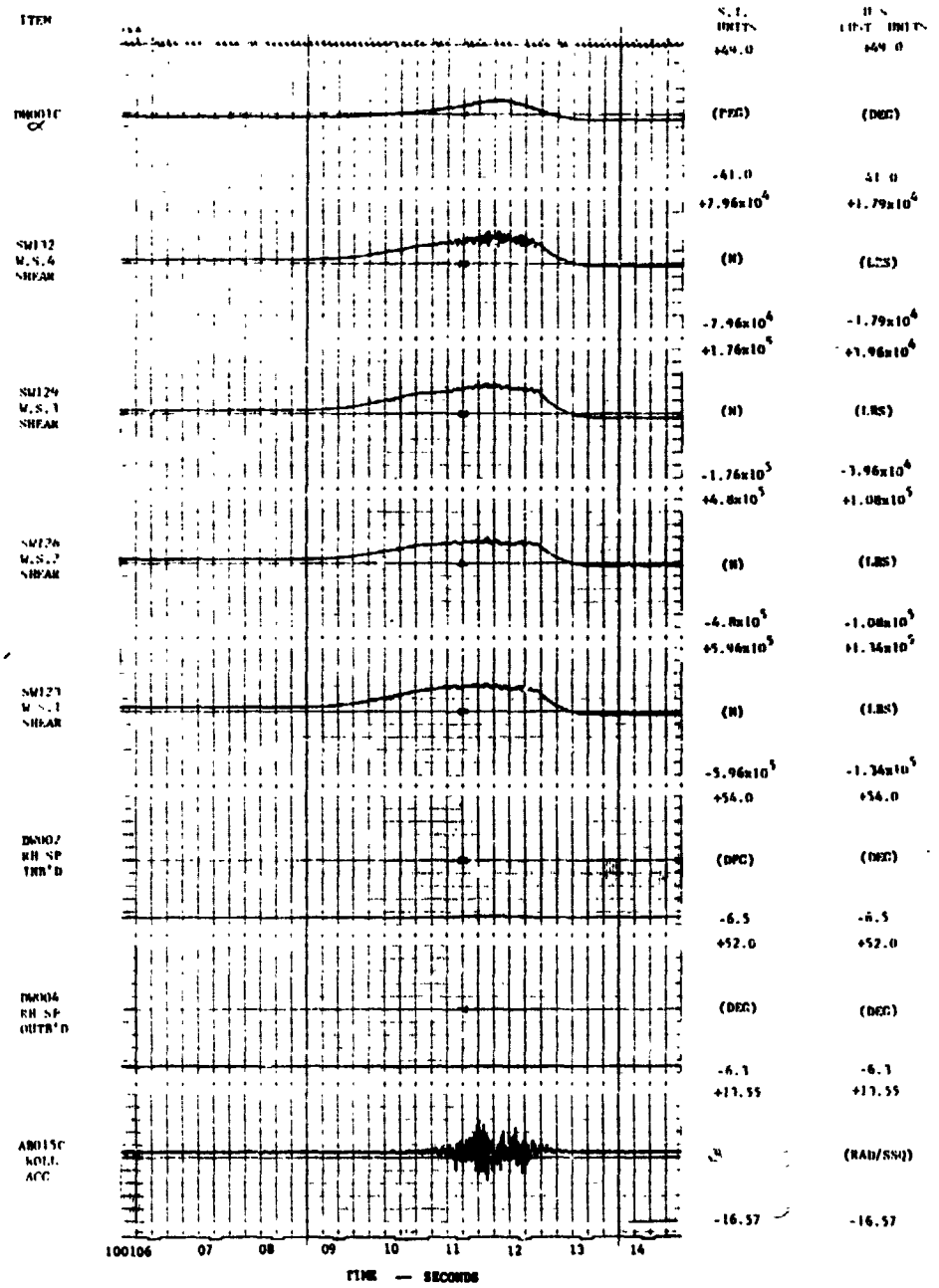

(c)

Figure A-8. Continued

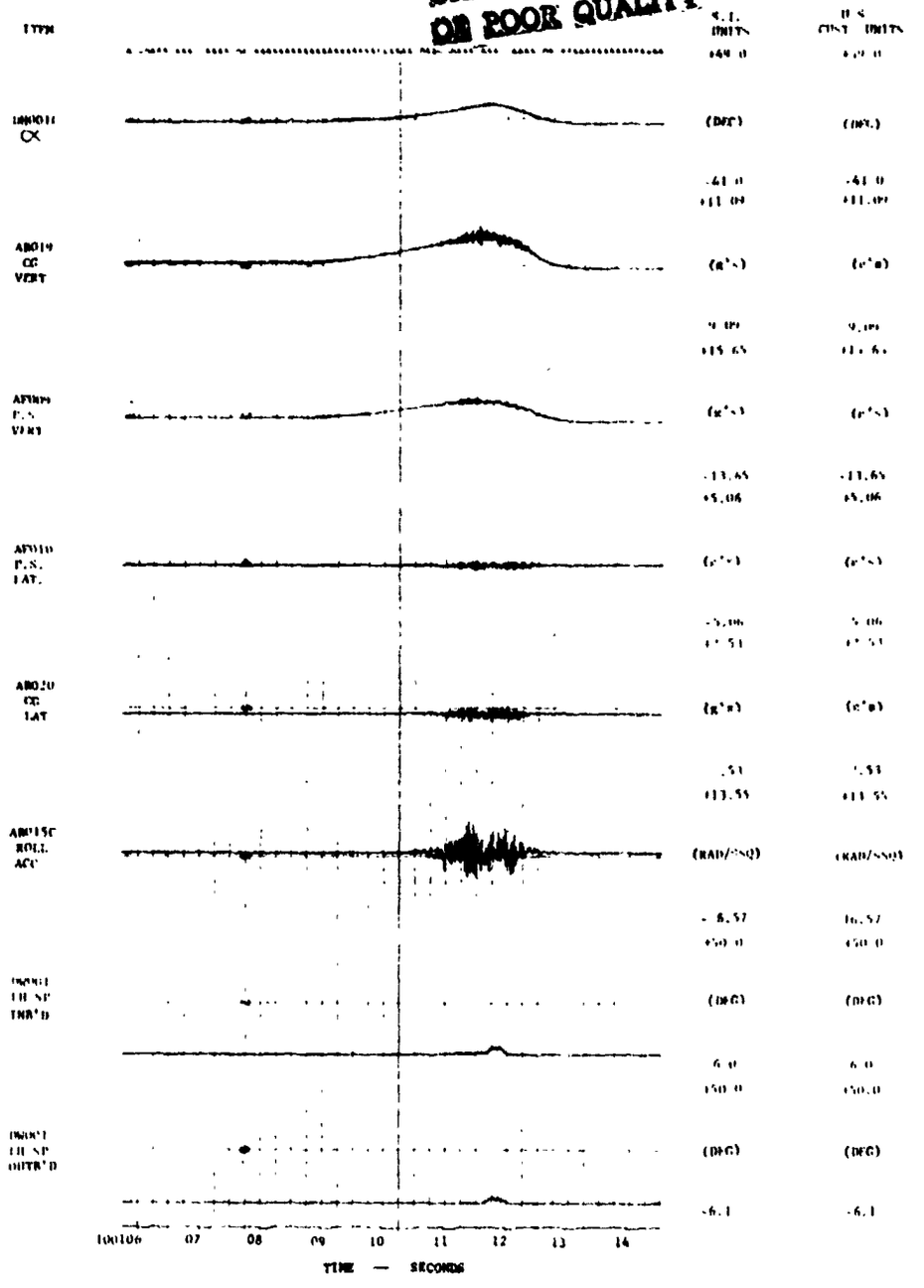

(d)

Figure A-3. Continued.

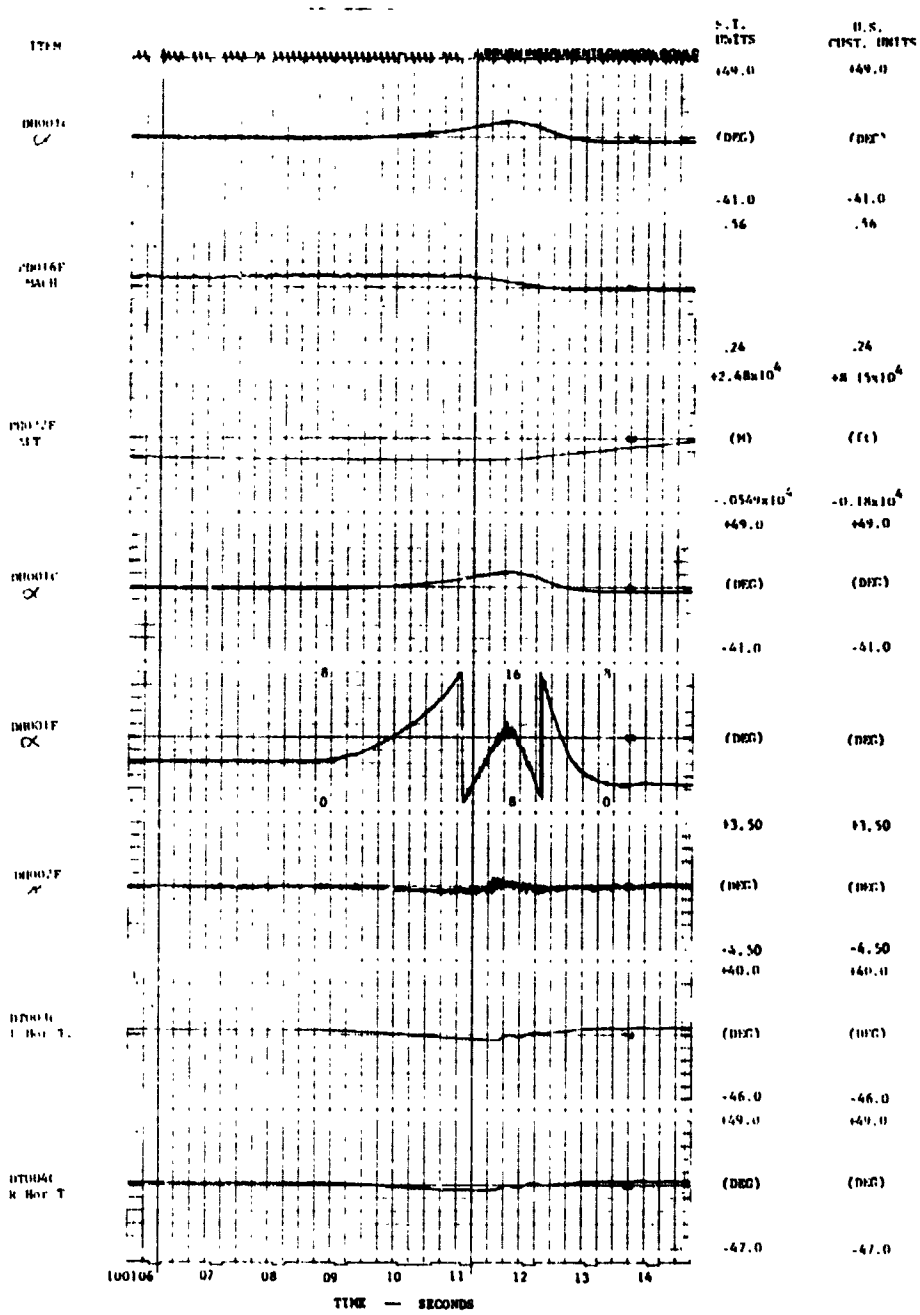

ORIGINAL PAGE IS OF POOR QUALITY

(e)

Figure A-3. Continued

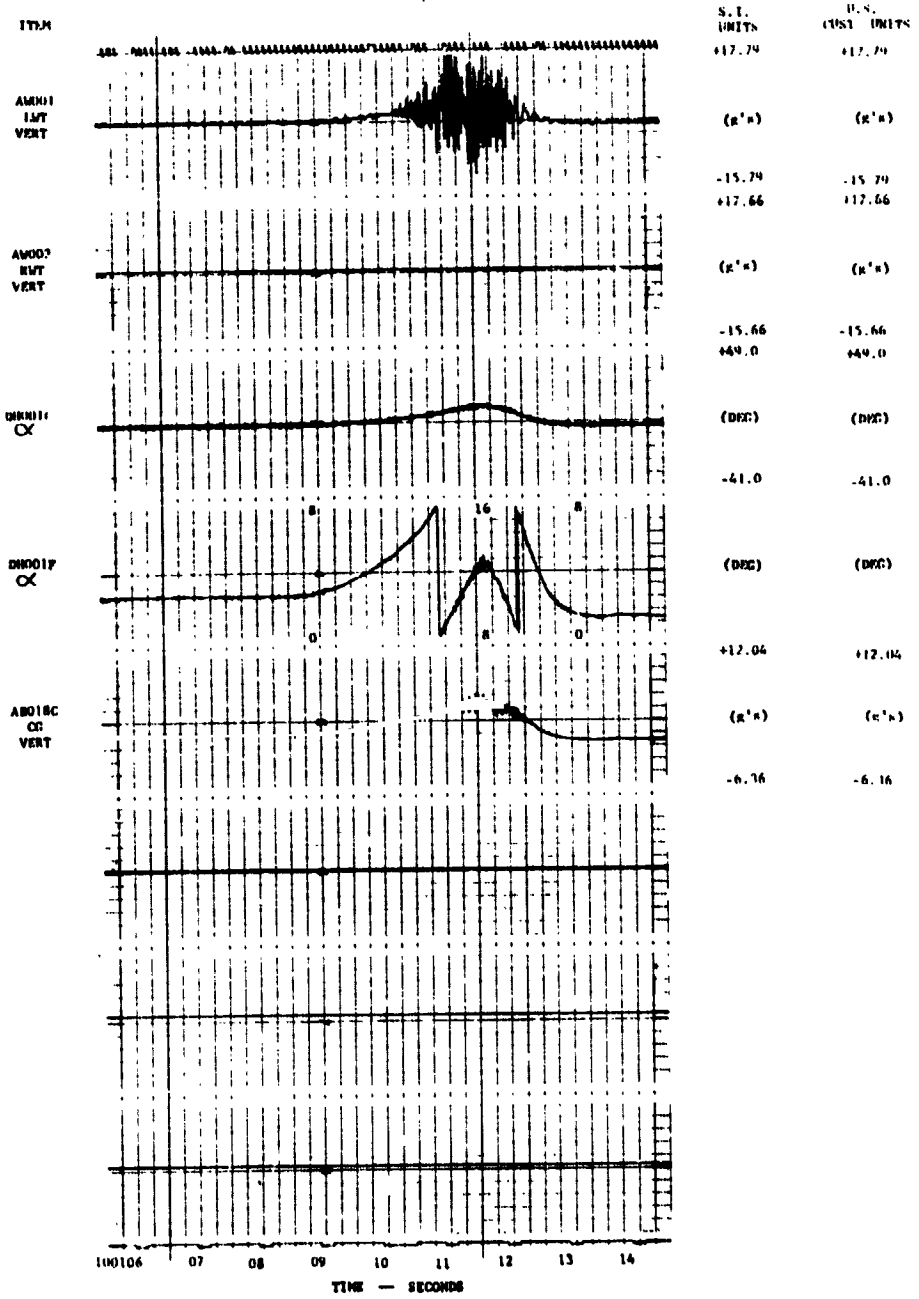

(f)

Figure A-3. Concluded

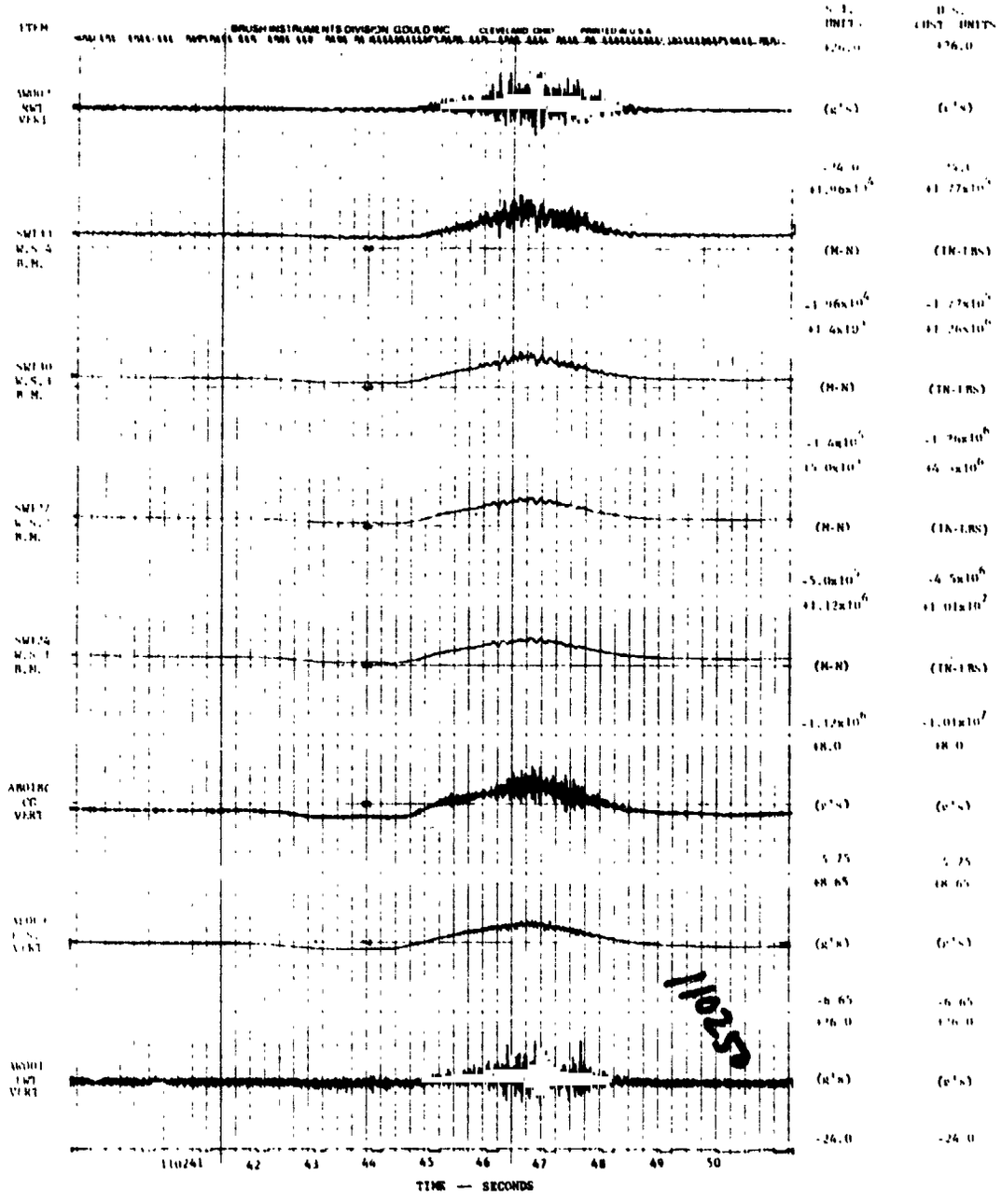

(a)

Figure A-4. TIME HISTORIES OF INSTRUMENTATION OUTPUT FOR ROLLER COASTER, FLIGHT 60- RUN 10

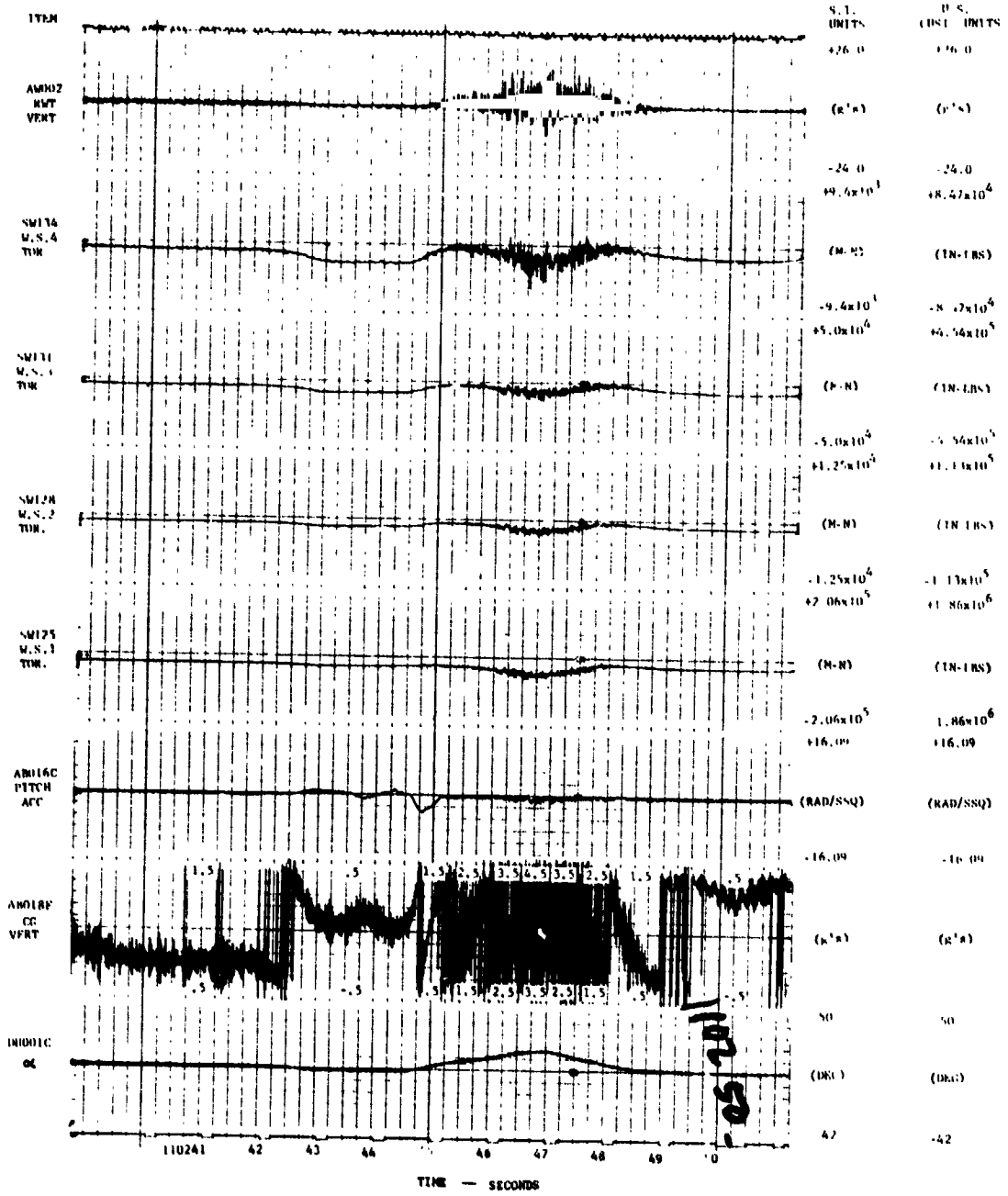

(b)

Figure A-4. Continued

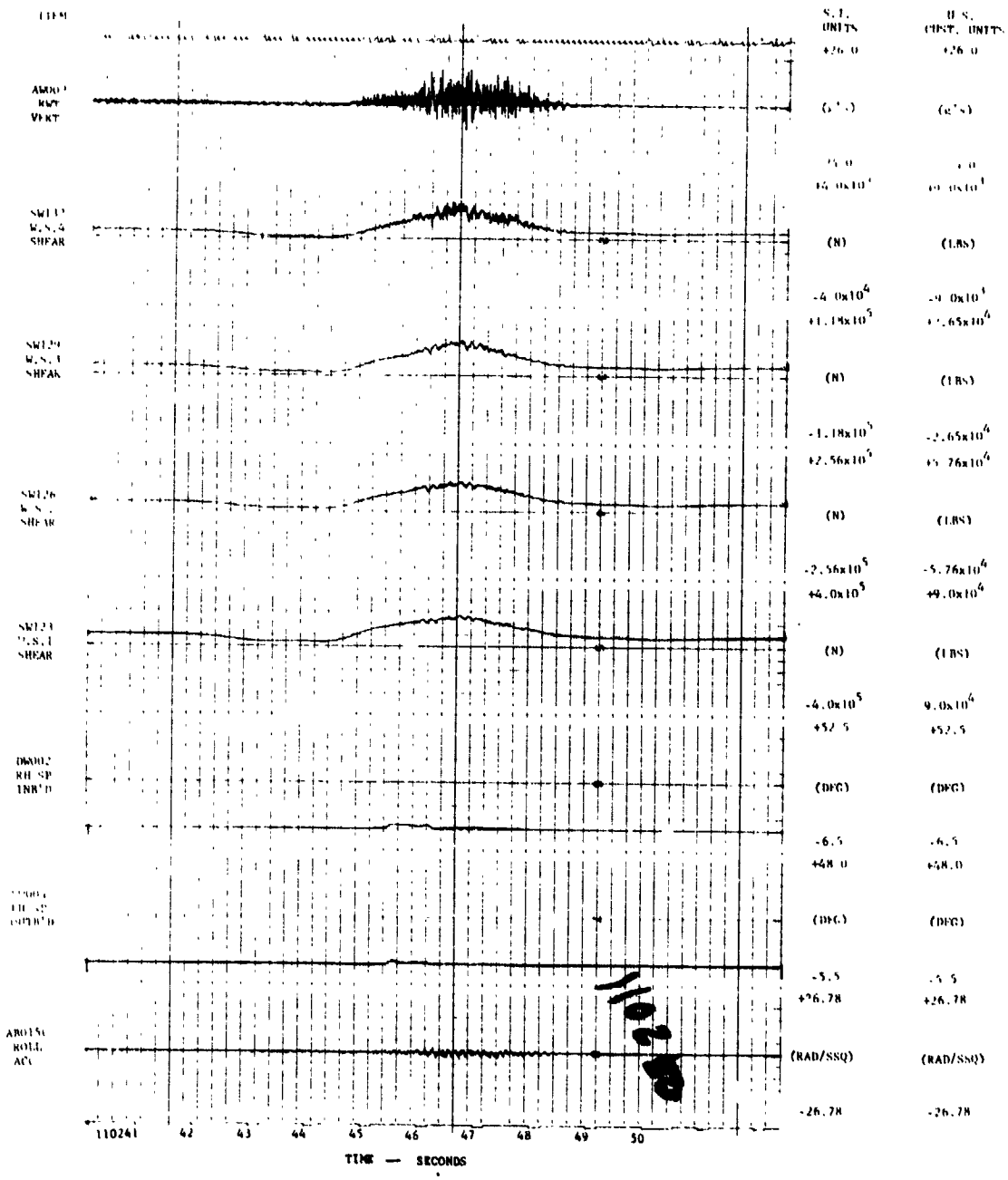

(c)

Figure A-4. Continued

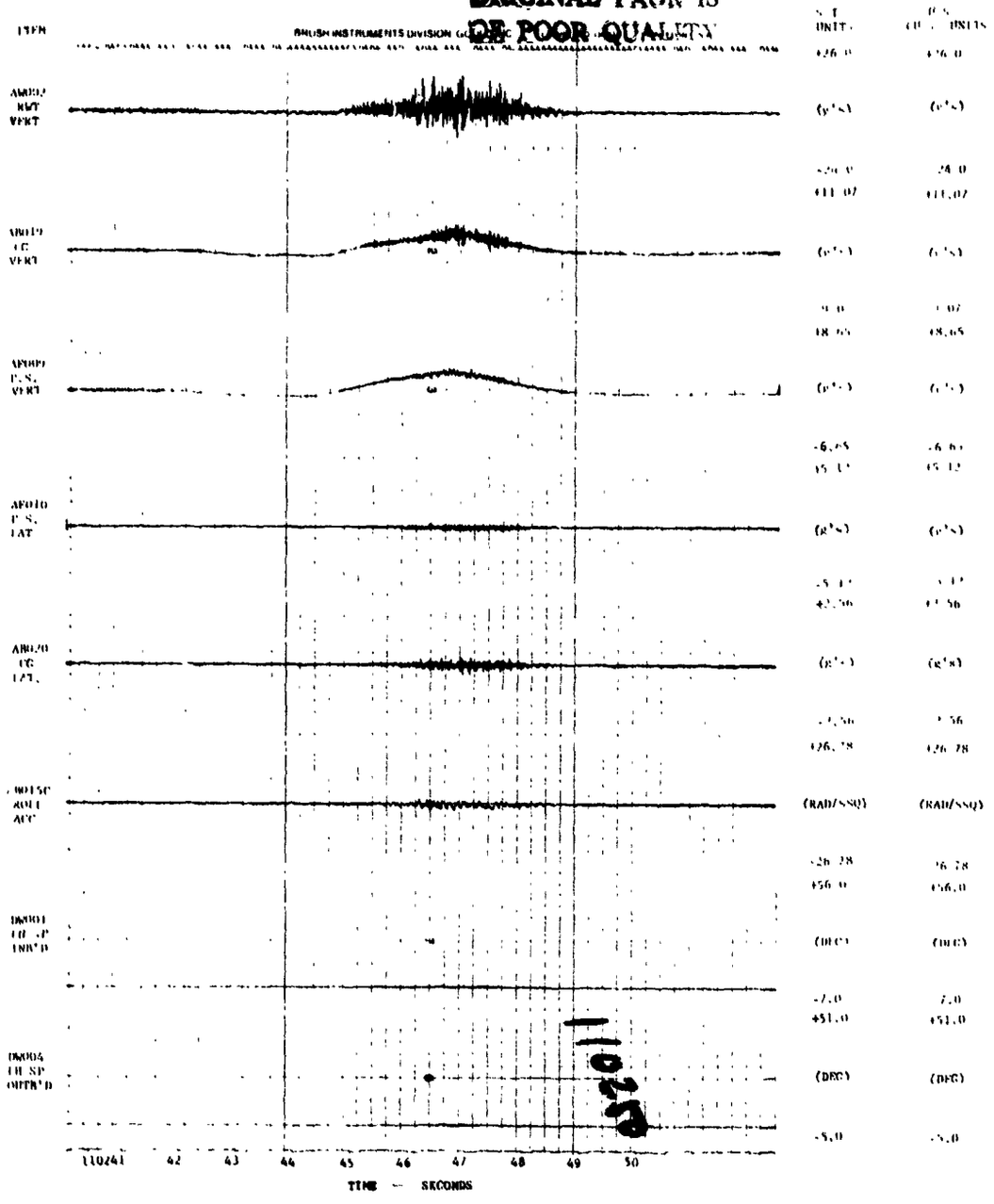

(d)

Figure A-4. Continued

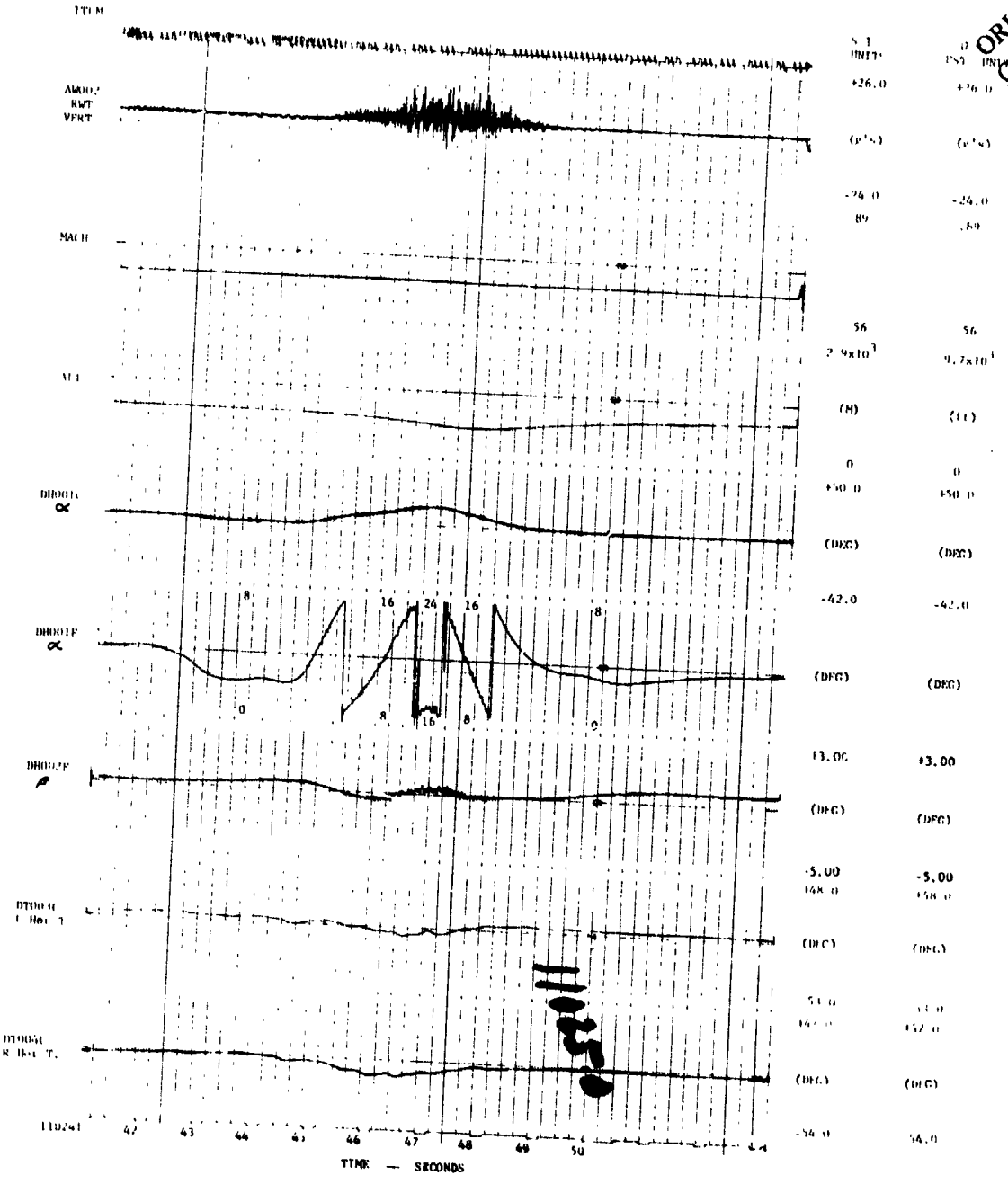

(e)

Figure A-4. Concluded

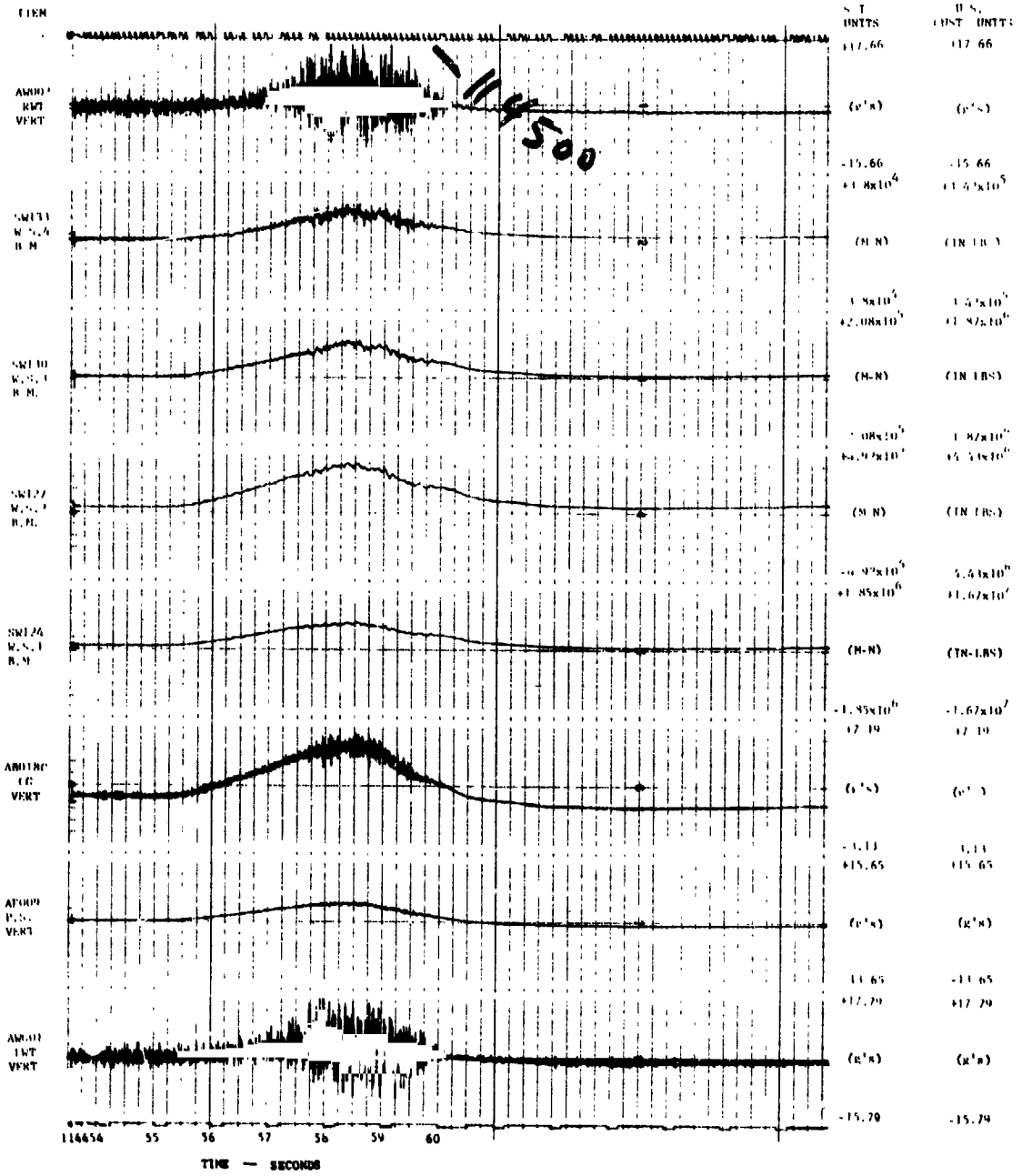

(a)

Figure A-5. TIME HISTORIES OF INSTRUMENTATION OUTPUT FOR PULLUP, FLIGHT 78, RUN 4

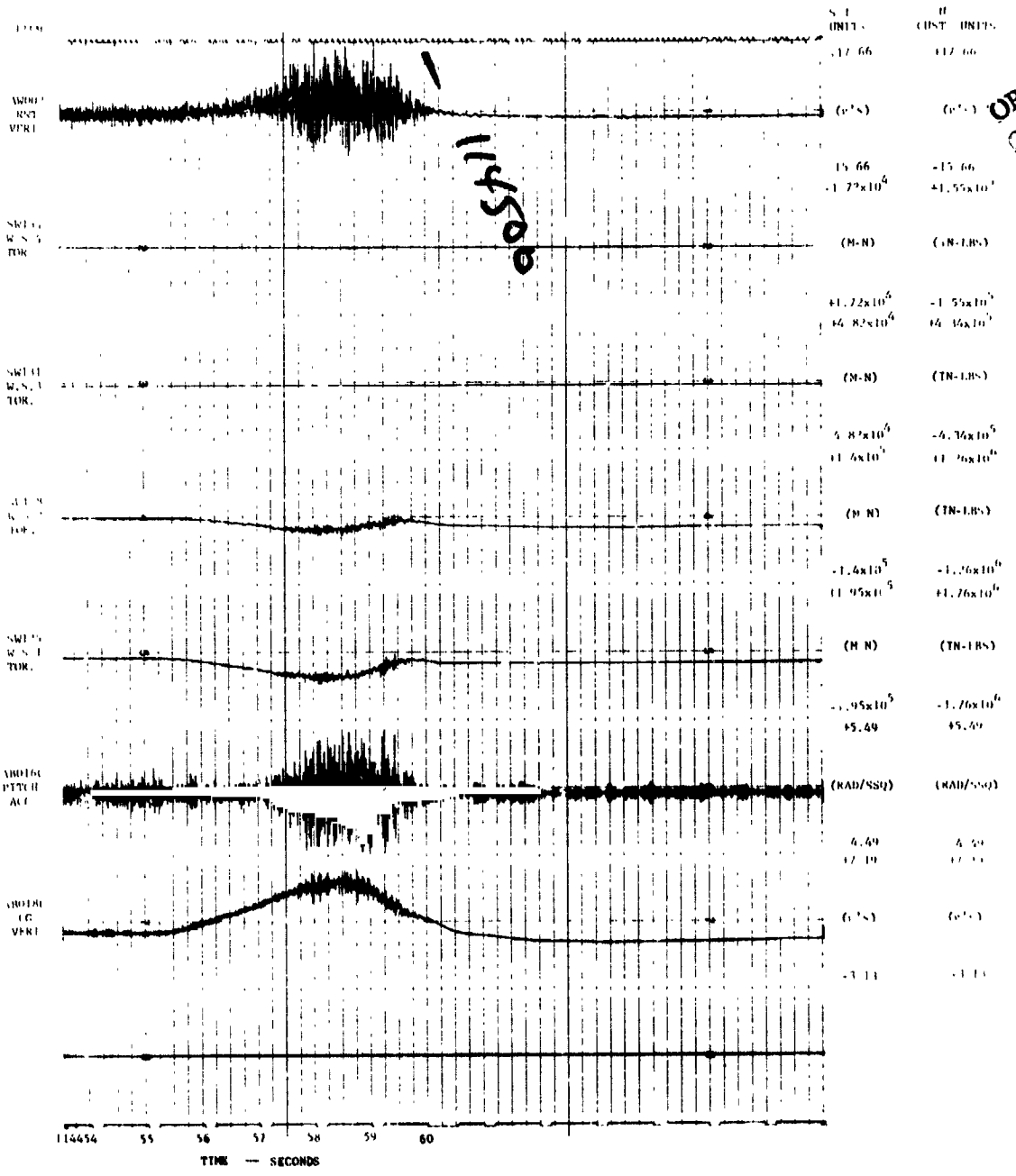

(b)

Figure A-5. Continued

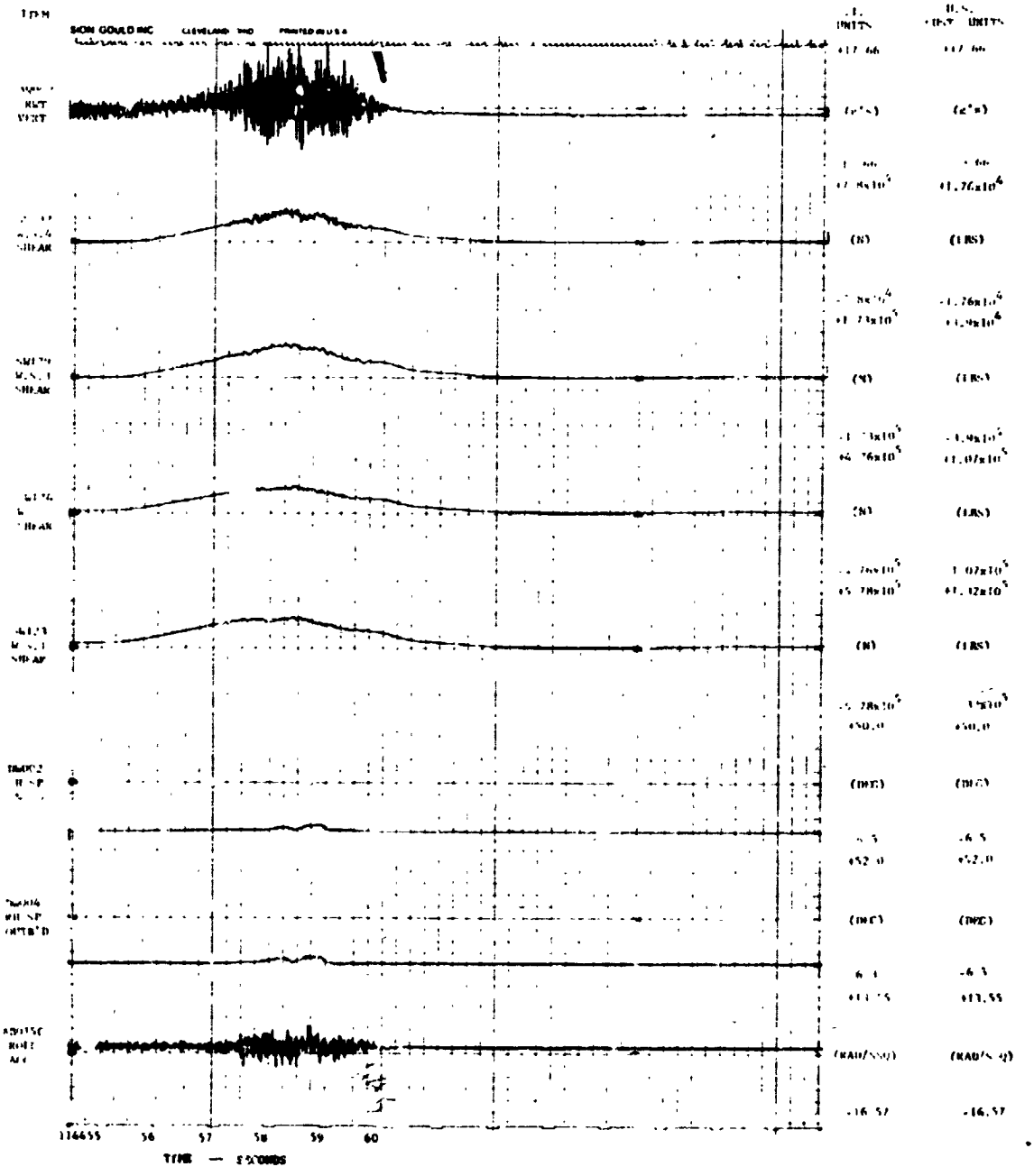

(c)

Figure A-5. Continued

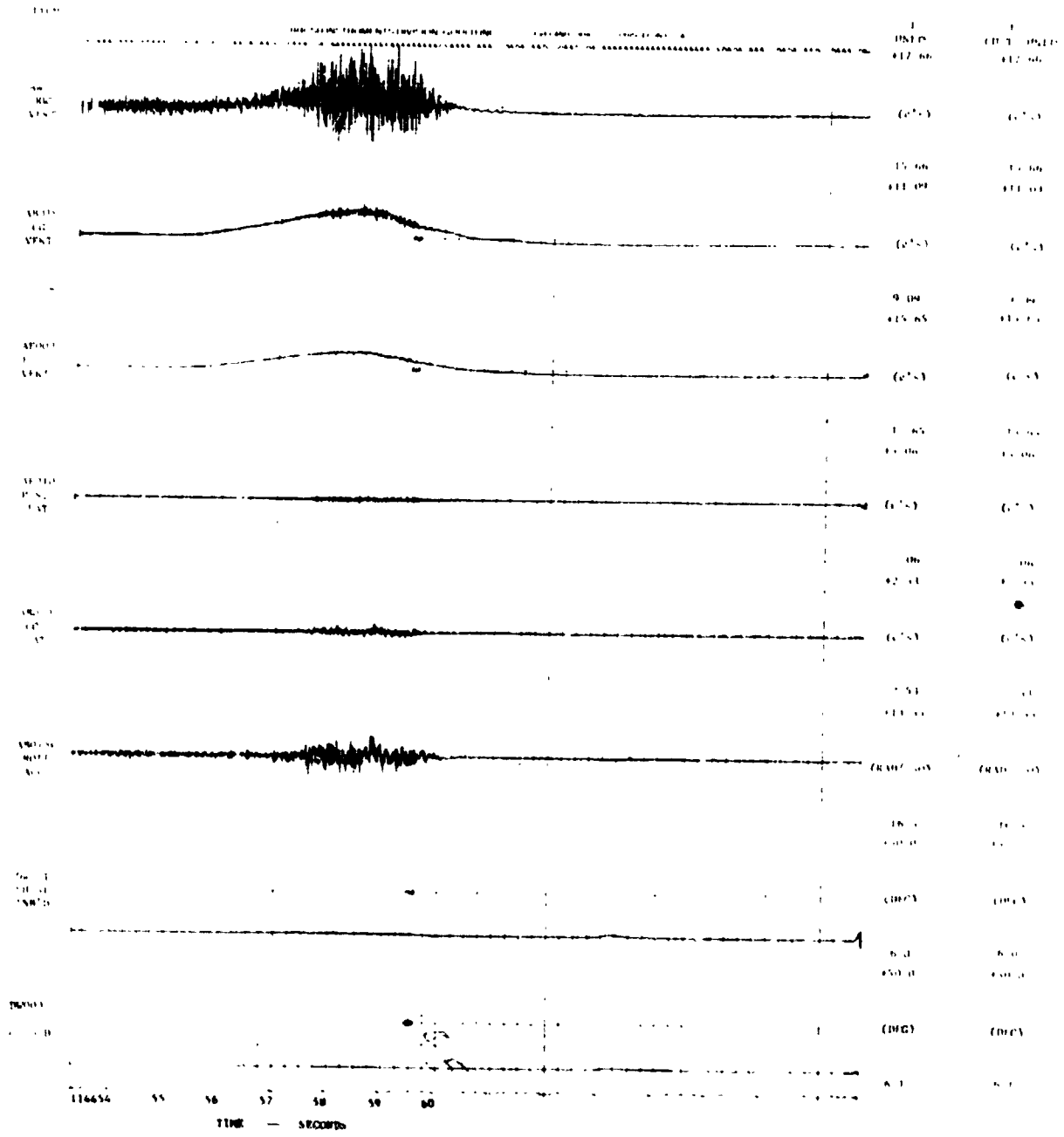

(d)

Figure A-5. Continued

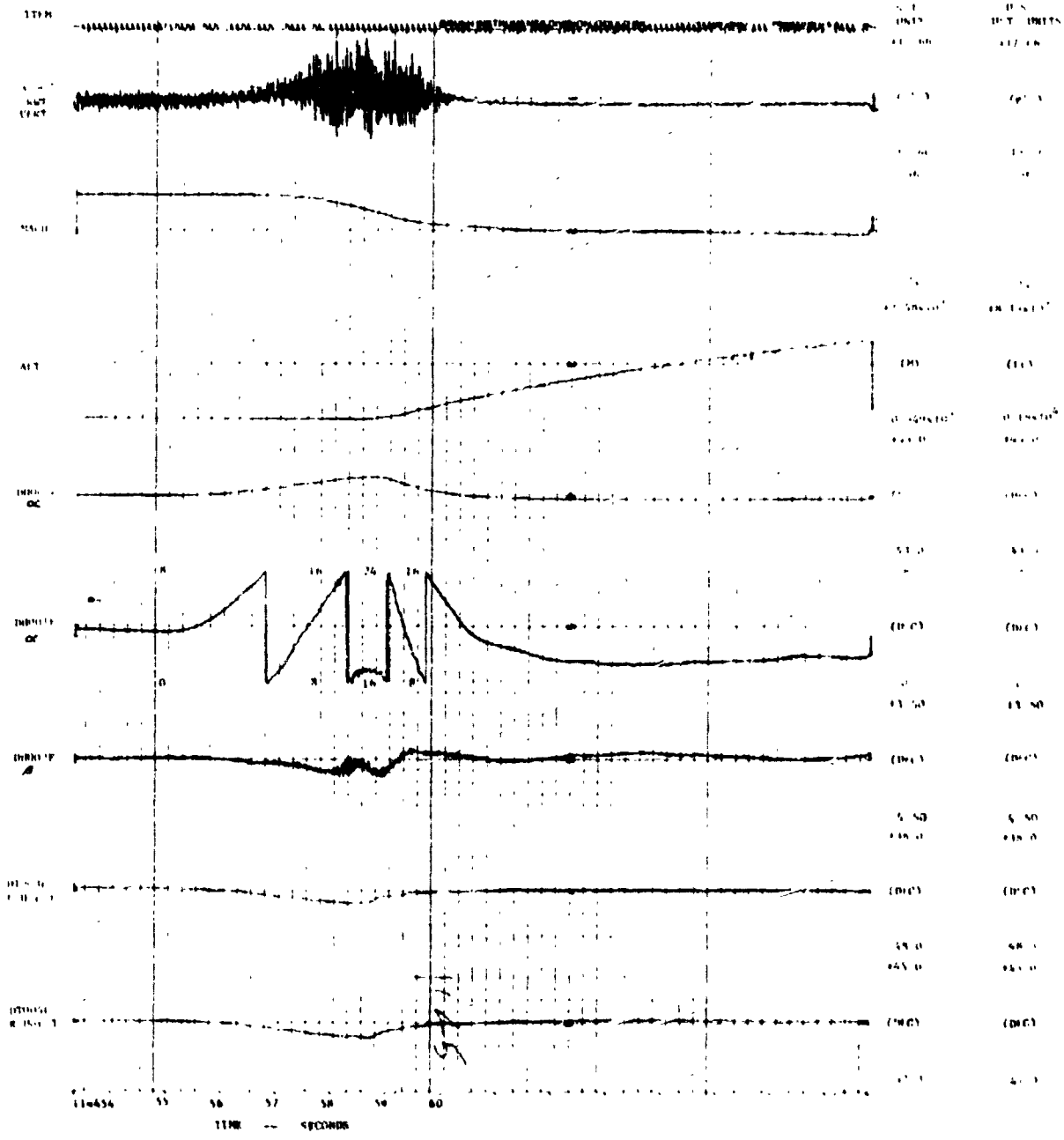

(e)

Figure A-5. Concluded

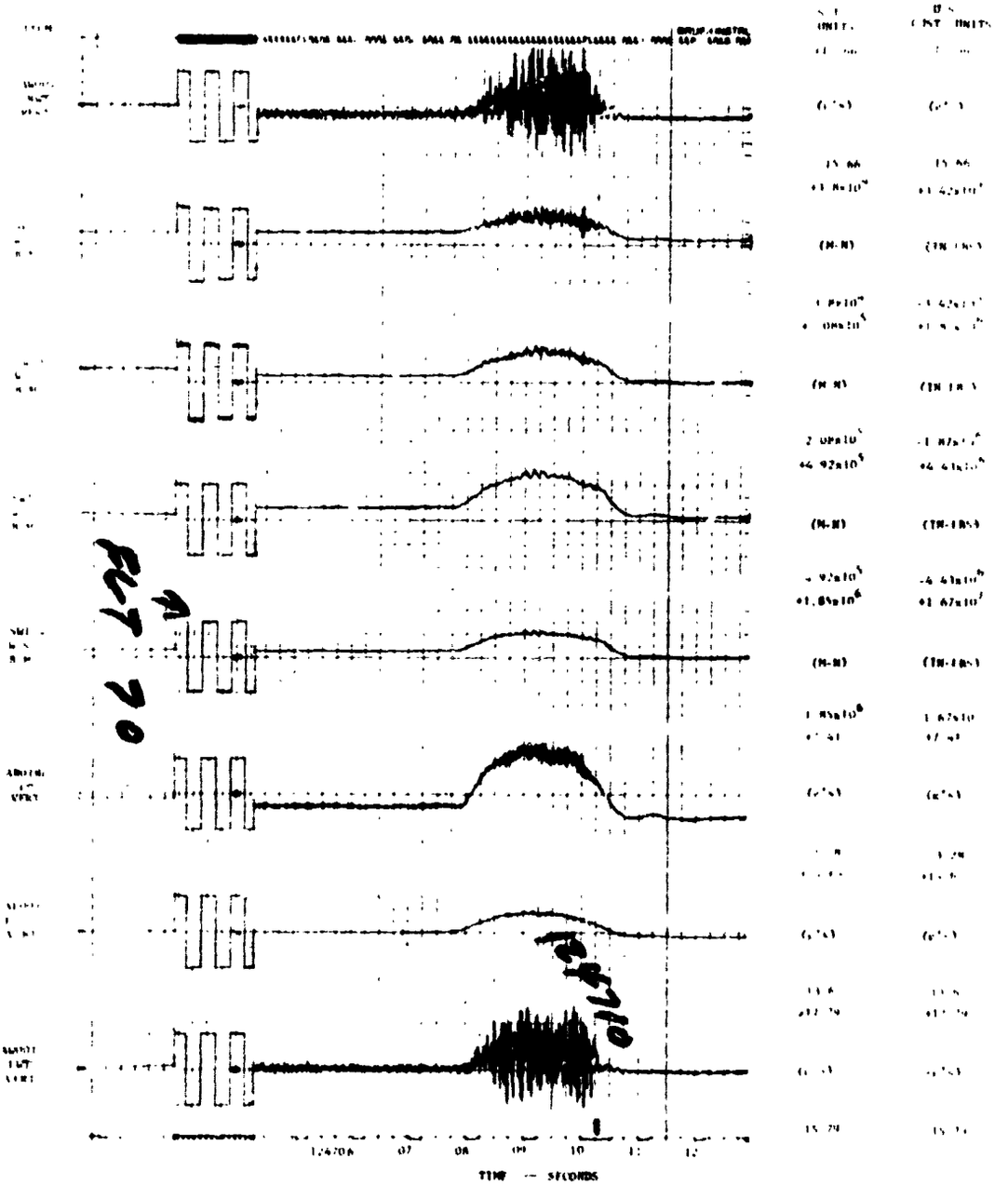

(a)

Figure A-6. TIME HISTORIES OF INSTRUMENTATION OUTPUT FOR PULLUP, FLIGHT 70, RUN 2

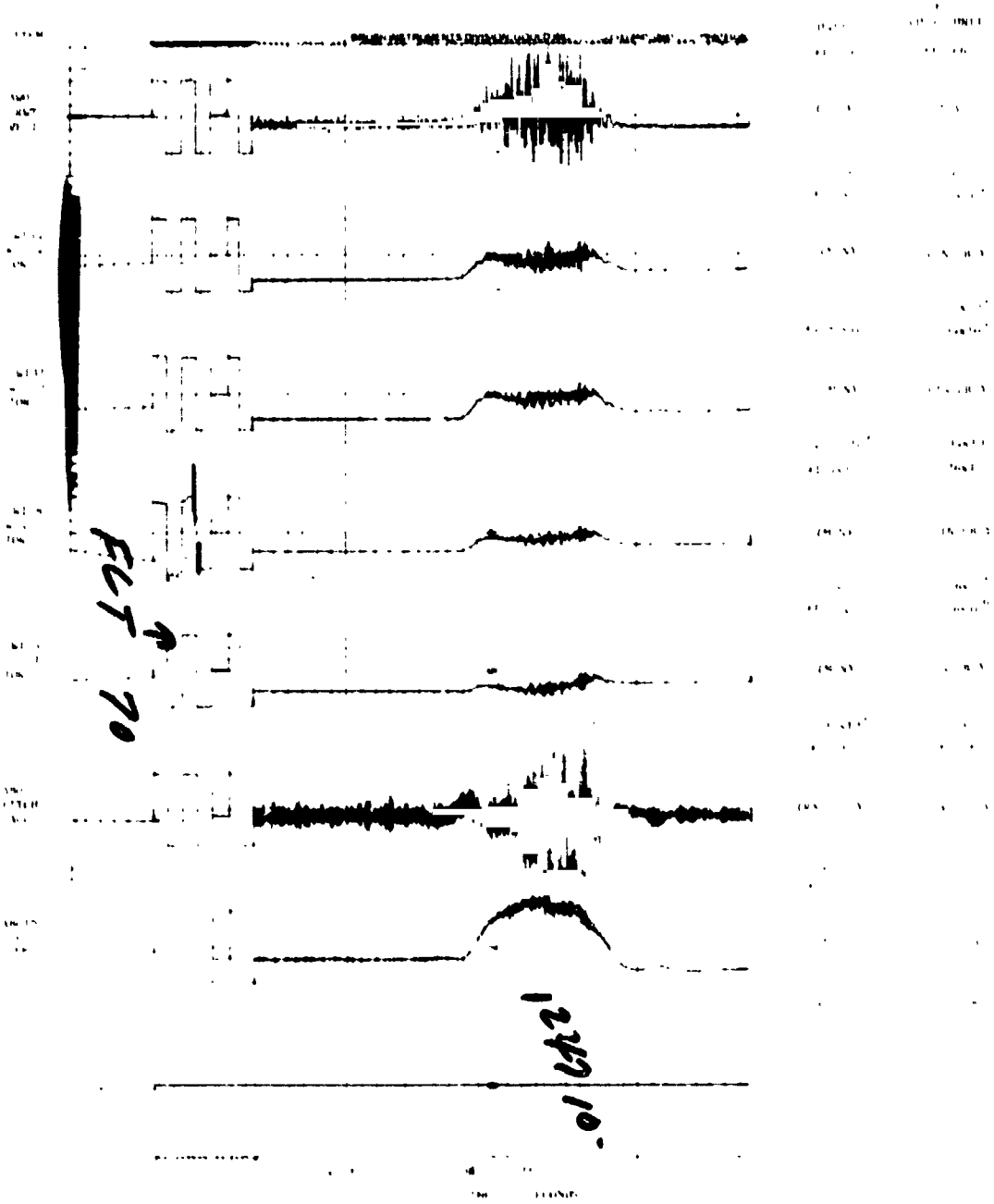

(b)

Figure A-6. Continued

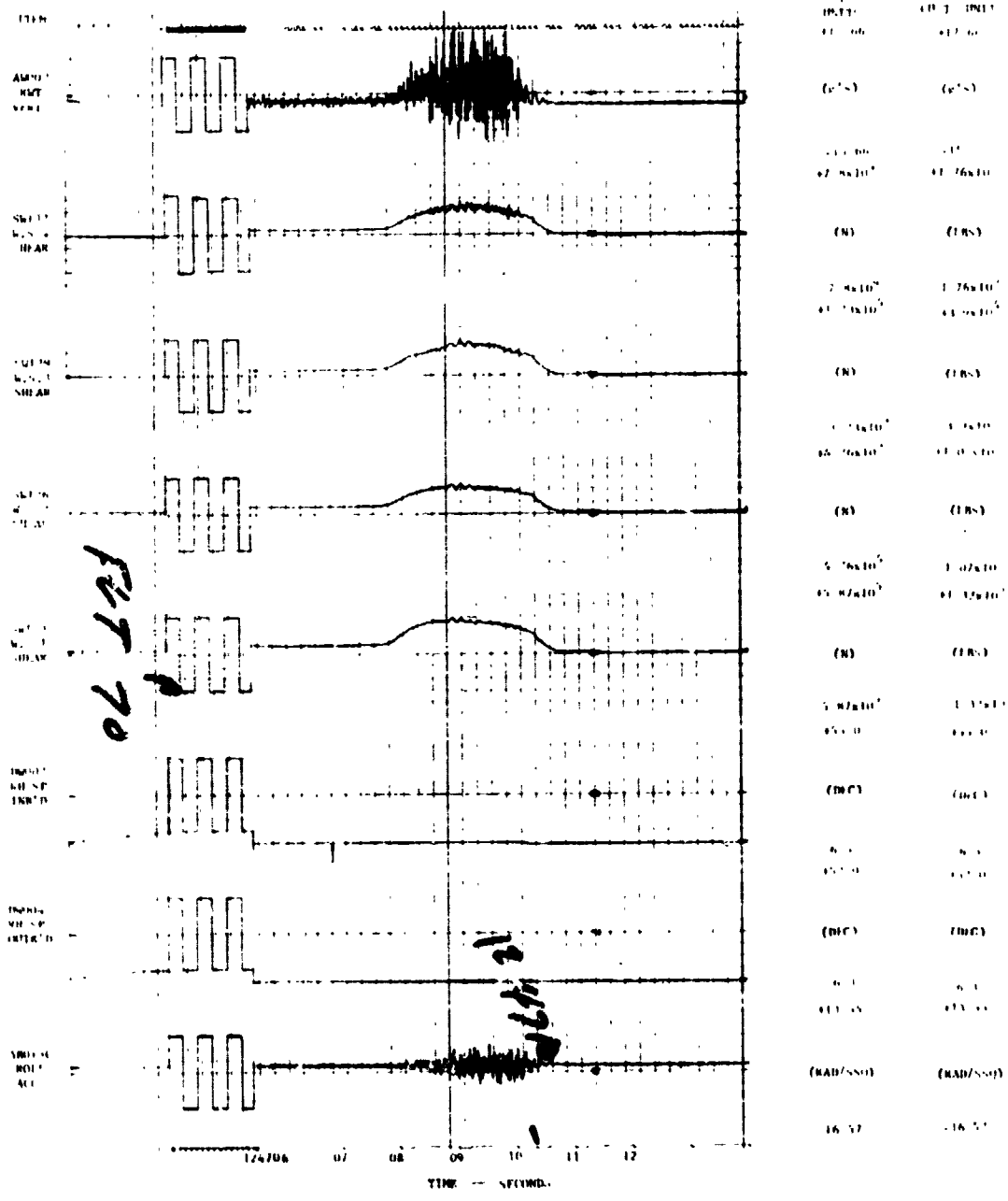

(c)

Figure A-6. Continued

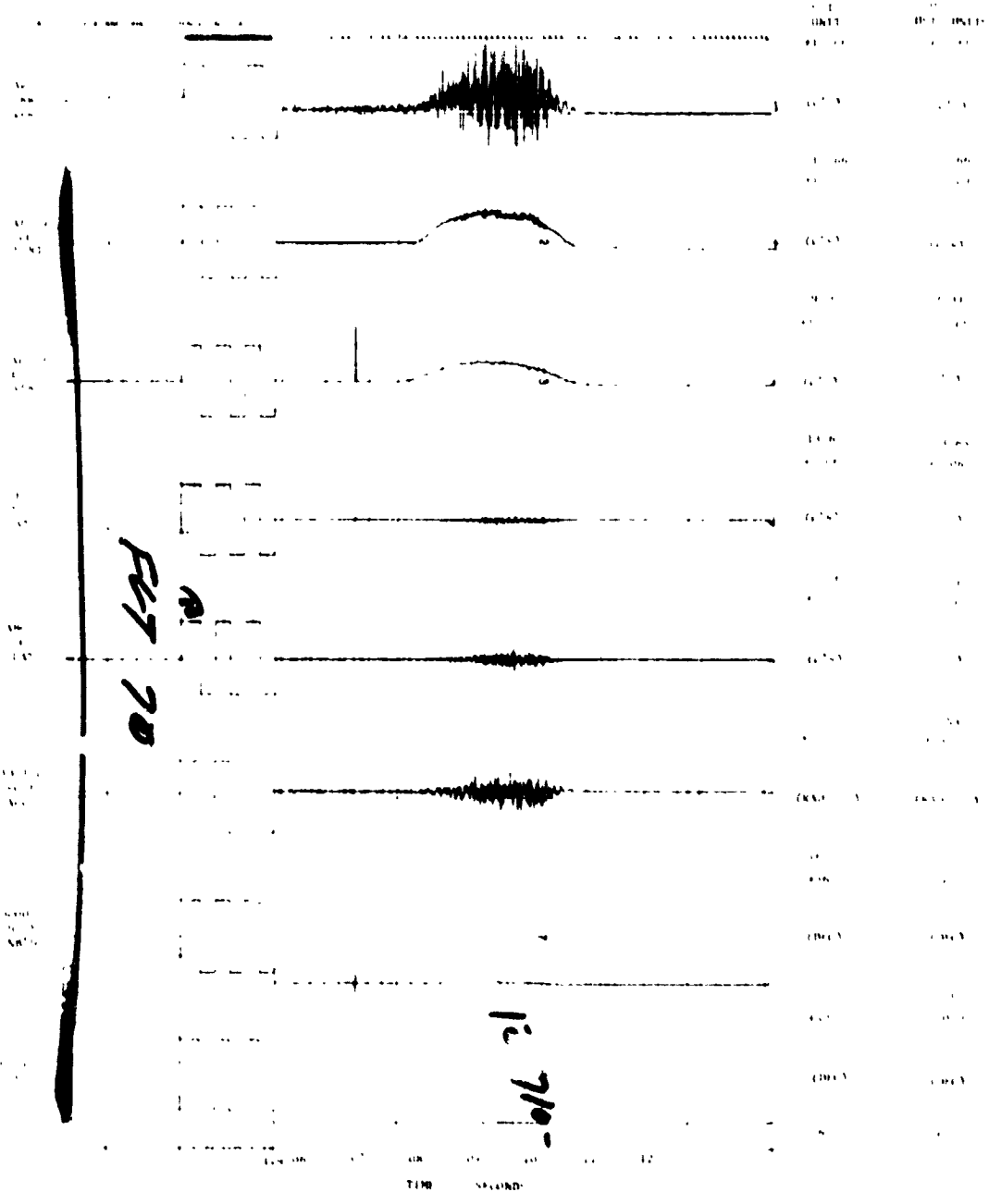

(d)

Figure A-6. Continued

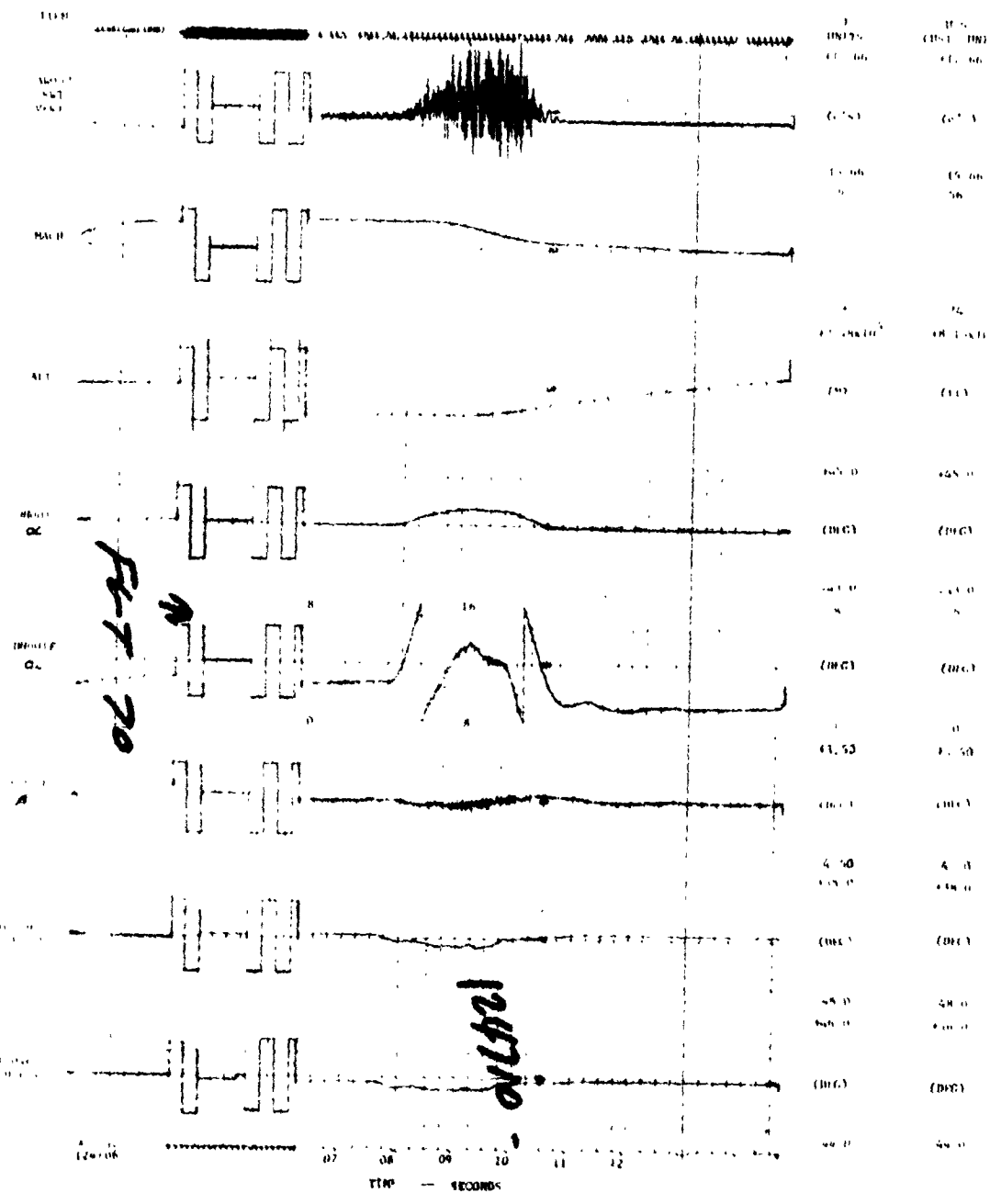

(e)

Figure A-6. Concluded